

OSLO METROPOLITAN UNIVERSITY
STORBYUNIVERSITETETMaster's Degree in
Structural Engineering and Building Technology
Department of Civil Engineering and Energy Technology

MASTER THESIS

THESIS TITLE: System Identification and Finite Element Model Updating of the Stange Railway Overpass	DATE: 09.06.2021
	NUMBER OF PAGES / APPENDICES: 89 / 3
AUTHOR(S): <ul style="list-style-type: none"> Jakob Braaten Johnsen Mathias Torp 	SUPERVISOR(S): Emrah Erduran

IN COLLABORATION WITH: Bane NOR	CONTACT PERSON(S): <ul style="list-style-type: none"> Kameran Aziz Ian Willoughby
------------------------------------	--

SUMMARY:

This study presents the implementation of a complete sensitivity-based, manual and iterative finite element model updating process of a 48.6 m long, continuous concrete railway bridge. Initial correlation of modal parameters between documentation-based finite element model and experimental data have indicated a considerable mismatch, with poorly correlated mode shapes and significant natural frequency errors. Through manual tuning, comprehensive sensitivity analyses, and finite element model updating, critical, undocumented structural parameters were identified, quantified, and incorporated in the updated finite element model. Resultingly, a satisfactory modal parameter agreement was achieved, and physically realistic updated parameter values were identified.

3 KEYWORDS:

Finite element model updating

System identification

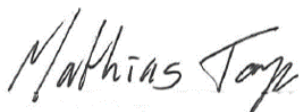
Railway bridge

Foreword

This thesis is prepared for the Department of Civil Engineering and Energy Technology at Oslo Metropolitan University within the field of Structural Engineering and Energy Technology. The thesis is the conclusion of our Master of Science degree (MSc.) and counts a total of 30 ECTS credits. The work is concluded within a period of 6 months, from January to June 2021. The thesis is a collaborative study between student authors Jakob Johnsen and Mathias Torp, with Bane NOR as a partner.

The Department of Civil Engineering and Energy Technology at Oslo Metropolitan University offers a highly relevant and interesting in-depth study through its specialization in structural engineering, which is firmly linked to the AEC industry and its development. With a specialization in structural engineering, topics like system identification and assessment of a structure's dynamic behavior have been especially relevant and interesting for us. By selecting a highly relevant topic for our master thesis that can take us further into the theory behind this, in addition to gaining practical experience and providing value for our partner, the wish is to gain indispensable experience and further promote our interest in complex structural engineering at an early stage in our careers. The topic of system identification and finite element model updating is perceived to be highly relevant for the future of structural engineering. It could provide the industry and society with great value and benefits as the present and future demands on our civil engineering structures are continuously increasing.

We would like to express our gratitude to all of those providing input, guidance, and help for this thesis, with special consideration to our partners from Bane NOR, Senior Bridge Engineer Ian Willoughby and Kameran Aziz. Special gratitude is also expressed to our supervisor, Associate Professor Emrah Erduran, and Ph.D. Candidate Kültigin Demirlioğlu from Oslo Metropolitan University.



Mathias Torp



Jakob Johnsen

Oslo, 09.06.2021

Abstract

This study presents the implementation of a sensitivity-based finite element model updating process on a 48.6 m long, continuous, concrete railway bridge located in Stange, Norway. Lack of documentation and uncertainties surrounding the structural system and dynamic responses have prompted the need for system identification and development of an updated finite element model that can more accurately represent the as-built structure.

The railway bridge under investigation was instrumented to perform system identification, and operational condition output-only vibration data was collected. Using the Covariance-driven Stochastic Subspace Identification method implemented in MATLAB, four dominant, distinct, and recurring modes were identified. By developing a simplified, documentation-based initial finite element model and performing modal analysis, significant discrepancies between the experimentally and analytically identified modal parameters were observed. Correlation of experimental and initial analytical modal parameters gave an average mode shape correlation of 61 % and average natural frequency error of 23.7 %, indicating a considerable mismatch between the documented and as-built structure. With observations made through visual inspections, undocumented changes to the structure were identified, confirming this mismatch. Through the implementation of these changes in the initial finite element model, manual tuning, comprehensive sensitivity analyses, and manual iterative finite element model updating, the errors between the experimental and analytical modal parameters were successfully minimized. The average mode shape correlation was increased to 89 %, and the natural frequency error was reduced to 9.8 %, indicating a very good modal parameter agreement between the experimental and analytical results.

This study has successfully identified and implemented an effective and complete method of finite element model updating applicable for railway bridges. Critical structural parameters have been identified, and their influence on the modal parameters and dynamic behavior has been thoroughly investigated. The manual finite element model updating process has generated indispensable first-hand knowledge of understanding structural systems and dynamic behavior of railway bridges, which, combined with fair engineering judgment, have contributed to the success of this study.

Table of Contents

Foreword.....	i
Abstract.....	ii
Table of Contents	iii
Table of Figures.....	v
Table of Tables	vii
1 Introduction	1
2 Study Purpose	4
3 Research Question	6
4 Methodology	7
5 Limitations.....	12
6 Theoretical Background for Finite Element Model Updating	13
6.1 Operational Modal Analysis.....	13
6.2 System Identification	13
6.3 Correlation of Modes.....	15
6.4 FE-model Updating	17
7 The Stange Railway Overpass.....	21
7.1 Background and Issue	22
7.2 Initial FE-model	26
8 Modal Identification of the Physical Structure	31
8.1 Sensor Hardware.....	32
8.2 Hardware Installation	33
8.3 Sensor Configuration	34
8.4 Data Processing.....	37
8.4.1 Organizing and Pre-processing of Acceleration Data	37
8.4.2 Time-history Acceleration Data	41
8.4.3 Forced-, Free-, and Ambient Vibration	43
8.5 System Identification	49

8.5.1	System Identification of the Stange Railway Bridge	49
8.5.2	Resulting Modal Parameters.....	54
9	Initial Correlation	60
9.1	Initial FE Modal Analysis	61
9.2	Refining and Manual Tuning of Initial FE-model.....	64
10	Finite Element Model Updating	68
10.1	Sensitivity Analysis	70
10.2	FE-model Updating	75
11	Verification of FE Computed Accelerations and Displacements	82
12	Conclusion	87
13	Future Work	88
	References	90
	Appendices.....	94
	Appendix A – Literature List	94
	Appendix B – Data Collection Report	98
	Appendix C – Complete FEMU Process	101

Table of Figures

Figure 1. Flowchart of general FEMU methodology.....	7
Figure 2. Flowchart of stages in identification of final sample for literature list.....	11
Figure 3. SSI-cov flowchart [25].	15
Figure 4. Mode shape correlation using the MAC. (i) good correlation, (ii) poor correlation [28].	17
Figure 5. Sensitivity-based, iterative FEMU process flowchart.	21
Figure 6. Aerial photo of Stange railway overpass [34].	22
Figure 7. Stange railway overpass side elevation [35].	22
Figure 8. General layout of Stange railway bridge (side elevation view).	23
Figure 9. General layout of Stange railway bridge, (i) bridge deck and column cross-section, (ii) abutment plan view.	23
Figure 10. Stange railway bridge 3D-view.	24
Figure 11. Abutment detail elevation view.....	25
Figure 12. Abutment detail cross-section.	25
Figure 13. Modelled cross-section with ballast.	28
Figure 14. Cross-section including pier caps.....	28
Figure 15. (i) Bearing ELASTO-BLOKK NBv [48]. (ii) Visual inspection of the bearing.	29
Figure 16. Extruded view of FE-model in CSiBridge.....	31
Figure 17. 2D-view with springs representing elastomeric bearings.....	31
Figure 18. Unquake sensor and datalogger setup [52].....	32
Figure 19. Accelerometer and datalogger installation.	34
Figure 20. Sensor configuration nr. 1. [mm].....	36
Figure 21. Sensor configuration nr. 2. [mm].....	36
Figure 22. Typical cargo train time-history acceleration plot.....	39
Figure 23. Typical express train time-history acceleration plot.....	40
Figure 24. Typical local train time-history acceleration plot.	40
Figure 25. Max. accelerations recorded based on 92 train crossings.....	42
Figure 26. Example of time-history acceleration plot vibration phases; (1) forced vibration, (2) free vibration, (3) ambient vibration.....	44
Figure 27. Observed effect of duration on natural frequency and damping ratio [56].....	45
Figure 28. Free vibration start and duration difference between sensors.....	46
Figure 29. Changes observed in natural frequency due to duration increment ex. 1.	48
Figure 30. Changes observed in natural frequency due to duration increment ex. 2.	48
Figure 31. Flowchart of the stabilization criteria [13].....	50

Figure 32. Stabilization diagram generated by the SSI-cov algorithm.....	50
Figure 33. Resultant displacement and modal components [42]......	52
Figure 34. The 4 obtained modes of the Stange railway bridge from experimental data.....	55
Figure 35. MAC correlation of the extracted experimental mode shapes.	57
Figure 36. Linear vs. spline approximation.	60
Figure 37. Experimental modes vs. initial analytical modes.....	62
Figure 38. Experimental vs. initial analytical MAC correlation.	63
Figure 39. Concrete slabs underneath the deck extensions.....	65
Figure 40. Concrete slab underneath deck extensions in relation to bearing.....	65
Figure 41. Modified deck cross-sections. (i) deck (ii) deck with column-cap.	67
Figure 42. 2D-view of refined FE-model with soil-springs.	67
Figure 43. Experimental modes vs. modes from refined and manually tuned FE-model.	69
Figure 44. Experimental vs. analytical MAC correlation.	70
Figure 45. Correlation of experimental and analytical MAC-optimized mode shapes.....	78
Figure 46. Experimental vs. analytical MAC-optimized modes.	79
Figure 47. Load model HSLM-A [59].	83

Table of Tables

Table 1. General guidelines for the scoping review.....	8
Table 2. Search table with identified key terminology and concepts.....	9
Table 3. Search string evolution and recorded hits per database.	9
Table 4. Concrete material properties specified in CSiBridge.	27
Table 5. Modelling parameters.....	30
Table 6. Average max. accelerations recorded for train types.	42
Table 7. Modal parameter criteria set for the stabilization diagram [26].	50
Table 8. Share of data from each sensor configuration.....	55
Table 9. Modes identified dependent on train direction.	57
Table 10. Experimental vs. initial analytical natural frequencies.	64
Table 11. Typical values of the modulus of subgrade reaction, k_s [65],[66].....	66
Table 12. Experimental vs. analytical natural frequencies.	70
Table 13. Parameters selected for sensitivity analysis with lower and upper bounds.....	71
Table 14. Effect of parameters on the analytical mode shapes assessed using MAC.	73
Table 15. Effect of parameters on the analytical natural frequencies.	74
Table 16. Parameter values in the MAC-optimized FE-model.	78
Table 17. Natural frequencies of experimental and analytical MAC-optimized modes.....	79
Table 18. Results of the FE-model updating process for the identified modes.....	82
Table 19. Load model HSLM-A10 [59].....	83
Table 20. Experimental vs. analytical accelerations.	85
Table 21. Experimental vs. analytical displacements.....	85

1 Introduction

Finite element modelling has developed to become a widely used technique during recent decades. Originating from the development of the finite element method (FEM) by the University of California and the Boeing company in the 1960s [1], the method allows the engineer to discretize and thus simplify the most complex of structures. However, even though the modelling technique has proven to accurately estimate structural behavior and therefore be an excellent tool for design purposes, a mismatch between physical structures and their finite element model (FE-model) counterpart was shortly identified [1]. Thus, with a background in a lack of correlation between analytical and experimental results, the concept of calibrating FE-models to the extent where they can more accurately render the actual structural behavior was formed. Today, the calibration process is formally known as finite element model updating (FEMU) [2].

In the 1990s, Friswell and Mottershead published "*Finite Element Model Updating in Structural Dynamics*" [3], of which the presented theory and concepts of calibrating numerical models based on acquired structural data are widely cited in literature [4]–[9]. Even though the idea of calibrating FE-models may sound simple, Živanović et al. [10] presented FEMU as a sum of 4 sequential stages: initial modelling, data acquisition, manual model tuning, and model updating. The stages themselves can be seen as independent, but in FEMU, they are interconnected through the identification and calibration of modal parameters. Modal parameters, such as natural frequency, mode shape, and damping ratio, are properties of the structure and describe how a structure will naturally respond when excited by an arbitrary force. Thus, if a structure's modal parameters can be identified, the structural behavior can as well.

By using prototypes within the aerospace industry, structural response data could easily be acquired by monitoring the prototypes. Thus, validating the FE-model counterpart and quantify the level of agreement with the physical measurements could be executed with minimal extra effort [1]. However, unlike the aerospace industry, producing prototypes to conduct real-condition testing is not economically feasible for unique, large-scale structures, such as railway bridges [10]. Thus, identifying the structural condition and performing FEMU for such structures requires specialized techniques of varying complexity that can be

significantly labor-intensive. Subsequently, identifying and discussing the essence and significant benefit of allocating resources into FEMU of the railway infrastructure is vital to clarify.

Railways and their associated infrastructure are critical aspects of transporting goods and passengers, both domestically and internationally, worldwide. Continuous research and development of infrastructure- and train technology are increasing the demands on the already existing infrastructure, which is rapidly aging. In 2005, European railway infrastructure estimates indicated that over 35 % of the railway bridges were over 100 years old, while only 11 % were less than ten years old [11]. In an effort to secure that the railway infrastructure can withstand current and future demands of increased train loads and speed, substantial research is being conducted to develop and streamline methods for structural assessment and monitoring. In a survey, as a part of a study by Olofsson et al. [11], owners of railways in Europe were asked to state a top 10 priority list for research areas relevant for railway infrastructure. Among the top three priorities listed, both *"better assessment tools"* and *"verification of theoretical dynamic factors for both design and assessment"* were included. As system identification and FEMU both can be good candidates for such research, the need for development and further incorporation of such techniques becomes highly relevant and can greatly benefit the assessment of the aging railway infrastructure. Understanding the benefit and importance of FEMU for maintenance and reuse of the railway infrastructure is key. However, understanding the origin to why a poor level of agreement between physical measurements and their numerical counterpart can occur in the first place, is equally important.

FE-models are numerically estimated, digital structures widely used in structural design. However, depending on region, experience, and project demands, the reference design code can vary. Thus, the FE-estimated structural behavior can not only differ from the as-built structure but also between FE-models. Moreover, time and deterioration are also a source of error. As the structure ages, the concrete strength increases, and deterioration and damage to various extent can occur. Subsequently, as a consequence of time and environment, the initial premises presented in the documentation may be outdated during the service life. Thus field-observed responses can be challenging to reproduce in a documentation-based FE-model. In general, the discrepancies identified by field testing usually originate from material

properties, uncertainties in geometry and boundary conditions, and inaccuracy in the discretization of the FE-model [12]. Živanović et al. [10] express the increasing need for rectifying FE-models of both new and existing structures through FEMU, as increasingly slender structures are becoming easier to excite. Even though Živanović et al.'s statement is based on the developments within footbridges, rectifying larger structures, such as railway bridges, are still highly relevant as the infrastructure ages.

It is widely acknowledged that FEM only gives estimations. However, rather than compensating with safety factors in design, FEMU can help quantify the error and thus develop FEM. Even though FEMU is well established in both mechanical and aerospace engineering [1], standardized techniques guaranteeing successful model calibration while maintaining a physically meaningful structure do not exist in structural engineering. Thus, FEMU in structural engineering demands competence in FE-modelling, modal testing, and various alternative calibration techniques to obtain a high-fidelity, updated FE-model.

Fundamental in FEMU is the identification of the structure, both through the available documentation as well as visual inspections. Thus, an initial FE-model based on the best engineering judgment can be formed. Essential in this process is to identify boundary conditions, possible damage, and generally the physical parameters that presumably affect the dynamic behavior and subsequently the ability to calibrate the FE-model later on. In that way, a set of expectations and a basis for comparison is formed ahead of data acquisition and modal parameter identification. There are different approaches to collecting data and performing a system identification. More and more common is the operational modal analysis (OMA) [13]. In OMA, structural responses are measured, where the typical measurand is acceleration. However, to get a structural response, the structure needs to be excited. Unlike in experimental modal analysis (EMA) [14], the forces exciting the structure in OMA are not known, leading to the need for specialized techniques to extract non-contaminated modal parameters from the collected data. When the modal parameters are identified and compared to the initial analytical parameters, the manual tuning of the FE-model can commence. At this stage, the goal is to manually change details in the FE-model to increase the correlation with the experimentally obtained modal parameters. In that way, the probability of obtaining a satisfactory calibrated FE-model increases as details can be altered and errors erased. Finally, a "formal" updating is performed either through continuous

manual tuning and optimization or through automatic updating algorithms using specialized software. Whereas manual updating greatly benefits from controlling how each parameter affects the structure, the automated algorithms benefit from being time-efficient.

The benefits of numerical modelling through the finite element method for design purposes are indisputable. However, as a consequence of simplifications and uncertainty in parameters, performing modal analysis on numerically estimated models may result in significant deviations from the ones that are experimentally obtained. Whereas there is uncertainty related to design models, focusing on existing structures may be even more critical in the coming years. The railway infrastructure is aging, thus it is essential to develop applicable tools to better assess existing structures that can subsequently be subjected to suitable measures to extend the service life. The key to realizing the goal of standardizing functional calibration tools within structural engineering is continuous research and transparency. To further develop the research field and add to the knowledge within FEMU of large-scale structures with limited documentation, this study describes the complete process of conducting FEMU on the Stange railway overpass, presented as a sequential procedure until a satisfactory, calibrated FE-model is obtained. Throughout the study, all steps are presented in a descriptive matter so that the methods can be adapted and the engineering judgment can easily be interpreted.

2 Study Purpose

A major InterCity railway infrastructure development project in Norway has prompted Bane NOR, which is responsible for all railway infrastructure in Norway, to develop streamlined and effective methods and frameworks for assessing already existing railway bridges. This InterCity railway project's success partly relies on the possibility of utilizing some of the already existing railway bridges on railway lines that are due to be upgraded such that they can accommodate increased axle-loads and traveling speeds exceeding 250 km/h. Thus, of the approximate 2 700 railway bridges in Norway [15] that Bane NOR is responsible for, many will require a structural assessment to meet the present and future demands to secure the safety of the passenger and freight traffic.

As FEMU can be a powerful and effective tool for assessing already existing structures, Bane NOR wish, in collaboration with Oslo Metropolitan University, to develop a streamlined and

generally applicable framework for structural assessment of railway bridges through the use of system identification and FEMU. To accomplish this, a collaborative research project titled "NEAR: Next Generation Finite Element Calibration Methods for Railway Bridges" was initiated. One of the NEAR projects clearly stated goals is; *"NEAR will leverage the vibrations that naturally occur on the bridge under regular train traffic to develop a FE calibration method that will provide accurate estimates of the maximum accelerations and forces generated by train traffic»* [16]. With this stated goal, the NEAR project intends to develop methods and frameworks for FEMU that can be utilized and easily incorporated by Bane NOR in their work of performing structural assessment and analysis of their railway bridge structures.

The NEAR project was initiated in Q4 2020 and is set to conclude in Q2 2022. This thesis is developed in conjunction with initial work packages stated for the NEAR project in Q1 – Q2 2021, and its purpose and goal is to perform initial system identification and development of a preliminary updated FE-model of the Stange railway overpass. This will be done by developing a baseline FE-model of the railway bridge which will be updated according to experimental responses gathered from operational condition monitoring, where key aspects are identification of mode shapes, natural frequencies, and damping ratios. One of the main challenges outlined for this thesis is identifying and quantifying the bridge's uncertainties, especially its boundary conditions and subsequent structural behavior during operational conditions. This work will be of great importance for the development of an updated FE-model and the identification of modal parameters. To successfully accomplish this, all available documentation of the bridge will be assessed along with results from visual inspections and operational condition monitoring. From this, the most uncertain factors and parameters can be investigated and quantified with the intent to obtain a better understanding of the structural system and dynamic behavior. This will then lay the ground for further work in the NEAR project, where the end goal is to develop a highly detailed and high-fidelity FE-model that can accurately recreate the true dynamic behavior through the use of the developed framework and methods.

3 Research Question

As the purpose of this study is defined according to the initial work packages stated for the NEAR project, the relevant research question for this study is redefined to function as an overall goal that again depends on the completion of a series of sub-goals.

Overall goal:

- Perform initial modal identification and development of a preliminary updated FE-model of the Stange railway overpass while obtaining a good understanding of the dynamic behavior of the bridge using system identification techniques and experimental operational condition data.

Sub-goals:

- Collection of operational condition, output-only acceleration data from the Stange railway overpass.
- Experimental system identification of the Stange railway overpass based on the collected operational condition acceleration data to identify dominant, distinct, and recurring natural frequencies and mode shapes within a realistic frequency range.
- Development of an initial, documentation-based FE-model with the inclusion of modeling parameters that will allow for further manual tuning and finite element model updating to correlate experimental and analytical modal parameters.
- Perform finite element model updating using methods and techniques found relevant to minimize the difference between the experimental and analytically computed modal parameters.
- Through finite element model updating and assessment of initial and updated FE-modelling parameters, identify and quantify the most critical parameters that significantly influence the structure's relative stiffness and mass distribution, affecting its modal parameters.

4 Methodology

This chapter will focus on the scientific methodology chosen and used in this thesis. In addition to this, special consideration is also given to how FEMU has been approached and how initial studies have been conducted in preparation for this thesis.

To fulfill the purpose and achieve the stated research goals of this study, the fundamental research method utilized for this thesis is a quantitative method applied through a case-specific study regarding the specified structure. With the collection of quantitative, output-only operational condition data, the structural behavior of the railway bridge in question will be investigated and quantified through modal identification and analysis of accelerations and displacements. This data will then act as reference data of the actual structural behavior and used in the process of minimizing the difference between the experimental and FE-computed modal parameters through FEMU. A flowchart presenting the general FEMU methodology relevant for this study is shown in Figure 1.

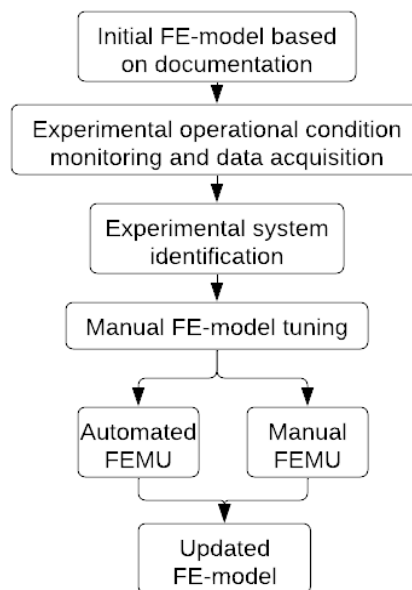


Figure 1. Flowchart of general FEMU methodology.

Preliminary studies in preparation for this thesis initiated in Q3 2020 and were concluded at the end of Q4 2020. The intention and goal of these studies were to obtain a general introduction and understanding of the field of FEMU with a focus on topics especially relevant for civil engineering bridge structures. As MSc. candidates, the field of FEMU in civil

engineering was a new and somewhat unfamiliar field of research, thus these initial studies were of great importance for a general understanding and for securing future work with the required level of scientific quality. The first preliminary study conducted in relation to this study was a scoping literature review focusing on identifying holistic and general characteristics of the research field in question. For a thorough introduction of what a scoping literature review is and how it can be utilized, see the study conducted by Arksey and O'Malley [17]. The most crucial factor acquired from this scoping literature review was a complete literature list with studies that provide unbiased and sound quality studies regarding FEMU of civil engineering bridge structures. From this sample of identified studies, it was possible to identify general trends within the field of FEMU, as well as detailed reviews of relevant FEMU methodology and techniques.

The first step for identifying a sample of studies relevant for future work was to review recommended studies by the project supervisor and other research fellows with good knowledge of FEMU. Of these recommended studies, the studies by Lorenzoni et al. [18], Chen et al. [12], and Reynders [13] were found to be especially helpful in this matter. After the preliminary review of recommended studies, the general guidelines for the literature search in the scoping review were decided. An excerpt of the guidelines determined is presented in Table 1.

Table 1. General guidelines for the scoping review.

1. General guidelines	2. Search database
<ul style="list-style-type: none"> • Sources: Online databases, journal articles, and conference papers • Timespan: last twenty years (2000 – 2020) • Full-text availability • English or Norwegian language 	<ul style="list-style-type: none"> • Oria • Elsevier Engineering Village • Scopus • Science Direct • Peer recommended and personal database

The general guidelines were decided to direct the literature search and establish standard limiting parameters of the search perceived to exclude studies of little relevance. The next step was to identify key concepts and terminology considered to be highly relevant within FEMU such that a search string for use in the different databases could be developed. Having a well-formulated search string is a crucial aspect for identifying relevant studies amongst the vast and overwhelming amounts of studies available in the databases. The key terminology

and concepts identified through simple literature searches and review of recommended studies are presented in Table 2.

Table 2. Search table with identified key terminology and concepts.

Concept 1	Concept 2	Concept 3	Concept 4
<ul style="list-style-type: none"> • Finite element model • FE Model • FEM 	<ul style="list-style-type: none"> • Updating • Calibration 	<ul style="list-style-type: none"> • Civil engineering • Structural engineering 	<ul style="list-style-type: none"> • Bridge

The concepts presented in Table 2 would then be combined using Boolean operators such as "AND" and "OR" to develop and evolve the search string used in the individual search databases presented in Table 1, column 2. The search string was evolved and refined through an iterative process and was proven to successfully produce highly relevant hits. The search string evolution and recorded hits per database are presented in Table 3. Note that after the third search iteration, the search was limited to only include published journal articles. This was done due to the assumption that acknowledged authors would more likely publish their studies in scientific journals. This assumption was also based on a preliminary review of a sample of conference papers identified through the search string that was concluded to be of little relevance and low quality.

Table 3. Search string evolution and recorded hits per database.

Search iteration	Search string	Oria	Engineering Village	Scopus	Science Direct
1	TITLE-ABS-KEY(((Finite element model) OR FEM OR (FE Model)) AND (updating OR calibration))	1 295	713	8 325	2 888
2	TITLE-ABS-KEY(((Finite element model) OR FEM OR (FE Model)) AND (updating OR calibration) AND ((civil engineering) OR (structural engineering)))	444	859	706	96
3	TITLE-ABS-KEY(((Finite element model) OR FEM OR (FE Model)) AND (updating OR calibration) AND ((civil engineering) OR (structural engineering)) AND Bridge)	106	761	159	16
After 3 rd search iteration, the search was narrowed to only include journal articles					
4	TITLE-ABS-KEY(((Finite element model) OR FEM OR (FE Model)) AND (updating OR calibration) AND ((civil engineering) OR (structural engineering)) AND Bridge)	106	573 ¹	70	16
¹ Including 116 duplicates between Compendex and Inspec → 457 unique journal articles					

The search string evolution was concluded after the fourth search iteration, and the identified studies were then collectively reviewed to exclude studies found to have less relevance. This was primarily done by review of the study title, keywords, and abstracts. Studies excluded in

this step were typically very narrow-focused or highly specific regarding the use of specialized methods and/or tools. This refinement process resulted in a sample of 312 studies that would go through a second more in-depth review performed individually by each project member. Studies selected by both project members were included in the final sample, and remaining studies were collectively discussed and included in the final sample if found suitable. As it was considered that the search string might not be able to identify all relevant studies, manual search techniques or a "hand-search", as described by Arksey and O'Malley [17], was conducted. From this, a few additional studies perceived to be highly relevant were identified and included in the final sample. After combining the studies identified using the search string in the databases, recommended studies, and studies found through a "hand-search", a final sample of 71 unique studies were concluded. During the search iterations, using the search string, it was observed that the recommended studies frequently appeared among the hits. This indicated that the search strings were of good quality and capable of producing highly relevant hits. A flowchart presenting the stages conducted in the process of identifying the final sample of studies is shown in Figure 2, and the complete final sample of 71 studies can be seen in Appendix A. Note that not all of the 71 identified studies are individually referenced in this thesis. However, they have collectively been essential for the scientific foundation. Where needed, additional studies and references have been identified for topics not covered by the identified studies as these are primarily focused on civil engineering bridge structures.

The second preliminary study conducted was a more in-depth literature review regarding FEMU in general, but also a review of methods and techniques more specific for civil engineering bridge structures. The primary purpose of this study was to utilize the previously identified sample of 71 studies to obtain a general understanding of the topic and conduct preliminary exercises in system identification using different software, such as CSiBridge and MATLAB. The combined results and the scientific foundation obtained from these studies have facilitated the case-specific study conducted in this thesis.

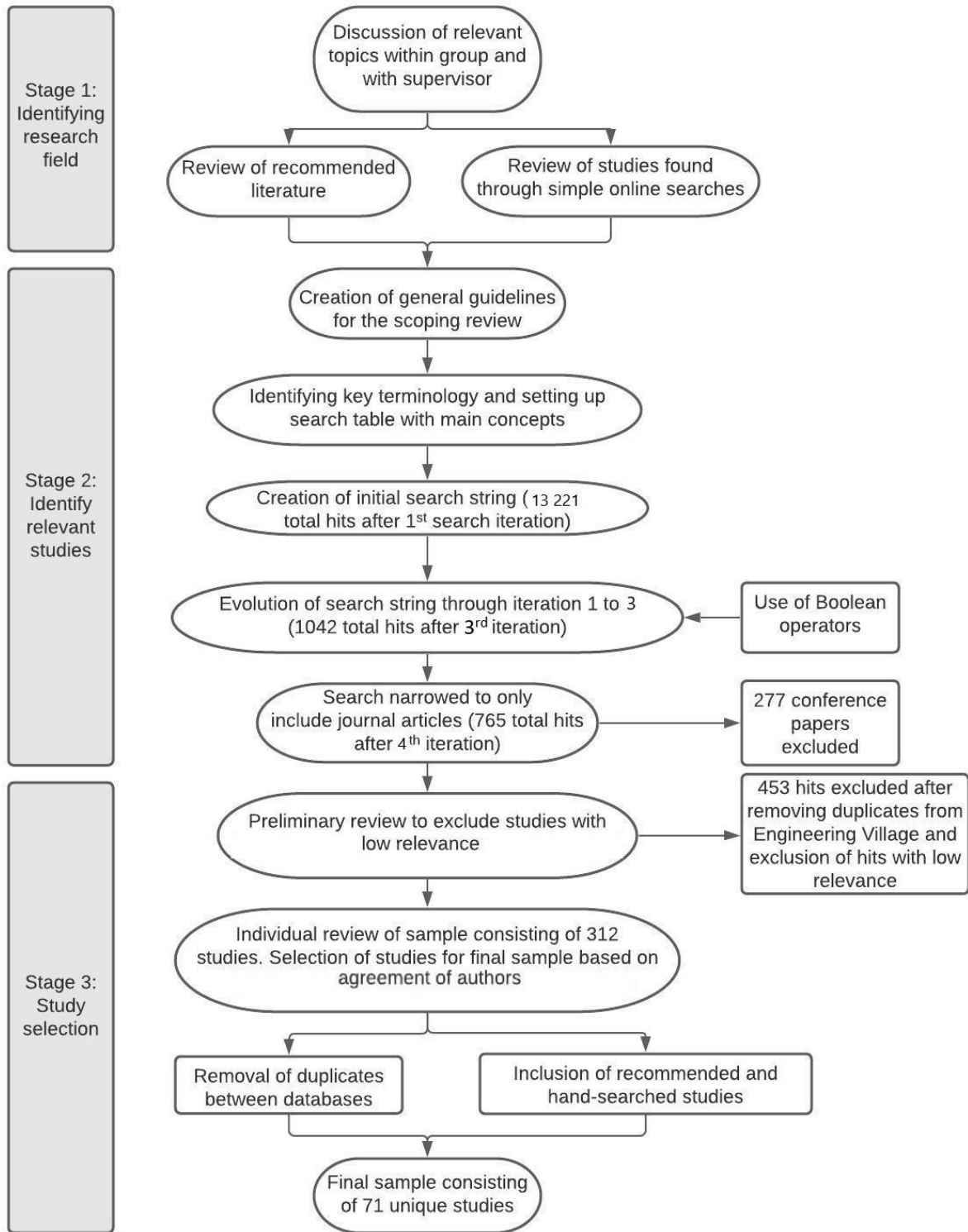


Figure 2. Flowchart of stages in identification of final sample for literature list.

5 Limitations

In order for this study to be holistic and feasible concerning time and scope, it has been necessary to impose certain limitations. This section will present the most general physical and chosen limitations imposed. Further and more detail-oriented limitations throughout the study will be presented where found relevant.

Physical limitations:

- Availability of sensor hardware at the time of structural monitoring has made it necessary to prioritize and limit the number of sensor locations and configurations. At the time of structural monitoring in this study, five complete accelerometer and datalogger systems were available.
- As the case-specific structure relevant for this study is located on an active railway line, the time available for monitoring was limited due to aspects of safety and practical feasibility. The time for monitoring of the bridge was approved by Bane NOR, starting at 15.12.2020, 09:00, and ending at 17.12.2020, 09:00.

Chosen limitations:

- As a consequence of the physical limitations regarding the availability of sensor hardware and time for monitoring, in addition to the geometry and symmetrical loading of the case-specific structure, only vertical responses will be assessed in this study. Thus, torsional-, transverse- and longitudinal responses will not be further assessed.
- To obtain a more in-depth understanding and a greater level of manual control of the case-specific structure's modal parameters with special regards to its physical parameters, automated and specialized FEMU software will not be utilized in this study.

6 Theoretical Background for Finite Element Model Updating

This chapter presents the basic theoretical framework utilized to perform the sensitivity-based FEMU conducted in this study. Stretching from data acquisition and system identification to the iterative calibration process, the theory put forward in the following sections forms the fundamentals of the study.

6.1 Operational Modal Analysis

Operational modal analysis (OMA) is a modal identification approach embracing experimental testing and modal identification through various system identification techniques. Opposed to experimental modal analysis (EMA), where the excitation source is known, OMA is based on output-only data, and thus it is also referred to as an output-only technique. Relative to EMA, OMA is more suitable for larger structures [19], such as bridges. Originating from the need to control the ambient environment as well as the excitation source, conducting EMA for larger structures can be challenging as the excitation source (typically a shaker) may only excite the structure to a limited vibration level [13]. Thus, even though OMA requires additional measures to extract modal information, it is still preferable for larger structures, such as the railway bridge investigated in this study.

6.2 System Identification

According to Reynders [13], system identification can be defined as "*the field of study where models are fitted to measured data*". System identification is a process of using specialized techniques on experimentally measured data to extract modal parameters. Furthermore, there are a variety of techniques to identify a system. Some can operate on time-dependent data directly, while others operate in the frequency-domain. The most common and widely used methods are Peak Picking (PP), Frequency Domain Decomposition (FDD), Enhanced Frequency Domain Decomposition (EFDD), Natural excitation technique – eigenvalue realization algorithm (NExT-ERA), and Stochastic Subspace Identification (SSI) [20]. In this study, a subspace identification technique is chosen based on the extensive literature review conducted to prepare for this study. The method has proven to be consistent and returned valuable modal data for several researchers [21]–[24].

The Stochastic Subspace Identification method (SSI) is a time-domain system identification technique, meaning that it can operate on the sensor data as a function of time directly [13].

According to Li et al. [25], the SSI method is acknowledged as one of the most advanced structural identification methods driven by output-only data, and it manages to overcome some typical shortcomings associated with the traditional frequency-domain methods, such as PP and FDD, typically related to closely-spaced modes and human error. Furthermore, the SSI method has developed into several sub-methods with different tweaks relative to the original SSI method. One of these sub-methods is the covariance-driven SSI method, SSI-cov.

The SSI-cov method combines the theory of system identification, linear algebra, and statistics [25], and it is, according to Reynders [13], "*a strongly consistent subspace algorithm*". The algorithm takes time-dependent data, such as measured accelerations per time unit, as input. The input matrix is required to be in the format of " $[n \times m]$ ", where n is the number of sensors, and m is the number of data points within the chosen time interval.

The first step performed by the algorithm is forming the "Hankel Matrix", which is a matrix based on the covariances of the sensor data [26]. From then, the Hankel Matrix can form the "Toeplitz Matrix", which can be described as a more compact version of the Hankel Matrix; it contains the same information, but the size of data is reduced. However, constructing the Toeplitz Matrix is optional as its objective is to reduce the computational effort [25]. Either way, the Hankel/Toeplitz Matrix is then decomposed through Single Value Decomposition (SVD) manipulation, and thus the system matrices can be formed. Based on the system matrices, the modal parameters can be extracted by identifying "stable modes" in a stabilization diagram. The very general steps of the SSI-cov method can be seen in Figure 3 and describes the steps from already detrended output data, to the extraction of modal parameters.

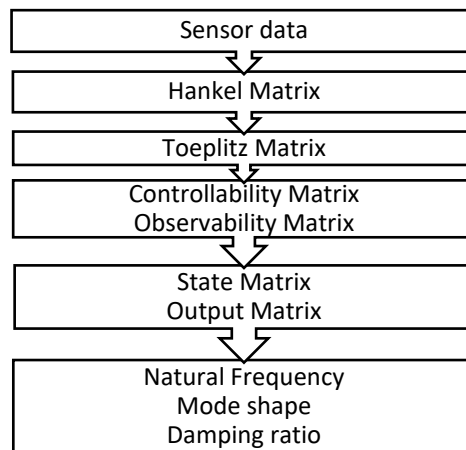


Figure 3. SSI-cov flowchart [25].

Modal parameters, such as natural frequency, mode shape, and damping ratio, are essential in verifying structural design and the safety of structures [13]. Thus, obtaining accurate experimental modal parameters through system identification techniques are essential in order to detect damage, quantify uncertainties and safely preserve the serviceability of a structure. Key to structural engineering, modal parameters describe how the mass and stiffness distributes in the system. Thus, with modal parameters as the comparand, the correlation between analytical models and experimental data can be controlled. Furthermore, in the calibration process, both natural frequency and mode shape are the two typical modal parameters incorporated as target responses in an objective function [27]. In the calibration process, the goal is to minimize the error between FE-computed and the experimental modes concerning the selected target responses. The objective function and modal parameters as target responses are further elaborated in Section 6.4.

6.3 Correlation of Modes

Correlation of modal parameters, such as mode shapes and natural frequencies, which have been extracted from both experimental data from the physical structure and by analytical modal analysis of an FE-model is a crucial step before, during, and after the model updating process. The correlation of modal parameters is to quantify and confirm that there exists some degree of correlation between the FE-model's and physical structure's dynamic responses [28]. There exist several different main types of correlation techniques which over the years have been modified for different applications. However, according to Sehgal and Kumar [28] and Moravej et al. [29], the most commonly used techniques are the Modal

Assurance Criterion (MAC) and natural frequency correspondence. The following sections will describe the general theory behind these two correlation techniques, which are relevant for this study.

As defined by Allemang [30], the Modal Assurance Criterion is defined as *"a scalar constant relating the degree of consistency (linearity) between one modal and another reference modal vector"*. The MAC-function returns a scalar between 0 and 1, which indicates the level of consistency and correlation between the mode shape vectors of two modal comparands. Here, a return value of 0 indicates no correlation, and a value of 1 concludes that the compared mode shapes are identical [30]. The mathematical formulation of the MAC can be seen in Equation 1 [31]. Here, ϕ_j and ϕ_l are the two mode shape comparands.

$$MAC(\phi_j, \phi_l) := \frac{|\phi_j^* \phi_l|^2}{\|\phi_j\|_2^2 \|\phi_l\|_2^2} \quad (1)$$

The MAC can have a variety of different applications depending on the case it is utilized on. In order to positively identify closely-spaced and complex modes, the MAC can be utilized to secure that the mode shape comparands are distinct and do not excessively overlap. This can be done by correlating a set of mode shape vectors to itself, where the ideal case would result in a MAC matrix with a unity diagonal and MAC values close to 0 for the remaining matrix. If the mode shape comparands are not distinct, meaning they overlap, larger MAC values will be present as peaks in the MAC matrix. When correlating a pair of experimental and analytical mode shape vectors, the ideal case is to see a MAC value close to 1 along the diagonal and close to 0 for the remaining matrix. An example of well and poorly correlated mode shape vectors are presented in Figure 4.

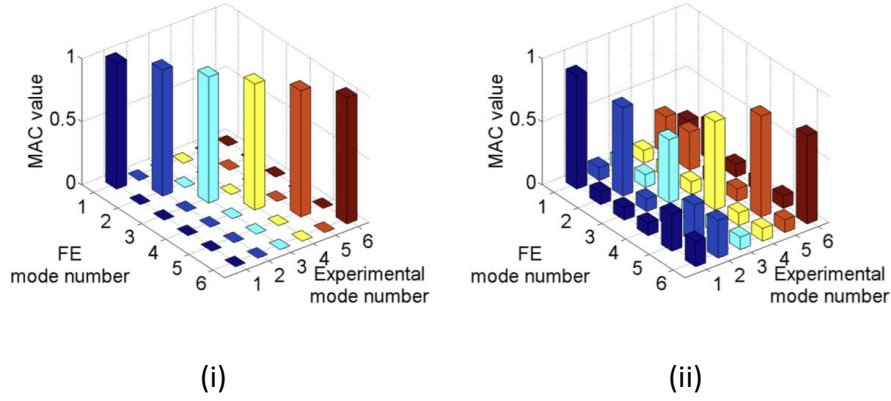


Figure 4. Mode shape correlation using the MAC. (i) good correlation, (ii) poor correlation [28].

The MAC solely assesses the mode shape vector of a mode, thus additional correlation techniques are often required when correlating sets of mode pairs. A very simple yet effective correlation technique is the quantification of the natural frequency correspondence between experimental and FE-computed mode pairs. This correlation technique provides a percentage frequency error between two mode comparands and can be very helpful when identifying mode pairs in addition to using the MAC. The mathematical formulation for the frequency error is presented in Equation 2, where f_{na} is the analytical natural frequency, and f_{ne} is the experimental natural frequency.

$$\text{Natural frequency error} = \left| \frac{f_{na} - f_{ne}}{f_{ne}} \right| \quad (2)$$

By combining the use of both the MAC and natural frequency correspondence, the analyst will have an effective and relatively simple way of correlating modes to ensure a sufficient level of correlation between mode pairs, which is considered to be indispensable when performing any kind of system identification and/or FE-model updating.

6.4 FE-model Updating

A large variety of different techniques for FEMU are commonly utilized in different fields of engineering. In general, these techniques all derive from two main categories, being the direct and iterative methods [29]. The iterative methods are recognized by initial values being assigned for a selected set of updating parameters and based on a sensitivity analysis of the

eigenvalues and eigenvectors of these updating parameters, an iterative model updating process is performed to reduce the difference between the experimental and FE-computed modal parameters [32]. The iterative methods update the selected parameters, which again indirectly update the mass, stiffness, or damping matrices affecting the modal parameters of a structure [20]. On the contrary, the direct methods are recognized by being non-iterative and having the mass, stiffness, or damping matrices directly updated in one single step. These direct methods are more computationally efficient and less time-consuming compared to the iterative methods, and based on equations of motion and orthogonality of modes, they are capable of reproducing the experimental data exactly [28], [29]. The advantage of the iterative methods, which have made these methods favorable and almost exclusively used for civil engineering applications [10], is that they provide the analyst with a larger sense of control of the parameters and updated parameter matrices that are physically meaningful [32]. The direct methods are mathematically sensible, but by updating the system matrices in one single step to reproduce the experimental results exactly, the physical realism of the updated parameters can be lost, and the updated parameter matrices might be hard to interpret physically. Using direct methods can also be very challenging for large and more detailed civil engineering structures defined with large amounts of degrees of freedom, as the mass and stiffness matrices would include many unknown parameters that could lead to ill-conditioned equations [27].

Regardless of the chosen method for FEMU, or if the method is either iterative or direct, the selection of proper updating parameters is crucial for successful FE-model updating. As concluded by Moravej et al. [29], *"Accurate parameter selection is the most pivotal step in FE model updating which still needs to be improved"*. The parameters that should be considered for use in an updating process are those that are perceived to greatly affect the total mass and stiffness properties of the structure, and at the same time, be related to some degree of uncertainty. Such parameters could be different boundary conditions, such as stiffness properties of bearings and possible soil-to-structure interactions or material properties of various structural elements. The amount of uncertainty related to these parameters can differ as the amount and quality of available documentation can significantly vary. Possible undocumented changes of the structure during its lifetime, in addition to a mismatch between the construction drawings and the as-built structure, could also add to this

uncertainty. For complex civil engineering structures, the identification and selection of updating parameters is a non-trivial task that can be both challenging and require experience and engineering judgment [32]. An effective way of aiding the selection of updating parameters is through a sensitivity analysis. A sensitivity analysis is not something unique for FEMU of civil engineering structures, rather, it is a widely used and generally applicable form of analysis where the purpose is to quantify how sensitive, e.g., an assumption, a parameter, or a calculation, is to change. For the case of civil engineering applications, a sensitivity analysis can be performed by individually changing an FE-model's parameters and performing modal analysis between each adjustment. The observed change in modal parameters of the FE-model can thus be used for quantifying the sensitivity related to the different parameters investigated. Proper selection of updating parameters can still be difficult after a sensitivity analysis since some FE-model parameters can be found to greatly affect specific modes while at the same time have a negligible effect on other modes. This all becomes a balancing act where careful consideration and fair engineering judgment are often used to select those parameters used for updating.

As iterative methods of FEMU are the most common methods for civil engineering applications, such methods are consequently chosen for the FEMU process in this study. Thus, direct methods will not be further discussed or utilized. Iterative FEMU can be conducted in several ways that can be adapted according to the desired level of manual control. One way of conducting iterative FEMU with a high level of manual control is to perform it as an optimization problem. By selecting a target response, such as mode shape or natural frequency, one or more updating parameters can be used to maximize the correlation between the experimental and analytical modal parameters. By performing continuous iterations of updating a parameter within a pre-defined range of allowable bounds, followed by modal analysis and correlation controls, one could decide on the optimal case with regards to the selected target response. This method provides the analyst with a high degree of manual control of the FEMU, but could also be more labor-intensive and time-consuming. This method of manual FEMU could also provide the analyst with a significant sense of understanding of the structural behavior. By providing first-hand experience of how the updating parameters affect the modal parameters, better engineering judgment throughout the FEMU process could be applied. A different approach of iterative FEMU is through

methods that implement an objective function, where the objective function's purpose is to minimize the difference between the analytical and experimental structural responses [29]. By solving the objective function with its required inputs, new and updated parameter values will be generated. The general concept behind the more manual optimization method and methods using an objective function is the same. However, where manual generation of updated parameters between iterations is required for the optimization method, the objective function will do this on itself, given the inputs for the FE-model's responses and parameter sensitivities.

The model updating presented in this study is based on the limited, linear Taylor expansion that expresses the changes in target responses as a function of change in parameters. The change in response can be expressed as in Equation 3 [33],

$$\mathbf{R}_e = \mathbf{R}_0 + \mathbf{S}(\mathbf{P}_u - \mathbf{P}_0) \quad (3)$$

where \mathbf{R}_e and \mathbf{R}_0 are the experimental and analytical response, respectively, and \mathbf{P}_0 and \mathbf{P}_u denote the current and updated parameter values, respectively. \mathbf{S} represents the sensitivity matrix, given in Equation 4 [27],

$$\mathbf{S} = \begin{bmatrix} \frac{\partial R_1}{\partial P_1} & \dots & \frac{\partial R_1}{\partial P_n} \\ \vdots & \ddots & \vdots \\ \frac{\partial R_m}{\partial P_1} & \dots & \frac{\partial R_m}{\partial P_n} \end{bmatrix} \quad (4)$$

where n and m are the number of parameters and responses, respectively. The sensitivity-based objective function adopted for this study is a Bayesian objective function as presented in Equation 5 [10],

$$J = \Delta \mathbf{R}^T \mathbf{C}_R \Delta \mathbf{R} + \Delta \mathbf{P}^T \mathbf{C}_P \Delta \mathbf{P} \quad (5)$$

where $\Delta \mathbf{R} = \mathbf{R}_e - \mathbf{R}_0$ is a vector representing the errors in target response, and $\Delta \mathbf{P} = \mathbf{P}_u - \mathbf{P}_0$ represents the vector of change in the updating parameters. \mathbf{C}_R and \mathbf{C}_P are diagonal weighing matrices of coefficients representing the confidence in the target responses and parameters, respectively. A larger confidence in the target response or parameter would be represented

by a larger coefficient. By using the linear relationship presented in Equation 3, the updated parameter values are calculated following Equation 6 [10],

$$\mathbf{P}_u = \mathbf{P}_0 + \mathbf{G}(\mathbf{R}_e - \mathbf{R}_0) \quad (6)$$

where the \mathbf{G} matrix, for a case with $n = m$, is given as in Equation 7 [10]. For the first iteration, \mathbf{P}_0 can be taken as the average between the upper- and lower bounds, b_u and b_l , for each parameter, respectively.

$$\mathbf{G} = \mathbf{C}_P^{-1} \mathbf{S}^T (\mathbf{C}_R^{-1} + \mathbf{S} \mathbf{C}_P^{-1} \mathbf{S}^T)^{-1} \quad (7)$$

The flowchart in Figure 5 presents the sensitivity-based, iterative FEMU process where iterations are completed until the acceptable level of correlation between the experimental and analytical FE-computed modal parameters is achieved.

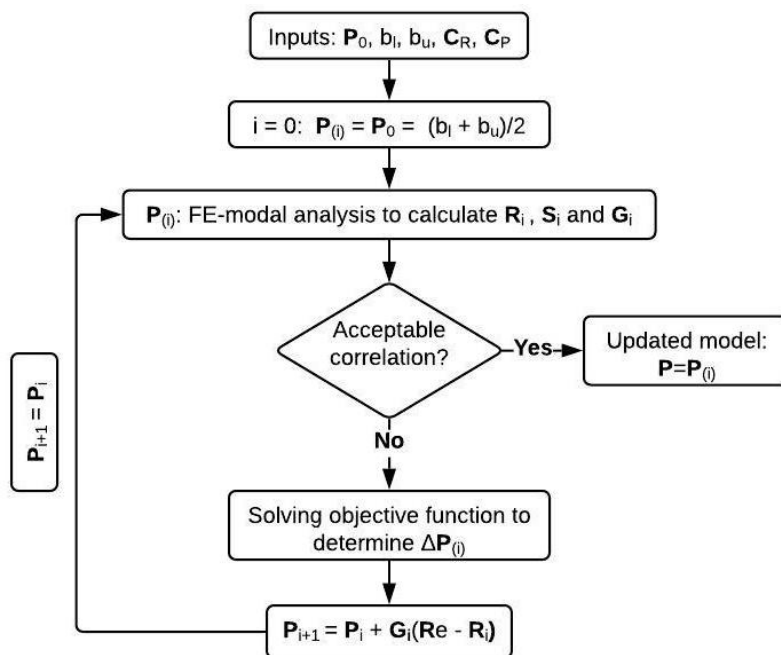


Figure 5. Sensitivity-based, iterative FEMU process flowchart.

7 The Stange Railway Overpass

This chapter will introduce the railway overpass selected for the case study in this thesis and the NEAR project, in addition to reasoning for selecting this specific overpass. Special consideration is also made to the development of an initial FE-model based on documentation with all modeling parameters initially included.

7.1 Background and Issue

The railway overpass under investigation in this thesis, the "Stange railway overpass", is a 48.6 m long, 3-span, in-situ cast, post-tensioned concrete overpass located in Stange near the city of Hamar, Norway. The overpass is located on the Dovrebanen railway line, where it crosses the Fv222 road, 2 - 300 m north of Stange railway station. The overpass consists of two identical but mirrored and completely separated bridge structures. Each bridge carries a single railway track where trains can pass in both directions. Of the two bridges making up the overpass, the bridge under investigation in this study is the most western located bridge, as seen outlined in Figure 6. A side elevation of the bridge in question is shown in Figure 7. The bridge located towards the east was exempted from further assessments as it was observed little-to-no train crossings in and around the time period of monitoring. The reason why the eastern bridge was hardly in use could not be confirmed at the time.



Figure 6. Aerial photo of Stange railway overpass [34].



Figure 7. Stange railway overpass side elevation [35].

The continuous deck of the bridge is supported on two elastomeric bearings at both ends of the bridge, which are anchored to concrete abutments. The bridge deck is additionally supported on two circular concrete columns with circular column-caps. According to available documentation, both the abutments and column foundations are founded directly on bedrock. In the "through" of the U-shaped bridge deck, a 0.6 m thick ballast layer of crushed rock is supporting concrete sills and a continuous and centric steel railway track. A general layout of the bridge can be seen in Figure 8 for a side elevation, and Figure 9 for a bridge deck/column cross-section and abutment plan view. A 3D-view is presented in Figure 10.

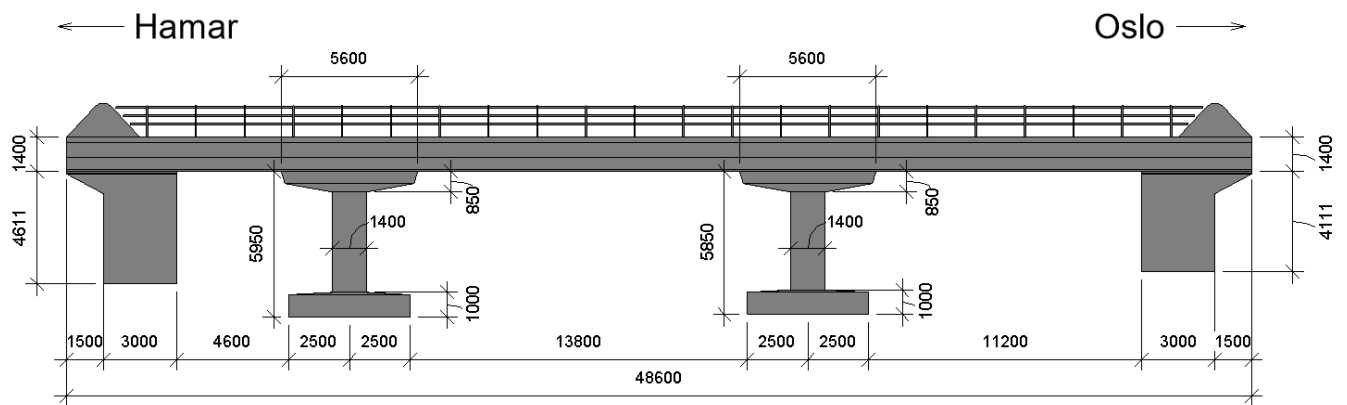


Figure 8. General layout of Stange railway bridge (side elevation view).

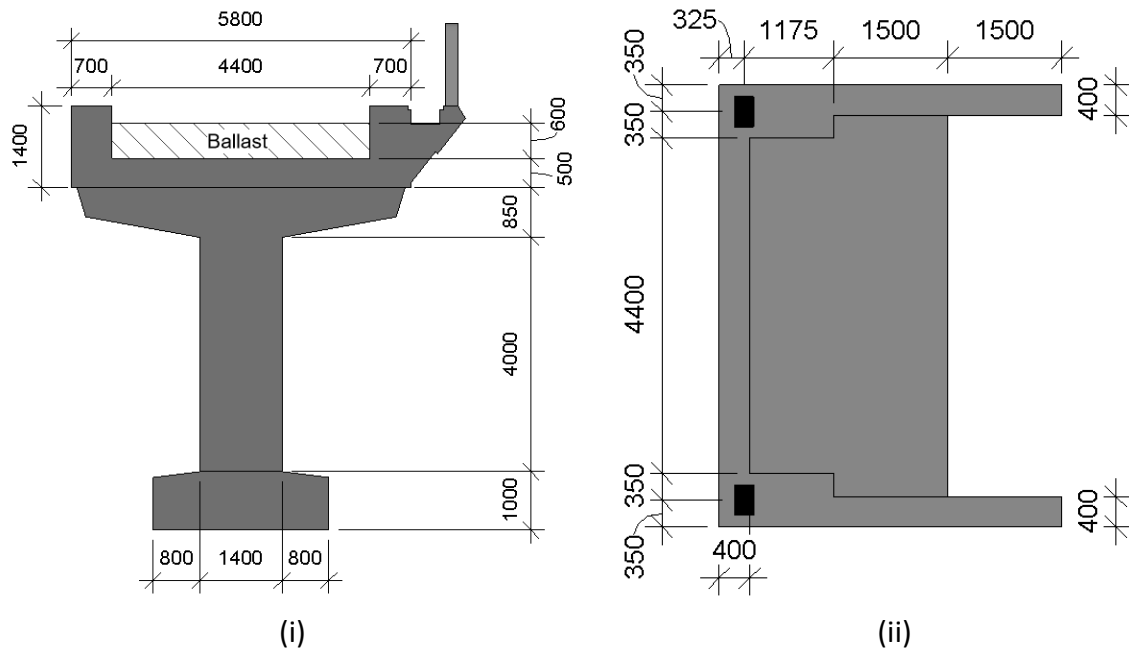


Figure 9. General layout of Stange railway bridge, (i) bridge deck and column cross-section, (ii) abutment plan view.

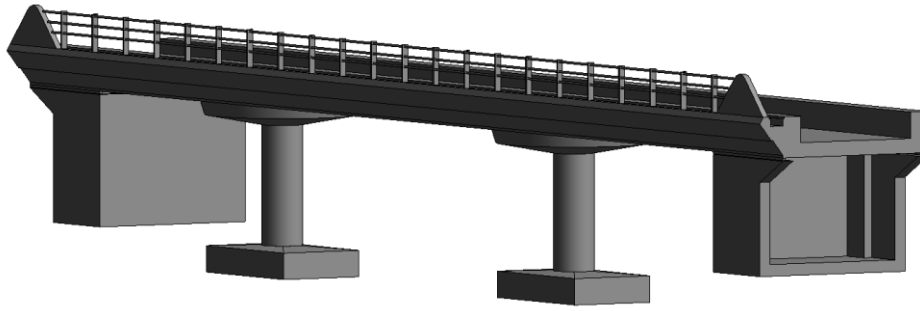


Figure 10. Stange railway bridge 3D-view.

The gathered documentation and construction drawings of the Stange railway overpass consist of a series of CAD drawings and structural hand computations dating from 1999. The CAD drawings are titled in a way that indicates that the overpass at some point between 1999 and 2004 underwent some structural modifications, but precisely what was done and why is not well documented. The bridge department in Bane NOR has not been able at this point to locate any earlier documentation of the bridge such that comparisons could be made. Therefore, the assumption is that the two bridges making up the overpass were originally designed and constructed during the '90s and were later modified for an unknown reason. One assumption supported by Bane NOR is that the original bridges did not extend beyond the location of the elastomeric bearings at the abutments. This design choice on the bridges differentiates the bridges from more common and similar beam-type bridges of this scale. According to the available construction drawings, this uncommon design choice leads to the 4.175 m deck extensions at each end of the bridge beyond the location of the bearings being free-floating cantilevers. According to drawings, there is a 111 mm gap between the bottom of the bridge deck and the top of the abutments, where a 90 mm non-structural concrete "skirt" comes down from the bottom of the bridge deck along the outside perimeter of the abutment. This leaves a 21 mm open gap between the bottom of the "skirt" and the top of the abutment, as shown in the abutment details in Figure 11 and Figure 12. There is no additional documentation regarding if these cantilevers are further supported by backfill or any possible soil-interaction. Terrain levels from documentation only indicate that the abutments are partly covered by backfill towards the top. The lack of early documentation has posed a challenge but has not limited the execution of this study as the as-built situation of the structure is what will be assessed. On the contrary, the lack of documentation has

further promoted the need for structural assessment and system identification of the overpass.

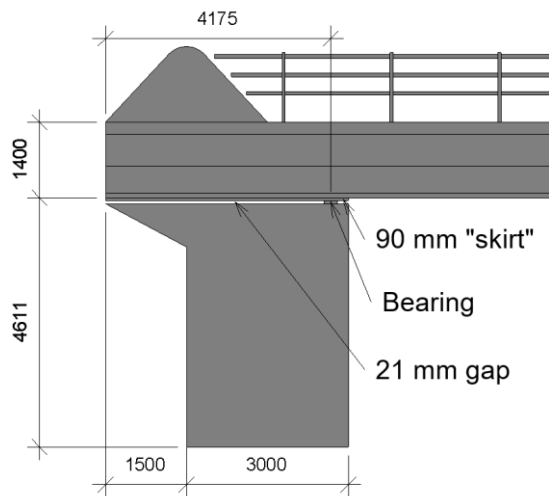


Figure 11. Abutment detail elevation view.

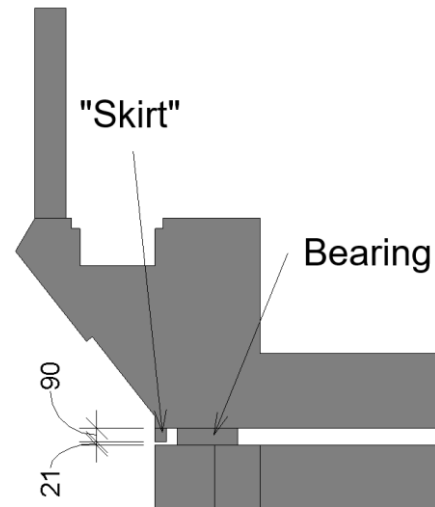


Figure 12. Abutment detail cross-section.

The Stange railway overpass is chosen as a case study for this thesis and the NEAR project due to this overpass being a part of the Dovrebanen railway line, which is currently being evaluated for increased traveling speeds exceeding 200 km/h. Prior to the initiation of the NEAR project, Bane NOR requested a structural assessment of the overpass to verify it for an HSLM-A train load from consulting civil engineering company's Rambøll and Sweco [36]. The structural assessment and HSLM-A verification by Rambøll and Sweco was performed by assessment of an FE-model based on the available construction drawings and documentation. Results of this FE-model assessment concluded with a maximum acceleration in the bridge deck of 35 m/s^2 ($\approx 3.6 \text{ g}$), located in the cantilevering deck extensions at a speed of approx. 150 km/h. A minimum acceleration of approx. 7.5 m/s^2 ($\approx 0.76 \text{ g}$) was recorded at the same location at a train speed of about 50 km/h. To put these recorded accelerations in perspective, according to standard NS-EN 1990 [37] section A2.4.4.2.1 (4), the maximum acceleration allowed for a railway bridge deck is 3.5 m/s^2 ($\approx 0.37 \text{ g}$), and a space shuttle during flight experiences a maximum acceleration of about 3 g ($\approx 29.4 \text{ m/s}^2$) [38]. As the resulting maximum and minimum accelerations from FE analysis are so large, these results are considered unrealistic and not an accurate representation of the actual dynamic behavior of the bridge. The analytical accelerations estimated by the documentation-based FE-model are

so significant that they most definitively would be felt by operators of the trains and passengers, but no complaints regarding this issue have been recorded. Furthermore, presented in the same report, calculations according to Eurocode 2 indicate that the calculated shear force in the bridge deck is about two times higher than the calculated capacity of the deck. However, calculating shear capacity is a common, non-trivial issue and is highly dependent on the design code, whereas the Eurocode 2 has been concluded to be very conservative in its estimations [39]. Thus, as visual inspections of the bridge have not concluded with any visual signs of shear damage or other degradation and the capacity is marginally satisfied according to NS 3473 [36], it is not further assessed in this study. The FE analysis results regarding accelerations have increased and somewhat confirmed the suspicion of these results not being realistic and a true representation of the structure. Thus, the need for a calibrated FE-model that can realistically represent the structure is expressed, becoming the basis for this thesis and the NEAR project.

7.2 Initial FE-model

To assess the structural behavior of the Stange railway bridge, it was decided to develop an FE-model based on the available documentation that can, later on, be compared to the experimental results. In the preparations for this study, a thorough investigation of modelling software was conducted. It was concluded that 75 % of the 42 studies investigated utilized SAP2000 [40] or Ansys [41] for FE-modelling. For the case of the Stange railway bridge, CSiBridge [42] was found to be a suitable, easy-to-use FE-modelling software. The software originates from the same developer as SAP2000, and thus it has the same interface and many of the same attributes. However, whereas SAP2000 is a software for structural analysis and design in general, CSiBridge is specialized to analyze and design both simple and complex bridge structures.

Before the modelling could commence, the FE-model's level of detail and complexity had to be assessed. Expressed in a study conducted by Brownjohn et al. [43], a model can be simplified to a certain extent. To make it applicable for modal updating, it needs a level of detail where parameters that affect the structural behavior are incorporated. Thus, even though a simplified model can produce valuable results, Brownjohn et al. express the issue of "over simplifying" FE-models that later on cannot be calibrated as they do not have the required level of detail. On the other hand, according to Daniell and MacDonald [44],

calibrating highly detailed FE-models containing a high quantity of parameters that practically do not affect the structural behavior can lead to an unnecessary amount of computational effort and possible ill-conditioning during calibration. Thus, for the case of the Stange railway bridge, it was decided to develop a simplified model, but ensured to include parameters that assumingly have a significant effect on the structural behavior. Subsequently, material properties, geometrical properties, boundary conditions, and bearings were set as the "main" parameters to include in the FE-model. Firstly, the material properties specified are presented.

For defining materials, CSiBridge allows the analyst to select a standard to compute material properties. Thus, for the Stange railway bridge, by selecting Europe EN 1992-1-1 [45] per EN 206-1 [46] and specifying the concrete quality B45 according to the bridge documentation, Table 4 expresses the concrete properties of interest defined in the model.

Table 4. Concrete material properties specified in CSiBridge.

Parameters	Values
Young's modulus of concrete bridge deck, girders and columns	36.0 GPa
Mass density of concrete bridge deck, girders and columns	2 548.5 kg/m ³

Subsequent to specifying concrete properties, both cross-sectional and global geometrical details were assessed. As seen in Figure 9, the cross-section is more or less symmetrical, and thus the center of gravity does not have any eccentricity of significance to cause excessive torsional movement. Furthermore, that is also why a beam-model, that cannot identify torsional modes, was found to be sufficient for modelling the bridge.

According to the documentation, the bridge deck has a 2-way cast water runoff ensuring that moisture does not excessively accumulate. Subsequently, the bridge deck is somewhat thinner at the location of the drainage pipes. However, the minor transverse- and longitudinal deck variation is assumed to not affect the structural behavior to a great extent, and thus it is not included in the FE-model. That is also the case for non-structural elements in general, such as sleepers, railings, and drainage pipes. The parameters are not incorporated as they are assumed not to affect the structural behavior significantly.

After assessing the geometry of the deck and girders, the resulting cross-section modelled in CSiBridge can be seen in Figure 13. The cross-section is symmetrical, has a deck thickness of

500 mm and a girder height of 1 400 mm. Note that for a model constructed for modal analysis, the mass and stiffness of the system are the parameters of interest. Thus, modelling reinforcement is not deemed necessary, as the mass density presented in Table 4 assumes that the cross-section is reinforced. Furthermore, even though the ballast is present in the figure, it is not included in the cross-section. Rather, it is modelled as a contributing mass source in the gravitational direction with a mass density of $1\,800\text{ kg/m}^3$ [47]. Subsequently, with an assumed continuous volume along the bridge, the equivalent load of the ballast corresponds to 47 kN per longitudinal meter.

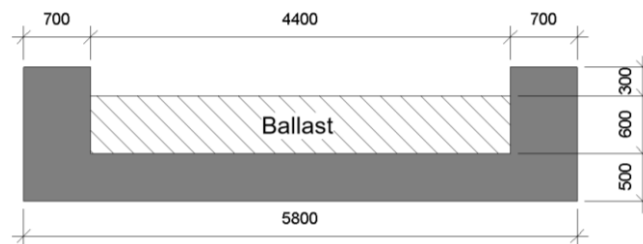


Figure 13. Modelled cross-section with ballast.

Even though the cross-section presented in Figure 13 makes up a significant share of the bridge span, the caps on top of the columns lead to some measures in the model. As seen in Figure 8, there are "column caps" or "pier caps" located in the connection between the columns and the bridge deck to avoid the phenomena of punching shear. These pier caps are assumed to have a significant effect on the global mass and stiffness. Thus, they are included by increasing the deck's thickness equivalent to the thickness of the pier caps for $2 \times 5.6\text{ m}$ of the bridge. The equivalent cross-section can be seen in Figure 14.

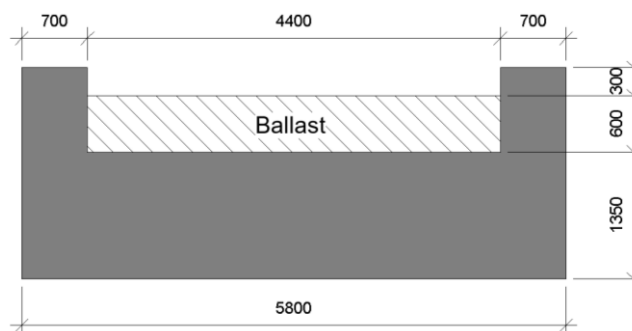


Figure 14. Cross-section including pier caps.

Subsequent to defining materials and setting the geometrical details, the boundary conditions are of great interest for identifying structural behavior. Presented in Section 7.1, the documentation indicates two versatile elastomeric bearings on top of each abutment and a rigid connection between the bridge deck and the columns. However, as the FE-model is a

beam-model, everything is modelled along the centerline. Thus, in the FE-model, the two bearings at each end are merged into one unit. The versatile elastomeric bearings are of type ELASTO-BLOKK NBv, manufactured by KB Spenneteknikk AS [48], which are cast into both the girders on top and the abutment below, with anchoring claws. An illustration of the bearings utilized at the Stange railway overpass can be seen in Figure 15 (i). Figure 15 (ii) shows how the westernmost bearing, located on top of the abutment closest to Oslo, appeared during visual inspection. Even though the bearings are versatile and thus are able to move in both the transverse and longitudinal direction (22 mm), it is mainly the vertical direction that are of interest for an initial FE-model. For the given 300 x 400 x 81 mm bearings utilized, the bearing has a Young's modulus, E , equal to 550 MPa [48]. In the FE-model, the vertical elastomeric properties were found to be an essential modeling parameter. Thus, it was decided to add springs representing the total stiffness of the bearings at each end.

According to Cook et al. [49], the spring stiffness can be expressed by the formula given in Equation 8, where E is the Young's modulus, A is the surface area of the connecting surface (300 x 400 mm), and L is, in this case, the height of the bearing, including both anchoring plates and rubber layers (81 mm). As the bearings are merged in the FE-model, the resulting spring stiffness, k , was set equal to 1.63×10^6 kN/m at each end of the bridge. The transverse- and longitudinal direction was, as a simplification, set as pinned and thus unable to move.



Figure 15. (i) Bearing ELASTO-BLOKK NBv [48]. (ii) Visual inspection of the bearing.

$$k = \frac{EA}{L} \quad (8)$$

The circular columns supporting the bridge deck are, according to the documentation, around the same length but not identical. As seen in Figure 8, the column supporting the span stretching towards Oslo is 100 mm shorter than the other. However, for FE-modelling purposes, the columns are assumed to have an equal height of 4.85 m, which essentially is the distance between the bottom of the bridge deck and the top of the foundation supporting the columns. Furthermore, as it is stated in the documentation that the columns are founded directly on bedrock, the boundary at the bottom of the columns is modelled as fixed. The diameter of the columns was both set to 1.4 m, according to the documentation.

To sum up the parameters incorporated in the initial FE-model formed to represent the structural behavior according to the documentation, Table 5 presents the details regarding material properties and boundaries especially. Note that geometrical properties are not included as the cross-sections are already thoroughly defined, and other global dimensions and distances are the same as in the documentation, see Figure 8.

Table 5. Modelling parameters.

Parameter	Value	Category
Compressive strength of concrete bridge deck, girders and columns, f_{ck} [MPa]	45.0	Material
Young's modulus of concrete bridge deck, girders and columns, E_c [GPa]	36.0	Material
Mass density of concrete bridge deck, girders and columns, m_c [kg/m ³]	2 548.5	Material
Poisson's ratio of concrete bridge deck, girders and columns, ν_c [-]	0.2	Material
Shear modulus of concrete bridge deck, girder and columns, G_c [GPa]	15.0	Material
Mass density of ballast, m_b [kg/m ³]	1 800.0	Material
Elastomeric bearing stiffness Hamar, k_{bH} [kN/m]		
x-direction	Pinned	Boundary
y-direction	Pinned	Boundary
z-direction	$1.63 * 10^6$	Boundary
Elastomeric bearing stiffness Oslo, k_{bO} [kN/m]		
x-direction	Pinned	Boundary
y-direction	Pinned	Boundary
z-direction	$1.63 * 10^6$	Boundary
Column foundations, k_{cf} [kN/m]	Fixed	Boundary

Even though the model is a simplification of the bridge itself, the resulting initial FE-model is perceived to be a valid representation of the bridge according to the available documentation

and thus gives a clear picture of how the bridge behaves. Subsequently, the initial FE-model was assessed, and the modal parameters were found to be reasonable for a bridge with cantilevering ends. The complete modal analysis of the initial FE-model is presented in detail in Chapter 9 after the experimental modal parameters are identified, thus the results are more comparable. An extruded 3D-view of the initial FE-model constructed in CSiBridge can be seen in Figure 16, with a supplementing 2D-view in Figure 17 to better visualize the elastomeric bearings. Both figures are oriented such that the longer span, located towards Oslo, is on the righthand side.

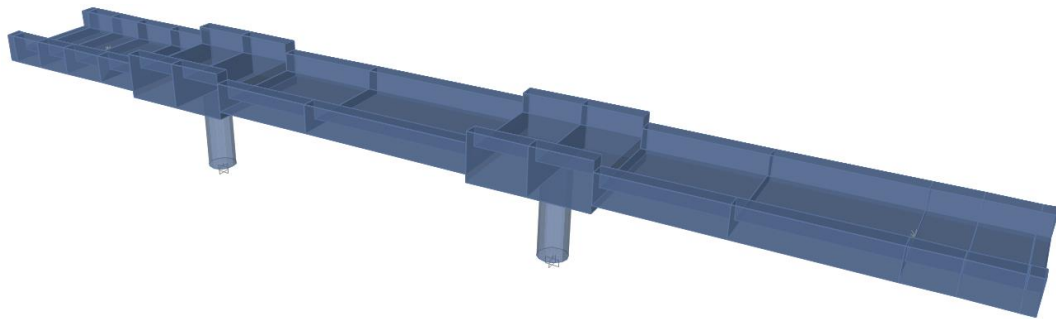


Figure 16. Extruded view of FE-model in CSiBridge.

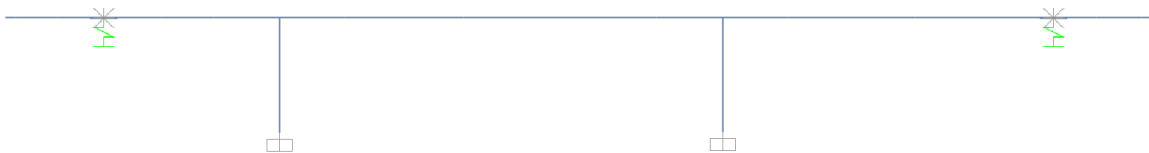


Figure 17. 2D-view with springs representing elastomeric bearings.

8 Modal Identification of the Physical Structure

This chapter regards the topics surrounding the complete process of collecting and analyzing operational condition acceleration data from the Stange railway bridge. The sensor hardware is presented along with a description of both installation of hardware and the different sensor configurations used. The process of system identification through the Covariance-driven Stochastic Subspace Identification (SSI-cov) method is discussed and the resulting modal parameters identified are presented.

8.1 Sensor Hardware

In this section, the sensor hardware available for the project will be presented along with project-specific limitations regarding the functionality and availability of the sensor hardware.

The continuous structural health monitoring (SHM) system available and implemented for this project consists of an accelerograph system supplied by Unquake [50]. The accelerometers in this system are produced by Analog Devices [51] and are 20 bit low noise, low drift, low power, 3-axis MEMS accelerometers with sampling rates ranging from 3.906 – 500 Hz. For most cases, a sampling rate of 250 Hz is recommended from the supplier, thus it will be possible to detect natural frequencies up until about 125 Hz. For the case of the Stange railway bridge, this sampling rate would be sufficient considering the natural frequency range which is typically observed in such structures. The sensors are individually coupled to dedicated dataloggers separate from the accelerometer housings to reduce noise and for ease of installation. The Unquake sensor and datalogger hardware setup are shown in Figure 18.



Figure 18. Unquake sensor and datalogger setup [52].

The Unquake datalogger and sensor hardware can be set up to be completely self-contained with its own power supply in the form of a 5V USB-powerbank and with an internal GPS – GNSS receiver for time-stamp and instrument synchronization. This feature ensures ease of installation and facilitates use on a wide range of different structures subjected to monitoring.

As informed by the supplier, the 3-axis (X, Y, Z) accelerometers vary in sensitivity and electronic noise level between the different axes, where the Z-axis has the lowest sensitivity and highest level of electronic noise. As a consequence, it is recommended that the Z-axis should be used as a complementary axis in three-dimensional measurements and not used as the main axis in two-dimensional measurements. The X- and Y-axis are described as being the most sensitive and least affected by electronic noise and should thus be used as the main axis for measurements.

The Department of Civil Engineering and Energy Technology at Oslo Metropolitan University has a total of seven of these self-contained sensor/datalogger systems. However, due to hardware malfunction, only five sensor/datalogger systems were available at the time required for this project.

8.2 Hardware Installation

Correct installation of hardware is a fundamental parameter for securing sufficient quality of the measured results. From the sensor/datalogger system supplier, it is recommended to mount thin steel plates to the structure using a high-strength, fast-setting adhesive and then securing the sensors to these steel plates using high-powered magnets. Careful consideration must be made to the sensor orientation such that the axes of the sensors are aligned with the axis of greatest interest in the structure, and at the same time avoiding the use of the local Z-axis of the sensor as this axis is least sensitive and prone to electronic noise.

The sensor installation on the Stange railway bridge was planned according to supplier recommendations, but due to the weather situation at the time of installation, securing the steel plates to the concrete structure using adhesives was not feasible. A recent snowfall combined with sub-zero temperatures had resulted in a thin layer of frost and ice on the exposed concrete surfaces, reducing the adhesive properties of the glue and not providing a positive bond between the concrete surface and steel plates. To secure a positive bond between the concrete structure and steel plates, in addition to the adhesive, a concrete drill was used to mount expansive concrete bolts. This solution secured a positive and permanent bond such that the sensors could be mounted to the steel plates using high-powered magnets. Figure 19 shows an example of the accelerometer and datalogger installation. For increased weather protection, the datalogger and power supply were placed inside a plastic

container. The magnetic GPS unit was also placed close to the accelerometer on the steel plate.



Figure 19. Accelerometer and datalogger installation.

As the vertical accelerations and deformations were of greatest interest, the local X-axis of the accelerometer was aligned to the vertical direction of the bridge structure. The local Y-axis of the accelerometer was aligned to the longitudinal direction, and the supplementary local Z-axis was aligned to the transverse direction. To secure proper installation of the accelerometers, a level was used to correctly orient the accelerometer housing in all directions. The sensors were all mounted on the exposed inside vertical concrete surface towards the top of the girders, above the ballast layer. This location was considered to be adequate given the dynamic behavior expected from the bridge due to the symmetric loading from the trains. Other locations were assessed, such as the underside of the bridge deck and top side of girders, but these locations were unfavorable due to practical feasibility and hardware limitations.

8.3 Sensor Configuration

Having introduced the sensor hardware available for monitoring the bridge along with hardware installation, this section presents the chosen sensor configurations perceived to generate the best data for system identification with regards to the sensor hardware and resources available.

To identify structural behavior, sensor location is vital. Thus, understanding what is desirable to achieve by locating a sensor in a specific spot is essential. The overall goal of monitoring the structure is to understand how the structure naturally behaves when excited by an arbitrary loading. This can be achieved by extracting and identifying the structure's mode shapes with the associated natural frequencies and damping ratios. However, if the sensors are not located strategically, a good visual representation of the mode shapes might not be feasible to obtain. One way to solve the issue of locating these sensors is to use an optimization algorithm, as performed by Bursi et al. [23].

To optimize the sensor configuration, a reasonable FE-model is needed. For the Stange railway overpass, utilizing an initial FE-model based on the bridge documentation to optimize the sensor configuration can be problematic. Previously, for this bridge, such FE-models have returned unrealistic results, and thus optimizing the sensor configuration based on these can lead to consequential errors in terms of extracting true modal parameters. Thus, even though optimizing the sensor configuration as a consequence of having a limited number of sensors seems like a reasonable solution, the bridge documentation raises doubts. Subsequently, instead of optimizing, it was decided to use engineering judgment to catch the structural behavior by using basic dynamics and structural understanding.

First and foremost, the critical and uncertain points of the structure need to be identified. Clearly, the spans stretching beyond the location of the bearings are of great interest, thus, one sensor at each end (1 and 5 from Figure 20) was deemed necessary to install. Furthermore, with around 48 hours available to monitor the bridge, it was decided to use two different sensor configurations, with two different targets. The first configuration's objective was to identify the global structural behavior and thus form a holistic understanding of the structure. The first configuration can be seen in Figure 20. In this configuration, the three remaining sensors (2, 3, and 4) are located in the middle of each span, as this is where the largest deformations are assumed to occur. Note that sensors 2 and 4 are mounted on the opposite beam of the remaining sensors. This was done in case torsional modes were to be of interest later on. However, due to more or less symmetric loading and cross-sectional stiffness properties, this sensor configuration is first and foremost intended to detect vertical modes.

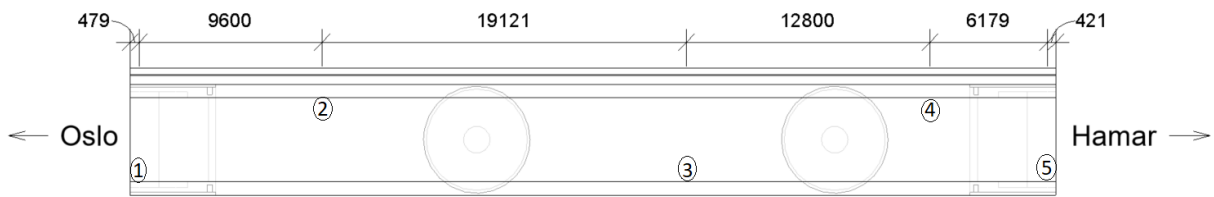


Figure 20. Sensor configuration nr. 1. [mm]

Furthermore, to both confirm global structural behavior as well as identify local structural behavior, the second configuration's primary objective was to assess the behavior of the assumed cantilevering deck extensions at each end of the bridge. The second sensor configuration has three common sensor locations relative to the first configuration; sensors 1, 3, and 5 remain in the same exact position. However, due to the uncertainty regarding the behavior beyond the location of the bearings, sensors 2 and 4 are now moved to the center of each abutment. In that way, a better representation of mode shapes in these areas can be identified, and the possible soil-superstructure interaction can be quantified. The second sensor configuration can be seen in Figure 21.

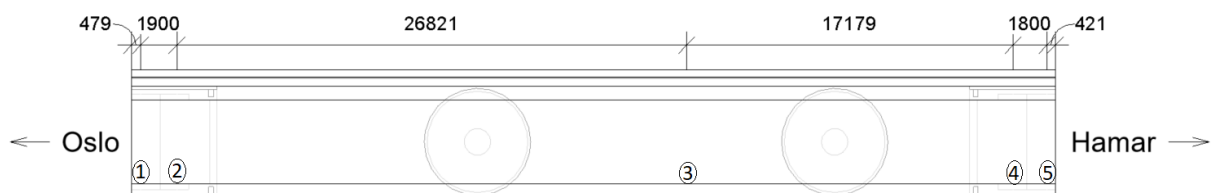


Figure 21. Sensor configuration nr. 2. [mm]

The presented illustrations are the two configurations utilized in the 48 hours available for instrumentation. Furthermore, the locations are based on the physical measurements collected during the installation of the sensors at site, thus sensor 3 has a minor eccentricity relative to the center of the mid-span. For more details regarding the process of the hardware installation and data collection itself, see the data collection report in Appendix B.

8.4 Data Processing

This section presents and discusses the processes undertaken to organize and pre-process the collected operational condition data from the Stange railway bridge, along with a more in-depth investigation of the acceleration data collected and identification of key input variables for use in system identification.

8.4.1 Organizing and Pre-processing of Acceleration Data

Before initializing data analysis and modal parameter identification, an important step is organizing and pre-processing the operational condition acceleration data collected from the structure. Depending on the number of sensors used and monitoring duration, the amount of data collected can vary significantly, but organizing this data properly will greatly benefit future work efficiency. Combinedly from sensor configuration 1 and 2, after about 48 hours of monitoring, approx. 10 GB of acceleration raw-data was collected from the Stange railway bridge. This data was recorded by the datalogger as .txt files and organized based on the recorded GPS time-stamps. The first step undertaken to organize the raw-data was to sort the data based on sensor location, sensor configuration, and time intervals recorded for each .txt file.

As the Stange railway bridge is located on an active railway line, Bane NOR provides a publicly available train schedule showing all planned trains operating on this specific railway line and at which times these trains are scheduled to pass each station. The relevant train schedule for the specific stretch that includes the Stange railway bridge is the “Blad Nr. 10, Eidsvoll – Dombås” [53], which is valid from Sunday 13.12.2020 until Saturday 11.12.2021. Following this schedule, a total of 122 trains were scheduled to cross the Stange railway bridge during the time of monitoring. Note that these are planned crossings and can deviate from the actual crossings due to this schedule not being live-updated. The schedule also includes basic information about the trains crossing in the form of a coded distinction on each of the trains operating on the line. This code is in a format of X(Y), where “X” is a two-to-five digit number, and “Y” is a one-to-three digit number.

Information from schedule train code:

- XX: Express passenger train not stopping at all stations.
- XXX: Local passenger train stopping at all stations.
- XXXX and XXXXX: Cargo train only stopping at certain stations.
- Y, YY, and YYY: No information regarding the specific train can be read from the “Y” index.
- If the last digit of the “X” index is an even number (2, 4, 6, 8), the train is traveling in the direction Hamar → Oslo.
- If the last digit of the “X” index is an odd number (1, 3, 7, 9), the train is traveling in the direction Oslo → Hamar.

Schedule train code examples:

- 41(2): Express passenger train traveling in direction Oslo to Hamar.
- 322(24): Local passenger train traveling in direction Hamar to Oslo.
- 5734(83): Cargo train traveling in direction Hamar to Oslo.

To begin investigating and perform a simple analysis of the collected data, a MATLAB [54] code detrending and plotting the time-history acceleration data was developed. Firstly, this code was solely used for identifying and localizing the train crossings amongst the acceleration raw-data. Based on the time for train crossings stated in the schedule, an individual search was performed with the MATLAB code for each of the crossings. Of the 122 scheduled train-crossings supposed to cross the Stange railway bridge during the monitoring, a total of 98 individual train crossings were identified and recorded. Of these train crossings, 48 were during sensor configuration 1 and 50 during sensor configuration 2. The remaining 24 scheduled crossings not identified are assumed to be either canceled or re-scheduled to a different time.

The quality of recorded acceleration data can vary significantly due to errors with hardware, hardware installation, software, and electronic noise in the sensors. Thus, being able to confirm some level of quality of the collected data is an important factor. The time-stamp data was deemed correct as the majority of train crossings were found either precisely at scheduled times or within few minutes of the scheduled time. As the self-contained datalogger/sensor hardware all had individual GPS units, a possible error could be if the individual GPS units recorded time-stamps out of synchronization in relation to each other. This possible error was rejected by assessment of the time-history acceleration data where it was possible to observe that the first recorded acceleration data of a train crossing was at one end of the bridge, while the last recorded acceleration data would be recorded at the

opposite end of the bridge. By comparing the scheduled direction of a train crossing to what could be detected in the acceleration data, the time-stamp relation between different GPS units could be confirmed and therefore considered to be correct.

From the recorded time-history acceleration data, it was also possible to observe apparent differences between the different train types operating on the line. Prior to investigating acceleration data, expectations of what the time-history acceleration plots would/should look like for the different train types were discussed. As the Stange railway bridge is located 200 - 300 m north of Stange railway station, it was a clear expectation to see a difference between trains stopping or not. Trains due to stop at Stange station would have lower traveling speed, thus having a longer duration of the time-history plot as it is crossing the bridge. It was also expected that the cargo trains would generate larger accelerations due to heavier axle-loads compared to the passenger trains. Using the developed MATLAB code, it was possible to extract time-history acceleration plots for all 98 identified bridge crossings, and it was possible to clearly differentiate the different train types from these. Prior expectations of what the time-history acceleration plots would/should look like proved to be correct and further confirmed that the quality of the collected acceleration data was good. Figure 22, Figure 23, and Figure 24 show typical examples of the time-history acceleration plots observed for the different train types. It can be seen that the cargo train generates the largest accelerations and has the longest crossing duration.

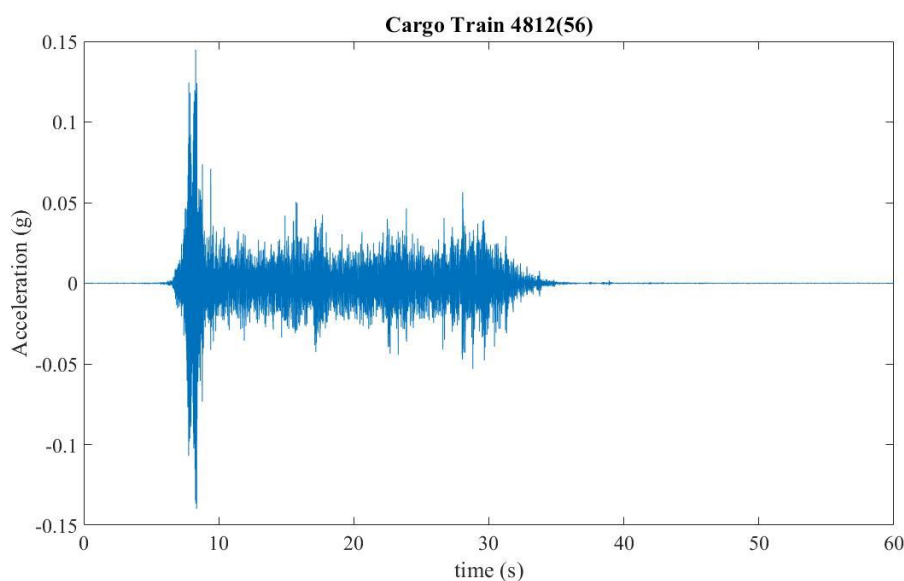


Figure 22. Typical cargo train time-history acceleration plot.

When comparing express- and local trains, it can be seen that the express train has a shorter duration and results in larger accelerations in the bridge deck, which is according to the prior expectations regarding how the time-history acceleration plots would/should look like. Utilizing this information combined with information of the trains from the schedule, it was possible to distinguish all 98 recorded train crossings. Of the recorded 98 crossings, there were 18 cargo trains, 11 express trains, and 69 local trains.

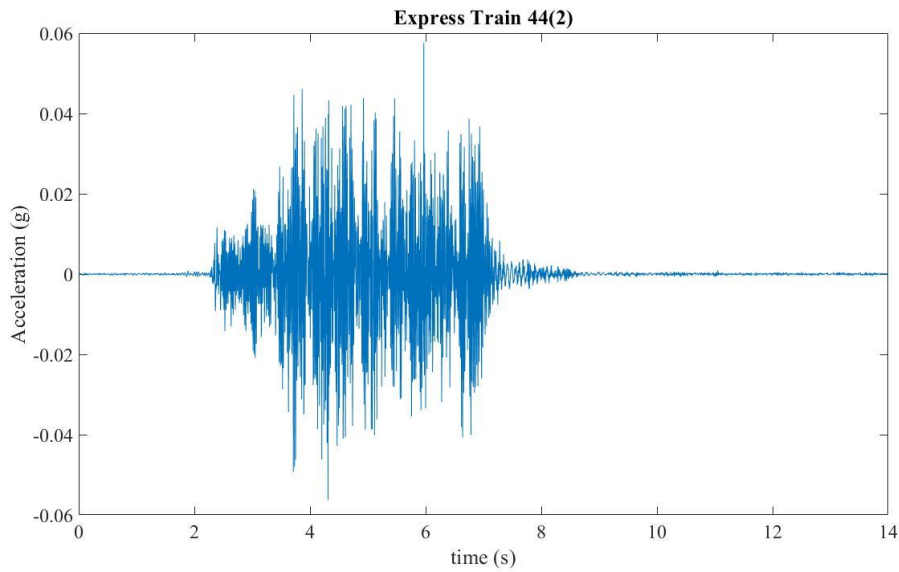


Figure 23. Typical express train time-history acceleration plot.

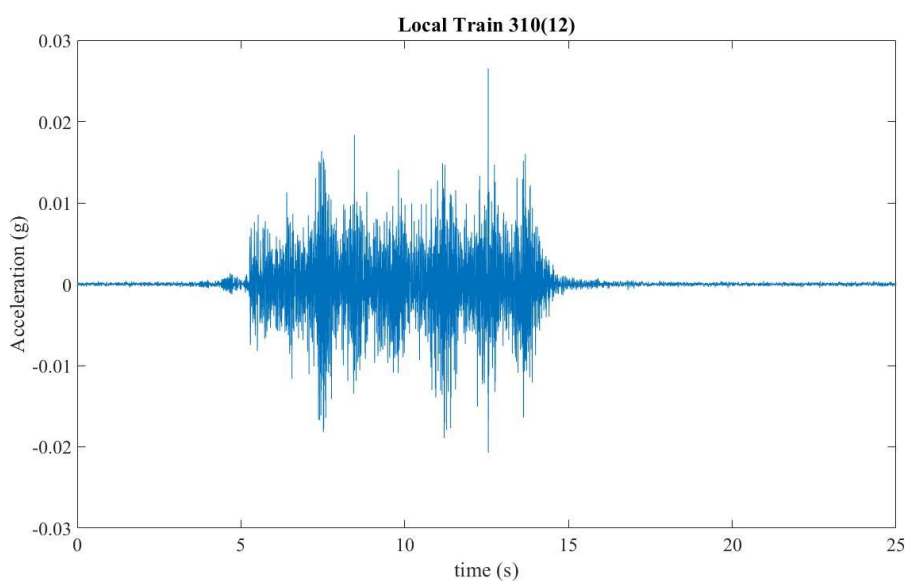


Figure 24. Typical local train time-history acceleration plot.

8.4.2 Time-history Acceleration Data

Recorded time-history acceleration data are the basis for future system identification of natural frequencies, damping ratios, and mode shapes using methods such as described in Section 6.2. This acceleration data can also provide important data of the structure on itself.

For the case of the Stange railway bridge, the preliminary acceleration estimations obtained by Rambøll and Sweco [36] through FEM analysis of a bridge model based on available construction drawings are assumed to be highly unrealistic. According to the Rambøll and Sweco report, the maximum acceleration observed in the bridge deck is 35 m/s^2 ($\approx 3.57 \text{ g}$). However, according to NS-EN 1990 [37] section A2.4.4.2.1 (4), the maximum acceleration allowed for a railway bridge deck is 3.5 m/s^2 ($\approx 0.37 \text{ g}$). As presented earlier in this study, this highly unrealistic maximum acceleration is a major part of the reason for prompting a complete FEMU procedure on the Stange railway bridge. Being able to then confirm that this maximum acceleration is indeed unrealistic and not the case for the physical bridge structure has been an important step in the process. This would confirm that the assumed complicated boundary conditions and unusual design of the bridge are coupled with uncertainty and will assumingly have a significant influence on the structure's dynamic behavior.

From all recorded train crossings during the 48 hour monitoring period, the recorded acceleration data from the bridge gives a maximum acceleration of 0.3275 g . This maximum value is based on a total of 92 crossings, where the remaining six crossings included what is assumed to be a sensor "bug" where a singular value had a significant peak value above the remaining duration of the crossing. Figure 25 presents maximum accelerations from all 92 recorded train crossings. The scatter plot includes acceleration data from 16 cargo trains, 9 express trains, and 67 local trains. Table 6 presents the average max. accelerations recorded for each train type. It can be seen that cargo trains and express trains generate very similar and the largest average acceleration, while the local trains generate about half of that recorded for cargo- and express trains.

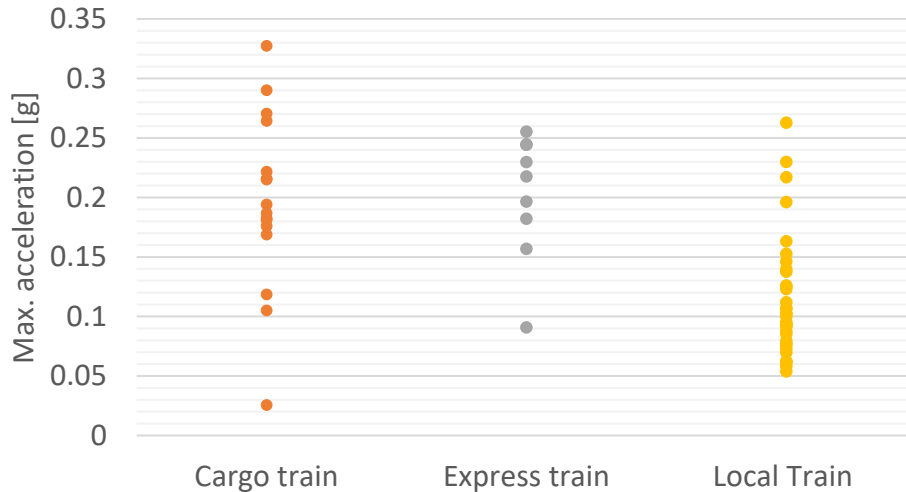


Figure 25. Max. accelerations recorded based on 92 train crossings.

Table 6. Average max. accelerations recorded for train types.

Train type	Average acceleration [g]
Cargo train	0.197
Express train	0.202
Local train	0.104

From Figure 25, it can be seen that the cargo trains have the largest variety considering the recorded maximum accelerations. This is assumed to be due to significant variations regarding the type of cargo train crossing, what is being transported and whether the train is loaded with cargo or not. It is assumed that the cargo trains have greater axle-loads than the express trains, but due to restrictions regarding traveling speeds on the bridge for cargo trains, the express- and cargo trains generate similar accelerations in the bridge deck. The effect of traveling speed on acceleration in the bridge deck is more evident when comparing express- and local trains. These trains are very similar in design and are assumed to be very similar considering axle-loads. The major difference is traveling speed when crossing the bridge as the express trains are not stopping at Stange station, while the local trains are either decelerating prior to stopping or accelerating after stopping at Stange station. Therefore, the local trains are crossing the bridge at a lower speed than the express trains, thus generating lower accelerations in the bridge deck.

As presented in Section 7.1, results from the FE analysis and structural assessment by Rambøll and Sweco indicated that maximum accelerations occur in the cantilevering extensions of the bridge deck. Whether this maximum acceleration occurs at the Oslo or Hamar side of the bridge is not specified. From the recorded time-history acceleration data, this was confirmed to also be valid for the actual bridge. Of the 92 previously discussed train crossings, 83 % had maximum accelerations recorded at Sensor 5 (Hamar side), and 8 % had maximum accelerations recorded at Sensor 1 (Oslo side). The majority (67 %) of the remaining crossings that had maximum recorded accelerations at other locations than Sensor 1 or 5 had maximum acceleration recorded at Sensor 2 and 4, from the second sensor configuration. These sensors are also located at the cantilevering bridge deck extensions, thus supporting the observation that the majority of crossings generate maximum accelerations in the cantilevering bridge deck extensions. From documentation and construction drawings, the abutments and cantilevering deck extensions are identical at each end of the bridge, and it is reasonable to assume that also the boundary conditions are identical. The observed location of the majority of the recorded maximum accelerations contradicts this assumption, indicating that the boundary conditions at each end of the bridge are not identical.

Based on the recorded operational time-history acceleration data from the Stange railway bridge and the consequent observations made, the previously assumed unrealistic high accelerations observed in FE analysis are confirmed not to represent the true behavior of the bridge. This proves that FE-models based solely on construction drawings are not typically an accurate representation of the structure [27], [33], thus prompting the need for a complete FEMU procedure to develop an FE-model that can realistically represent the structure, being the basis for this study.

8.4.3 Forced-, Free-, and Ambient Vibration

A time-history acceleration plot for a structure, in this case, a railway bridge, can be divided into three different main phases; forced-, free-, and ambient vibration. Forced vibration occurs when the excitation source(s), which are typically moving loads (e.g., pedestrians, vehicles, or trains), actively transfer loads to the structure. Free vibration initiates as the excitation source no longer affects the structure, but the structure is still moving/vibrating “freely”. As the structure comes to rest in its undeformed state, only ambient excitations will be present. Ambient vibration can be due to ambient conditions such as wind and

temperature acting on a structure. Note that the ambient vibration phase is most likely dominated by ambient excitations, but that electronic noise from the sensors could also be more predominant. These ambient vibrations and influence of electronic noise are typically very small compared to forced and free vibrations and can, in many cases, be viewed as “background noise” or a baseline excitation. Note that different terminology and definition of these vibration phases are common, but for the case of this study, the following presented definition is chosen. Figure 26 visually defines the different vibration phases of a time-history acceleration plot used in this study.

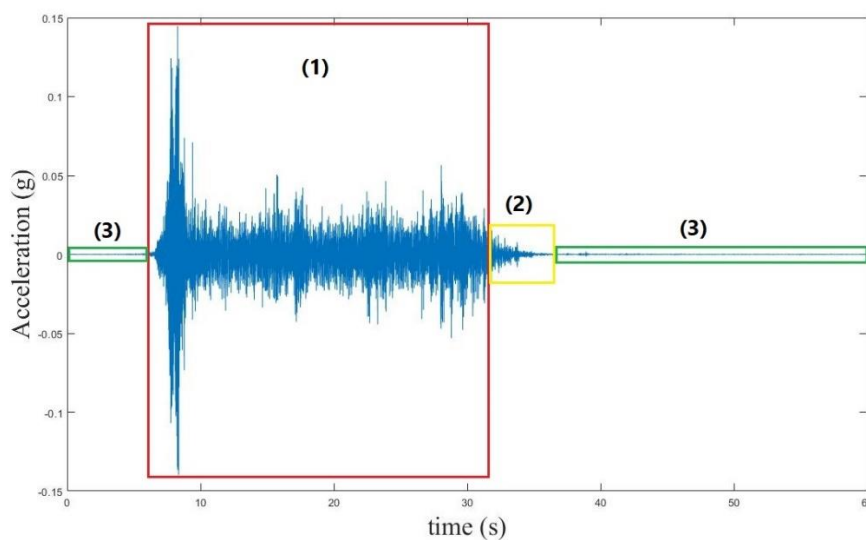


Figure 26. Example of time-history acceleration plot vibration phases; (1) forced vibration, (2) free vibration, (3) ambient vibration.

Important input variables for system identification methods, such as FDD and SSI-cov, is the definition of starting point and duration of the time interval of the time-history acceleration data used for system identification. Different approaches for determining these variables exist, but for many cases, this is often determined based on engineering judgment. The modal parameters of a structure (natural frequency, mode shape, and damping ratio) are “natural” or “inherent” parameters, meaning they only rely on the structure’s physical properties, such as stiffness and mass [55]. Thus, the loading on a structure will not affect the modal parameters. For this reason, choosing a time interval including the free- and/or ambient vibration phase will secure system identification based on acceleration data not affected by external loading other than minor ambient excitations. To successfully identify the natural modal parameters of a structure from the free- or ambient vibration phase, it is then required

that enough energy is present in the system to sufficiently excite the modes. A stiff system will typically retain sufficient energy in the relatively short duration of the free vibration phase to successfully identify its modal parameters. However, for other less stiff systems, this might not be the case. For such systems, it can be necessary to conduct the modal parameter identification over a longer duration and also include the ambient vibration phase.

For the case of the Stange railway bridge, which is a relatively stiff structure, the free vibration phase is deemed to retain sufficient energy for modal parameter identification. Determining the starting point and duration of this phase is still highly dependent on engineering judgment. The starting point is typically chosen to be at a point of time where it is estimated that the excitation source, in this case, the train, has left the bridge. The duration must be determined such that enough data is included, but this can be difficult to conclude on. Too short duration might result in a limited amount of modal parameters possible to identify. However, too long duration might affect the data negatively due to greater influence of ambient vibrations or noise. In a study by Ülker-Kaustell and Karoumi [56], the effect of duration on the identified natural frequency and damping ratio is discussed. Here, the identified natural frequency and damping ratio are shown to vary greater with short durations ranging from 0 – 5 seconds, while in durations exceeding 5 seconds, the frequency and damping ratio seem to start stabilizing. Figure 27 presents the observed effect of duration on natural frequency and damping ratio.

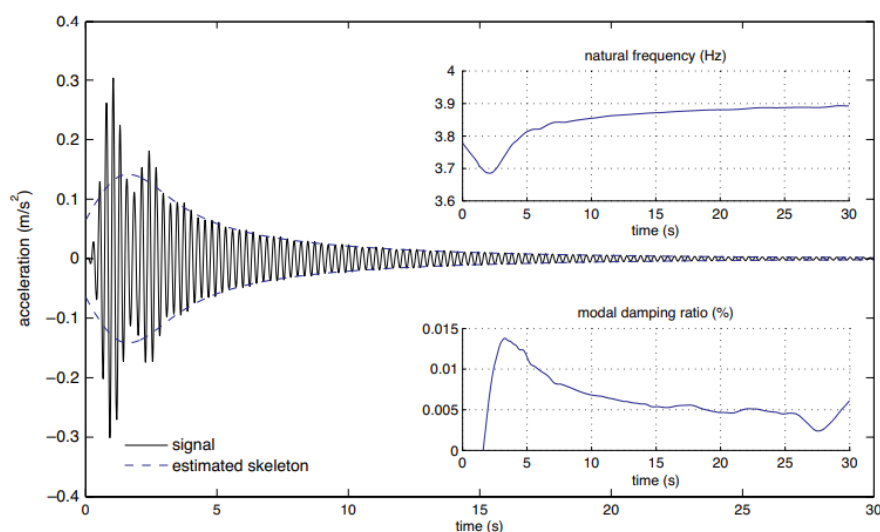


Figure 27. Observed effect of duration on natural frequency and damping ratio [56].

To avoid a highly time and labor-intensive process of determining the optimal duration for each individual train crossing, it was decided to determine a common duration used for all crossings. For each crossing, the starting point was individually determined based on the assumed start of the free vibration phase from Sensor 3. Sensor 3 was chosen due to this sensor being placed in the center of the bridge's middle span (see Figure 20 and Figure 21). It is acknowledged that this method might result in the inclusion of some acceleration data from the forced- and ambient vibration phases, as the train has not fully crossed the bridge at this point. The sensors behind the tail end of the train would, at this point, be well into the free vibration phase, while the sensors ahead of the train would still not have initiated its free vibration phase and vice versa. Figure 28 visually presents this effect by depicting an excerpt of a time-history acceleration plot of a train traveling from Hamar to Oslo (Sensor 5 to Sensor 1). From this figure, a reasonable estimate of when the free vibration initiates at Sensor 3 would be at time 31.27 s ($X = 31.27$). At this time, it can be seen that Sensor 1 is still in the forced vibration phase, while Sensor 5 is vibrating freely. If one would choose to define the starting point of the free vibration phase when the train has entirely left the bridge at Sensor 1, which would roughly be at time 32.5 s, there would be very limited data left to analyze on the remaining sensors, and possibly not enough energy retained in the system for successful system identification.

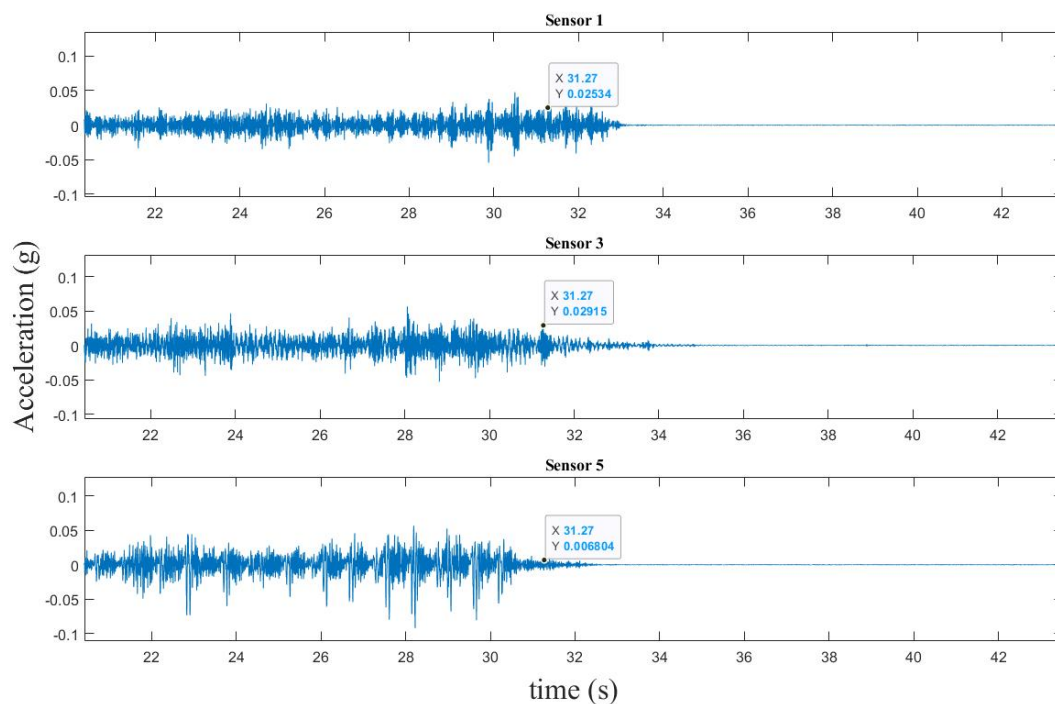


Figure 28. Free vibration start and duration difference between sensors.

Considering that the bridge is relatively short (48.6 m), it can be challenging to determine a common start- and end-point of the free vibration phase when considering all sensors at once. To secure sufficient data and contribution from all sensors, defining the starting point of the free vibration phase from Sensor 3 is therefore deemed favorable in this case. Including enough data and securing contribution from all sensors have outweighed the possibility of thus including acceleration data from the forced vibration phase.

Having identified and selected an individual starting point of the free vibration phase of all train crossings, the next step is determining the required duration of the sensor data used for system identification. To conclude on a suitable duration used on all train crossings, it was decided to investigate how the selected duration would affect the resulting natural frequencies. As described by Ülker-Kaustell and Karoumi [56], it can be expected to see some variation of the natural frequency as the duration is altered. To investigate this effect, an FDD algorithm incorporated in MATLAB [26] was used to identify natural frequencies from 12 randomly selected train crossings (4 cargo trains, 4 express trains, 4 local trains). The duration was manually increased from 2 – 8 seconds with 0.25-second increments, and the change of each individual frequency was recorded. FDD with peak picking was selected for this instance due to ease of use and simplicity, as well as having manual control of selecting the peaks/modes of which to investigate. Note that the purpose of using FDD in this instance is solely to investigate the effect of altering duration have on the natural frequency. No formal results would be extracted from this process other than evaluating the proper duration suitable for future use in system identification.

Figure 29 and Figure 30 presents two examples of observed changes to identified natural frequencies as the duration was increased from 2 – 8 seconds. A similar, but not as prominent, effect as observed by Ülker-Kaustell and Karoumi [56] can be seen for certain natural frequencies, where the natural frequency has some variation at short duration and stabilizes as the duration is increased. A key observation is that if a too short duration is used, not as many natural frequencies are identified. This is assumingly due to insufficient data from the time-history acceleration data being included, resulting in less excitation of modes due to less energy being included in the system identification period. As similar observations were made on the remaining train crossings investigated, a 5-second duration was considered to generate a sufficient amount of natural frequencies that have also stabilized. By also

considering the possible negative effect of too long duration, being an increased amount of noise from the ambient vibration phase, a 5-second duration was decided to use for further system identification.

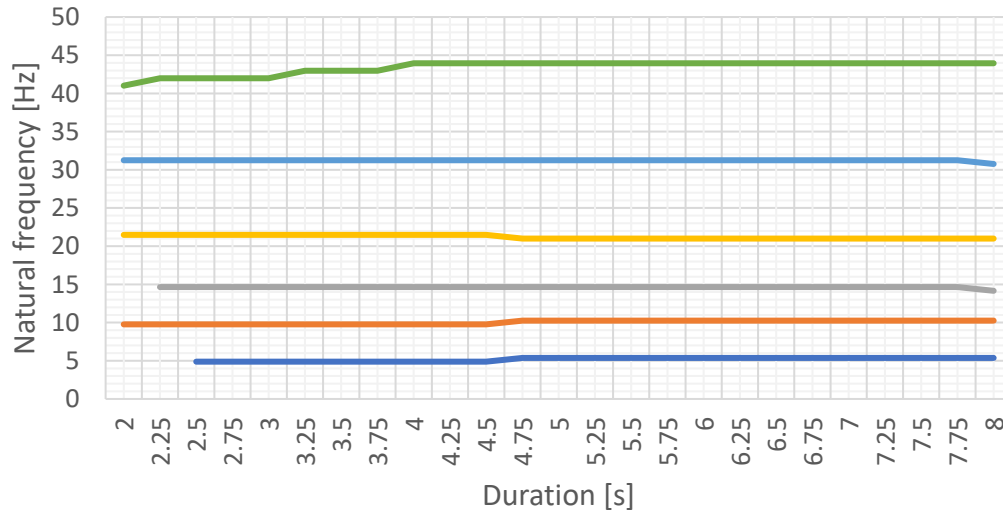


Figure 29. Changes observed in natural frequency due to duration increment ex. 1.

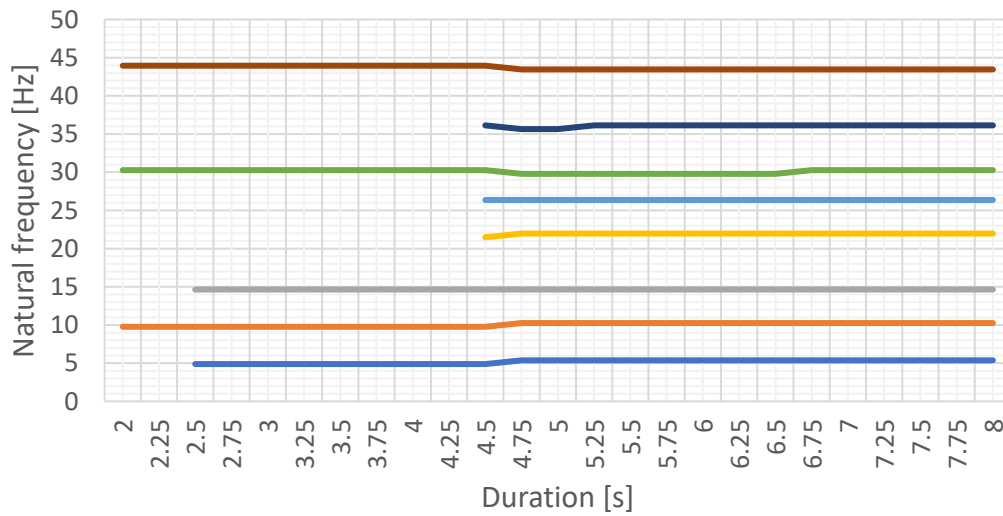


Figure 30. Changes observed in natural frequency due to duration increment ex. 2.

8.5 System Identification

This section aims to describe the process of extracting modal parameters from operational condition acceleration data and thus identify the structural behavior of the Stange railway bridge. As described in theory, a number of techniques are suitable for identifying a structure from output-only data. In the case of this study, the covariance-driven Stochastic Subspace Identification method was found to be the best option.

8.5.1 System Identification of the Stange Railway Bridge

To perform system identification of the Stange railway bridge, the OMA Toolbox for MATLAB, developed by Otto [26], was utilized. The toolbox contains a variety of different identification techniques, such as frequency-domain decomposition (FDD), data-driven Stochastic Subspace Identification method (SSI-data), and SSI-cov. The SSI-cov method was selected based on observed results in other studies utilizing this method, in addition to discussions regarding the benefits of this method with the project supervisor.

The SSI-cov algorithm in the OMA Toolbox takes three input arguments:

- Output-only data (sensor data), [Y]
- Model order
- Number of time lags used in the covariance calculation, s .
 - Can be set as 2 x model order [26]

With an accelerometer sampling rate of 250 Hz, the optimal duration found to be 5 seconds and five sensors per configuration, the input sensor data, [Y], was set to the following:

$$[Y] = \text{number of sensors} \times \text{sampling rate} \times \text{duration} = [5 \times 1 \ 250]$$

According to Li et al. [25], determining the model order is a crucial step in system identification with SSI-cov. However, even though it exists theoretical methods to decide the parameter, the methods lose their efficiency for ambient-excited, civil structures. To identify a suitable model order and overcome the issues related to noise, Reynders [13] proposed a stability diagram [25]. The theory behind the stability diagram is that true modes will occur more often than modes contaminated by noise. Thus, Reynders introduced a set of criteria for natural frequency (f_n), damping ratio (ζ), and mode shape (ϕ), ensuring that the modal parameters are consistent for a number of model orders. If one of the criteria are not met, an

“unstable mode” is detected, as there is too much variation between the model orders. A basic flowchart of the stabilization criteria can be seen in Figure 31. The concept is further exemplified with the stabilization diagram for the system identification of Stange bridge in Figure 32.

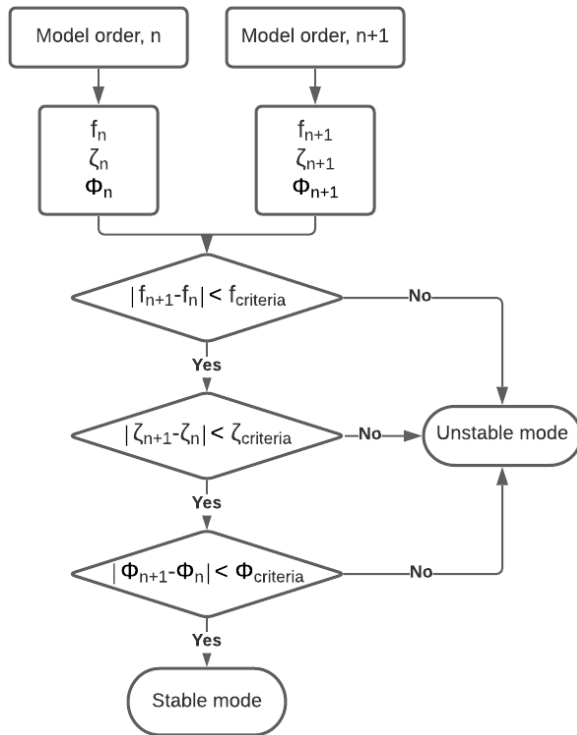


Figure 31. Flowchart of the stabilization criteria [13].

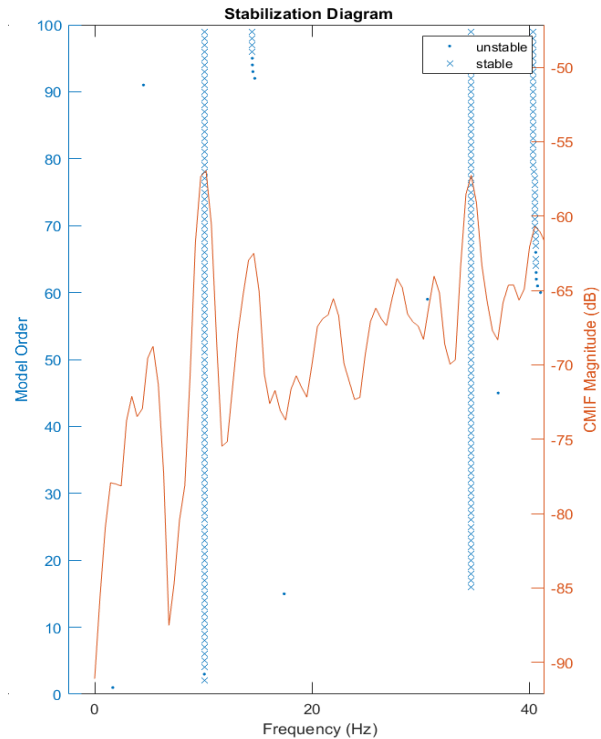


Figure 32. Stabilization diagram generated by the SSI-cov algorithm.

The criteria set, forming the stabilization diagram, and acting as “cut-off” values differentiating stable versus unstable modes, can be seen in Table 7. Here, the values given in the SSI-cov algorithm are discussed and conferred with the supervisor and concluded to be satisfactory in order to identify true modes.

Table 7. Modal parameter criteria set for the stabilization diagram [26].

Modal parameter	Acceptable error [%]
Natural frequency, f_n	2
Damping ratio, ζ	5
Mode shape, ϕ	2

In Figure 32, the stabilization diagram indicates up to four true modes within the frequency range of 0 - 40 Hz, and it can be seen that selecting a correct model order is very important in

this case, as the mode at 15 Hz would not have been identified for a low model order. However, even though the SSI-cov algorithm until now has avoided significant subjective choices, the sensor data can be more contaminated by noise and subsequently not be as “clean” as in Figure 32. Thus, setting the model order to extract modal parameters can be a challenging task. In the exemplified figure, the model order was set to 96 to ensure that the mode identified at 15 Hz was not excluded.

8.5.1.1 Selection Criteria

Even though the SSI-cov algorithm identifies stable modes, it does not necessarily identify true modes. The criteria set in the algorithm only focus on consistency and relative error. Thus, if a modal parameter is false for a given model order, the following model order can still be marked as a “Stable mode” if the modal parameters do not change more than the error criteria given in Table 7. Subsequently, defining supplementary criteria are essential in order to identify true, recurring, and dominant modes.

Firstly, from the stabilization diagram of every train crossing, an impression of the structural response can be read from the CMIF-curve, where the highest peak indicates the “strongest” mode identified [57]. Thus, to exemplify, the CMIF-curve in Figure 32 indicates modes at around 10 and 35 Hz, where the highest peaks occur. It can also be seen that this is where the “stable poles” are formed, meaning that stable modes for a number of model orders are detected. Thus, the first criteria for modal parameter identification is to ensure that stable modes occur for the highest peaks. Subsequently, if these are the true modes of the structure, one would also expect high peaks to occur around the same frequency for several train crossings. However, even though stable modes at a given frequency now can be detected, it is still questionable whether the mode shapes are realistic and distinct.

To identify dominant and distinct modes, the Modal Assurance Criterion (MAC) [30] features as a great tool. Presented in the theory, in Figure 4 (i) and (ii), there are two different scenarios using the MAC. In an ideal case, the modes are independent and represent the exact decomposition of the structural deformation [13], [28]. This case is conceptually presented in Figure 33, where the resulting deformation curve on the left is the summarization of the modes of vibration. To exclude modes that are not distinct, ϕ_j is set equal to ϕ_i in Equation 1. Subsequently, the diagonal will always be equal to 1. In Figure 4 (i), the values represent the

“ideal” MAC-values, as there is no correlation between the modes. In Figure 4 (ii) however, the case is somewhat different. Here, modes are shown to have a large correlation, but some of the modes do also excessively overlap. Consequently, the modes cannot be distinguished as distinct modes.

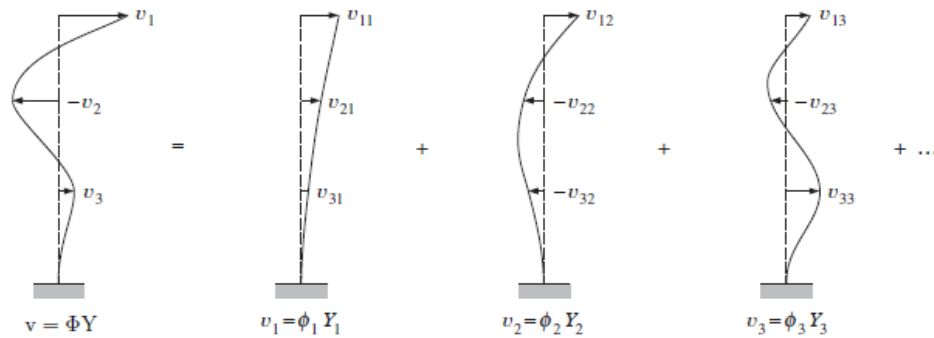


Figure 33. Resultant displacement and modal components [42].

Thus, using the MAC criterion could effectively help reduce the number of potential modes during modal identification. Selection of modes could still be challenging and require fair engineering judgment, but this process could be aided by selecting modes that:

- Are close to a high peak on the CMIF-curve.
- Have a “stable pole” in the stabilization diagram, meaning that a stable mode is detected for a number of model orders.
- Have a reasonable natural frequency (f_n) and damping ratio (ζ).

With a “reasonable natural frequency”, there are two important things to identify; what is the magnitude, and does the mode occur with the same natural frequency for a number of crossings. Firstly, to identify an applicable and reasonable natural frequency range, an in-depth investigation was conducted in the preliminary studies for this thesis. There, it was concluded that the vast majority of the studies investigated, which focused on civil engineering bridge structures, had a natural frequency ranging from 1 to 15 Hz. However, that sample was based on many different bridge structures with different sizes and design philosophies. Thus, even though the presented frequency range is not too inaccurate, some modifications are deemed necessary to make it suit the Stange railway bridge. According to Eurocode 2, section A2.4.4.2.1 (4) [37], the maximum natural frequency to account for should be set to the largest of the following values:

- 30 Hz
- 1.5 times the frequency of the smallest mode shape of the structure in focus
- The frequency of the third mode shape of the structure in focus

As the criteria for modal parameter extraction is currently being set, the second and third bullet point above cannot be assessed. Subsequently, the criteria left is 30 Hz. However, the Stange railway bridge is a relatively stiff structure as a result of having a large cross-section area relative to its length, which can lead to higher natural frequencies. Thus, it was agreed not to exclude the modes above 30 Hz in the system identification process. Moreover, assessing the same topic, Majka and Harnett [58] identified that an upper bound of 50 Hz usually covers the most frequent vibrations for railway bridges. Thus, to conclude on the natural frequency range, modes with a natural frequency above 30 Hz could be included as long as they are distinct and recurring for a number of train crossings. For this study, an upper bound of the natural frequency range is set to 40 Hz. An example of this can be seen in Figure 32, where stable modes up to around 40 Hz have been identified and included.

The damping ratio, ζ , does not function as a primary selection criterion. It is rather used as an additional criterion to ensure that the damping ratio is also preserved in a realistic range. According to Eurocode 1, NS-EN 1991-2:2003+NA:2010 [59], the theoretical structural damping can be set to 1.32 %, given a prestressed bridge with a maximum span of 18 meters, as the Stange railway bridge. However, even though damping ratios for railway bridges can be roughly estimated, they are conflicting as many factors can affect their magnitude [58]. Thus, in discussion with the supervisor, it was decided to set a cut-off value to around 10 - 12 %. Meaning that modes with damping ratios above this percentage were excluded, as they assumingly would not be realistic.

By using SSI-cov, and the further described selection criteria, the structural system of the Stange railway bridge was identified with recurring, dominant natural frequencies and mode shapes, and with reasonable damping ratios. Even though the presented methodology of identifying the system to some extent, in the end, requires some degree of engineering judgment to practically pick the modes, the premises set, the quantity of data, and the level of consistency of the resulting modal parameters have ensured and confirmed that the results are unbiased and minimally exposed to subjective choices. Furthermore, based on the

number of available sensors and time to monitor the bridge, the resulting modal parameters are found to be satisfactory to understand the structural behavior of the Stange railway bridge. The resulting modal parameters are thoroughly presented in the following section, with some interesting findings relative to available documentation.

8.5.2 Resulting Modal Parameters

After performing SSI-cov modal identification on acceleration data from a total of 98 train crossings, distributed on two sensor configurations, four distinct, recurring, and dominant modes were identified. To ensure comparability between the modes internally, as well as with the analytical FE-model, some mathematical measures were found necessary to apply. Moreover, the mathematical measures are also applied to obtain continuous and more realistic mode shapes.

Firstly, the two sensor configurations were combined by taking the average deformation for each mode at the location of the sensors. As Sensor 2 and 4 are moved towards the bridge ends in the second configuration, combining the configurations practically results in having seven sensors (see Figure 20 and Figure 21), as each mode is based on seven sensor locations. However, linearly combined modal values from seven sensor locations alone do not result in smooth, continuous mode shapes. For that purpose, spline interpolation [60] is deemed necessary to conduct. Lastly, the mode shapes are normalized at their individual absolute maximum to obtain mode shapes with coordinates between -1 and 1.

After performing the presented mathematical measures, the following four mode shapes presented in Figure 34, with corresponding natural frequencies and damping ratios, were obtained. Note that $x = 0$ on the x-axis (Bridge span) of Figure 34 represents the Oslo side of the bridge, while $x = 48.6$ represents the Hamar side. The scaling of the mode shapes is also highly exaggerated for a better visual representation in the figure, especially relative to the geometric shape of the bridge in the background only intended to provide a visual reference.

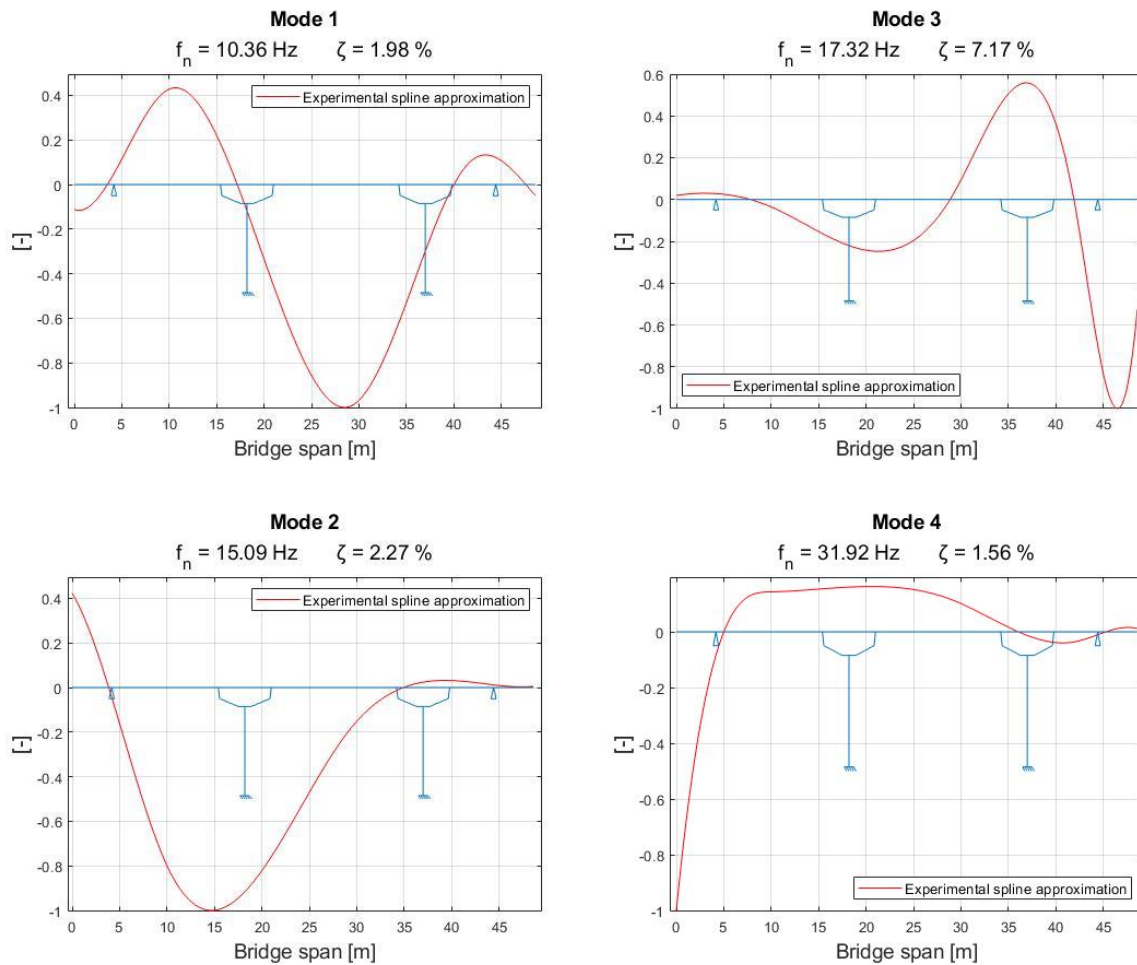


Figure 34. The 4 obtained modes of the Stange railway bridge from experimental data.

The modes presented above were found to be recurring and dominant throughout the system identification. Furthermore, the share of data between the sensor configurations are presented in Table 8. There, it can be seen that both sensor configurations significantly contribute, but as assumed earlier on, the first sensor configuration is the major contributor to the resulting modal parameters.

Table 8. Share of data from each sensor configuration.

Modes	Mode 1	Mode 2	Mode 3	Mode 4
Data from configuration 1	60 %	60 %	52 %	46 %
Data from configuration 2	40 %	40 %	48 %	54 %

The first mode of vibration (Mode 1) was found to be the most recurring mode of the ones identified. For this mode, the maximum deformation occurs in the center of the mid-span,

and the motion flattens out towards the ends. Interestingly, the values at the bridge ends are small relative to what could be expected from a bridge with cantilevering ends.

Similar to Mode 1, the second mode of vibration (Mode 2) was slightly easier to identify with the first sensor configuration. This mode has a slightly higher natural frequency and damping ratio, but it is still within reasonable limits. The maximum deformation occurs in the span at the Oslo side, close to the column. In practice, the location of maximum deformation of the mode shape was expected to occur in the middle of the span. However, it is acknowledged that the number of sensors and the interpolation of the data may have caused an eccentricity.

The third and fourth mode of vibration expresses a cantilevering behavior at each end. Assessing the natural frequencies of the modes, there are again some interesting results relative to what is expected from the theory. From theory, the natural frequency (f_n) of a system is dependent on two things; stiffness and mass, as presented in Equation 9 [55]. As the boundary conditions are the same at both ends of the bridge according to the documentation, the equation expects the cantilevering mode at the Oslo side (Mode 4) to have the lowest natural frequency as a consequence of having the longer span and subsequently a larger total mass. However, this is not the case with the experimental data. According to the natural frequencies of the third and fourth mode, there is an uncertain parameter that makes the Oslo side stiffer than the short-spanned Hamar side, which again is something that the documentation does not express.

$$f_n = \sqrt{\frac{k}{m}} \quad (9)$$

Furthermore, in Figure 35, the MAC correlation values of the four extracted modes are presented. It can be seen that the correlation between the modes is low in a holistic perspective. Even though the correlation control indicates a 37 % correlation between the second and fourth mode, their maximum deformation is at different locations. As the MAC criterion is calculated as the normalized scalar product of two sets of vectors, it does not consider any other modal parameters, such as natural frequency. As concluded by Pastor et al. [61], *“the MAC gives no information about the frequency correspondence and can*

sometimes show good correlation between modes that have significant frequency separation". From this conclusion, in addition to assessing the shape of the modes and location of maximum deformation, Mode 2 and 4 are concluded to be truly distinct despite the 37 % MAC correlation found between them.

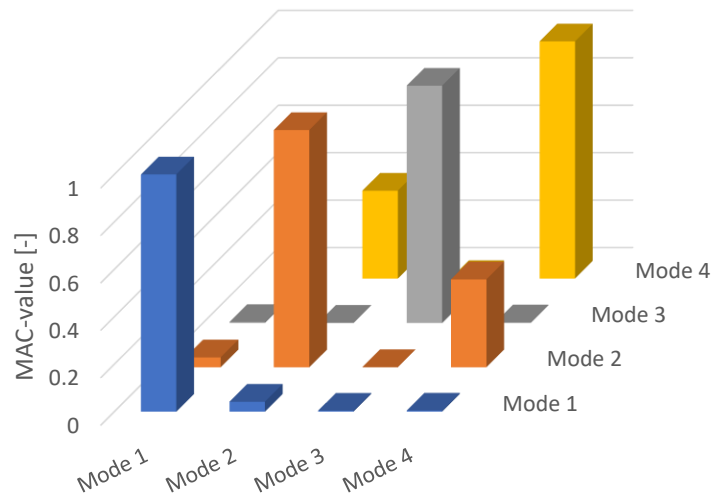


Figure 35. MAC correlation of the extracted experimental mode shapes.

8.5.2.1 Observations

Directional dependency of modes

From system identification and FEMU theory, it is common knowledge that the modal parameters only rely on the inherent structural properties of a system, such as stiffness and mass. Thus, the modal parameters should not be reliant on the forcing function of the load, in this case, the train crossing the bridge and in which direction it is traveling (Oslo to Hamar or Hamar to Oslo). Considering this, an interesting observation made on the identified experimental modes is that there seems to be a directional dependency on some of the modes. Table 9 presents evidence of this partial directional dependency by providing a percentage for each mode regarding which direction is dominant.

Table 9. Modes identified dependent on train direction.

Modes	Mode 1	Mode 2	Mode 3	Mode 4
Oslo → Hamar	51 %	25 %	0 %	100 %
Hamar → Oslo	49 %	75 %	100 %	0 %

For Mode 1, an almost completely even distribution is shown, where both traveling directions of the trains are close to equally dominant. Mode 2 is less even in its distribution, where the majority of train crossings exciting Mode 2 is in the direction Hamar to Oslo. The trend is assumingly that as the maximum deformation in the mode shapes shift from the middle of the center span towards the ends, the directional dependency increases. This assumption is backed by observing that Mode 1, which has maximum deformation in the middle of the center span, shows no evidence of directional dependency. Whereas Mode 2, which has its maximum deformation in the span on the Oslo side, between the abutment and column, has a more significant directional dependency favoring the trains arriving from Hamar. The assumption regarding possible directional dependency is further strengthened by the clear directional dependency observed for the third and fourth mode. Both of these modes, which have their maximum deformation at the bridge ends in the cantilevering bridge extensions, respectively, are shown to be 100 % directionally dependent. Meaning that Mode 3 is only identified from trains crossing from Hamar to Oslo, and Mode 4 is only identified from trains crossing from Oslo to Hamar.

The directional dependency is assumingly due to the energy dissipated in the system from the forcing function in all cases (traveling directions) is not sufficient for exciting all modes. Meaning that the modes are there, but not enough energy is present in the free vibration phase used for system identification to detect them using analytical methods. Tests were performed by increasing the duration of the data used for system identification such that more of the ambient vibration phase was included. This would increase the total amount of recorded energy such that more modes could be excited. By doing this, the directional dependency of the third and fourth mode was reduced, with the modes being excited and possible to detect from trains traveling in both directions. However, the data quality was heavily reduced and less predominant as the data was more affected by noise. Thus, there were peaks beginning to show at the frequencies of the third and fourth mode, but the stability of these was insufficient, and the low CMIF magnitude did not allow for clear identification of distinct modes at the relevant frequencies.

Vertical displacement of columns and foundations

According to the bridge's available documentation and construction drawings, the two concrete columns are rigidly connected to concrete foundations that rest directly on bedrock. This would imply that the vertical movement of the column/foundation system would be highly restricted. However, in Figure 34, it can be seen that the columns are somewhat able to move vertically as the bridge deforms, implying that modelling the columns as constrained to bedrock might not be the best approximation. It is acknowledged that a mode shape is a more theoretical shape and should not be confused with actual deformations occurring during a train crossing. However, the mode shapes that are calculated based on experimental data indicate that vertical movement of the column/foundation system should be considered. Due to a limited amount of sensors and time available for the collection of data, consequent prioritizations did not allow for placement of sensors on top of each column in this study. As the mode shapes are more theoretical and based on collected data from the presented sensor configurations, the possible vertical displacement of the column/foundation system could not be confirmed nor rejected. Thus, this possible phenomenon will not be further discussed as the collected data would not allow for positive confirmation

Mode shape approximation

One clear disadvantage of having a limited amount of time and sensors available for monitoring is visualized in Figure 36. The figure expresses the difference between the linear approximation and spline interpolation of the third mode shape. From the sensor data, the deformations are below 0.04 for all cases but the cantilevering end. Subsequently, it can be seen that the linear approximation of the mode shape gives a relatively flat mode shape. However, when the data is interpolated using a spline function to obtain a continuous shape, the deformations become larger at locations where the linear approximation expects values close to zero. These approximations are again a result of not having an unlimited amount of sensors available for the operational condition monitoring. Ideally, more sensors could be used to capture a more complete and exact mode shape, but in this case, priorities regarding the sensor configurations and available hardware did not allow for this. In the case of Mode 3, it is difficult to decide on the best approximation as there is such a significant difference between the estimates. Thus, the issue of Mode 3 especially is still to be concluded until a

comparison with an analytical solution is performed. For now, the spline interpolation is used as a reference. Note that the aspect of a significant mismatch between the linear and spline approximations is only true for Mode 3, as the case for the remaining mode shapes show a high correlation between the linear and spline approximations.

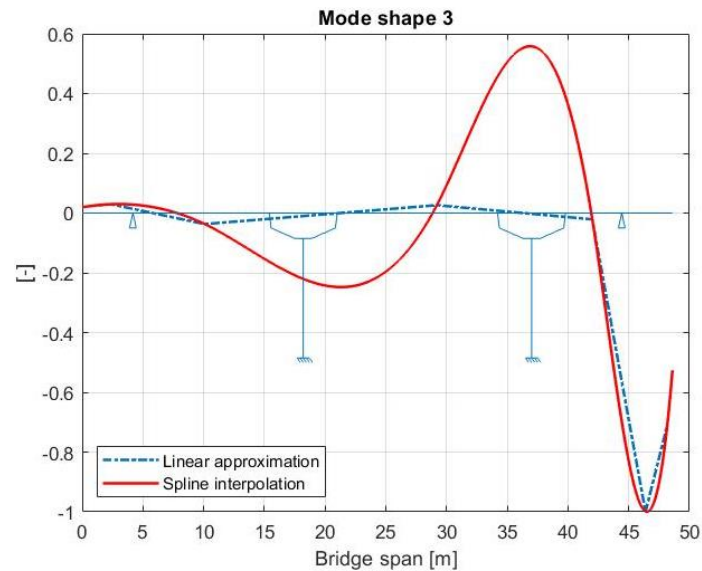


Figure 36. Linear vs. spline approximation.

Throughout the system identification, the identified modes were found to be recurring, dominant, and distinct. Even though the mass contribution of each mode to the total deformation is yet to be assessed, the extracted mode shapes did not all fit the expectations based on theory and documentation of a bridge with cantilevering ends. Thus, a strong perception based on the results acquired from the experimental operational condition monitoring indicates a mismatch between the physical as-built structure and the documentation. Moreover, the difference can hopefully be expressed when performing an initial correlation between the experimental results and the documentation-based FE-model.

9 Initial Correlation

In this chapter, the resulting experimental modal parameters will be compared and correlated to their analytical counterparts from the initial FE-model. Evidence of a mismatch between the documented and as-built structure is confirmed. By including additional modeling parameters and manual tuning, the intention is to bring the analytical modal parameters closer to the experimental results and to a level considered acceptable for a non-updated FE-model.

9.1 Initial FE Modal Analysis

After identification of the experimental modal parameters, the first steps towards obtaining analytical modal parameters from the initial FE-model using CSiBridge was conducted. From this, an initial correlation between the experimental and analytical results could be conducted to assess the initial FE-model, which is solely based on the available bridge documentation.

From the analytical FE-model, an infinite amount of modes can be identified if a cut-off value is not set. For the FE-model in question, a cut-off value of 20 was conservatively set to ensure that enough modes were included. However, for all practical purposes, the number of modes is not the deciding factor. Rather, it is how much the modes of vibration identified contribute to the structure's total deformation. Thus, in CSiBridge, the “*Modal Participating Mass Ratios*” are of great importance. The parameter expresses a scalar between 0 and 1, indicating the level of contribution to the overall response from the respective modes [62]. According to the FE-model, the first 20 modes of vibration make up 99 % of the total vertical response of the structure. However, Chen et al. [12] express that the modes that cumulatively represent 90 % of the total deformation are the most important ones. Moreover, Mosavi et al. [27] highlight the limitation of including higher modes, as ambient vibrations generally excite the lower modes of the system (the modes with lower frequency). Thus, it was decided to include modes starting from the first mode of vibration and upwards. Furthermore, as only vertical modes are of interest, the first nine modes cumulatively made up over 90 % of the total response. The frequencies of the resulting nine modes was also confirmed to have a lower frequency than 40 Hz, which was set as an upper bound in Section 8.5.1.1.

Even though nine modes were found to be sufficient in order to accurately identify the overall vertical response of the structure, all nine modes could not be correlated. From the experimental results, a total of four dominant, recurring and distinct modes were identified. Thus, the nine modes of the analytical model were limited to four, as only four modes are reliably detectable in the experimental data. Despite that the number of modes was reduced, with the four experimentally identified modes as a reference, the same four modes were also identified in the FE-model. It implies that initial assumptions regarding the modeling parameters and structural system are within a realistic range and that the FE-model can be a candidate for future model updating. According to CSiBridge, these four modes make up 50 % of the total vertical response. However, as the FE-model is initial and solely based on the

documentation, adding the fact that the experimental results indicate a mismatch between the physical structure and the documentation, the presented percentage is not seen as a reliable reference to assess the modal contribution. The essential part is that the analytical model identified the four modes perceived to match the experimental modes. Resultingly, Figure 37 presents the identified analytical modes compared to the experimental counterpart, with the associated analytical- and experimental natural frequency, f_{na} and f_{ne} , respectively.

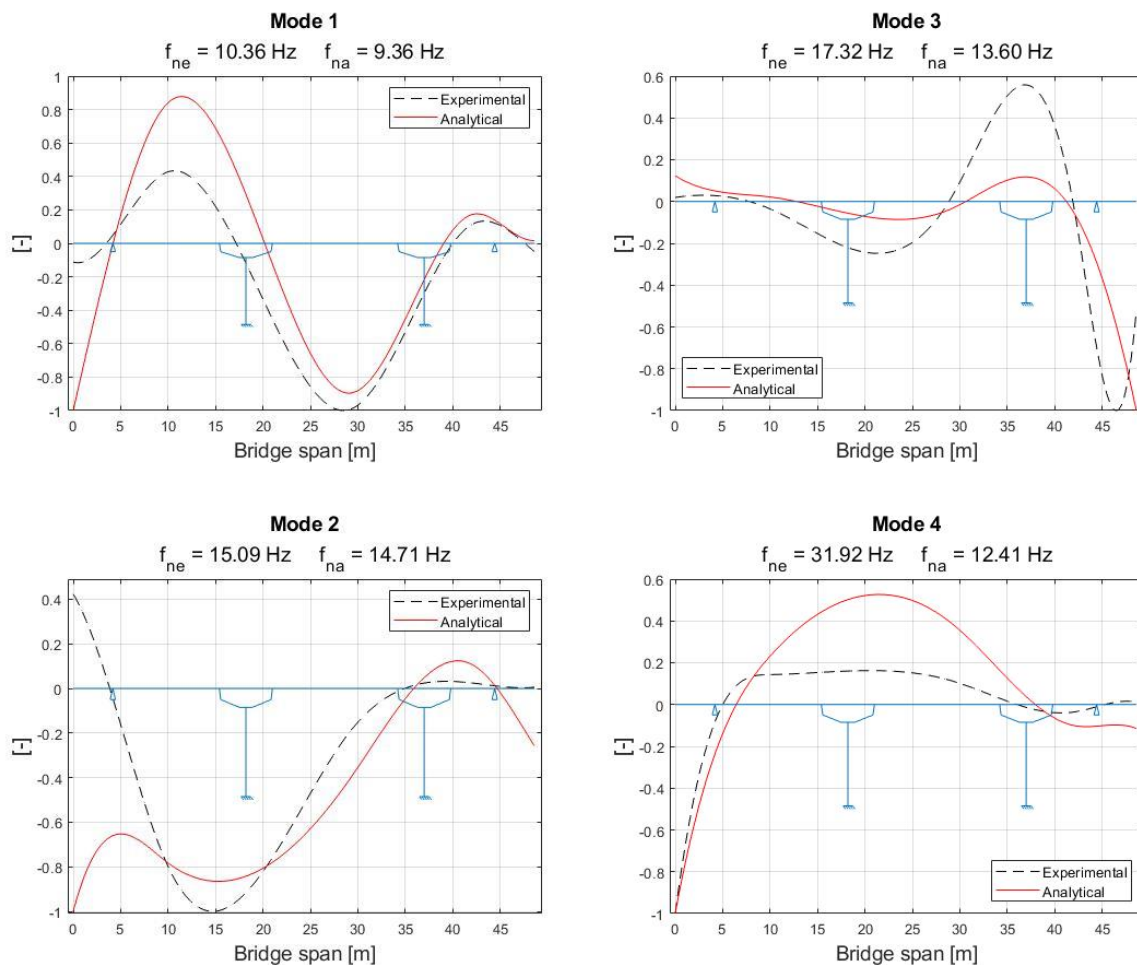


Figure 37. Experimental modes vs. initial analytical modes.

In addition to considering the modal participation mass ratios, the criteria used for selecting the analytical modes of interest were, most importantly, the mode shape, but also the associated natural frequency. From Figure 37, it can be seen that the third and fourth mode are the closest match regarding mode shape, while the first and second mode are the closest regarding natural frequency. An important observation made is that the cantilevering motions of Mode 3 and 4, at the bridge ends, the analytical model can more easily reproduce

compared to Mode 1 that flattens out towards the ends, especially at the Oslo side (Bridge span = 0 m). A MAC correlation of the experimental and analytical modes is presented in Figure 38, which confirms this observation. From the MAC correlation, it can be clearly seen that Mode 3 and 4 have the largest MAC correlation, with 84 % and 91 %, respectively, while Mode 1 and 2 have a 66 % and 2 % correlation, respectively. As described in theory, regarding MAC correlation, the ideal case is to see only correlation along the diagonal of the MAC plot, indicating clearly distinct modes with little overlapping. This is not the case with the initial MAC correlation, which for Mode 1 and 2 gives a low correlation along the diagonal in addition to some overlapping of other modes. In addition to the poor MAC correlation, the error between the analytical and experimental natural frequencies is found to be significant for some cases, as presented in Table 10. Although no consensus regarding lower cut-off values for MAC correlation and natural frequency matching between experimental and initial analytical has been observed, Ewins [63] propose an “acceptable” lower limit for MAC correlation of 80 %. Note that the acceptable lower limit stated by Ewins is not specified for use on an initial or updated model but acts as a general guideline. For the case of civil, structural engineering applications, Živanović et al. [10] state that MAC values exceeding 0.80 indicates “*very good mode shape agreement*”. In addition, Moravej et al. [29] state that if a natural frequency error between experimental and initial analytical FE-models exceeding 50 % is experienced, it is recommended that the initial FE-model is either manually tuned or altered.

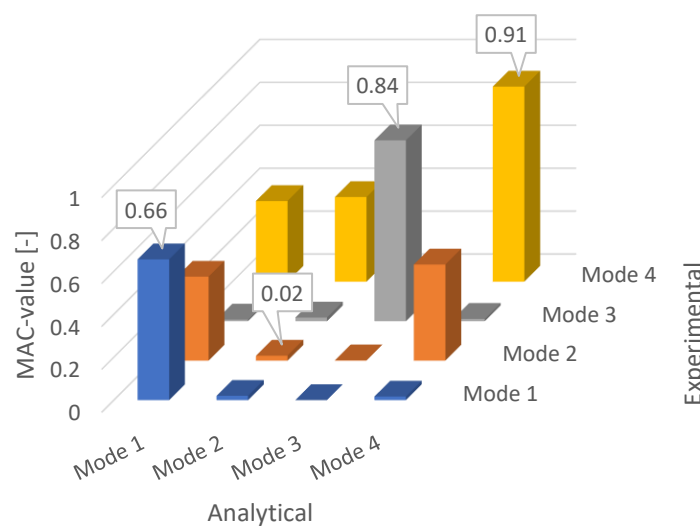


Figure 38. Experimental vs. initial analytical MAC correlation.

Table 10. Experimental vs. initial analytical natural frequencies.

	Mode 1	Mode 2	Mode 3	Mode 4
f_{ne} [Hz]	10.36	15.09	17.32	31.92
f_{na} [Hz]	9.36	14.71	13.60	12.41
Error [%]	9.7	2.5	21.5	61.1

The observation regarding how the initial FE-model is not able to properly generate the first and second mode of vibration, where the motion is restricted towards the bridge ends, has raised doubts if this model is a true and sufficient representation of the structure. The initial FE-model is modelled according to documentation, thus it has cantilevering deck extensions at both ends, which are not further supported. The initial FE-model is proven to successfully generate the cantilevering modes, Mode 3 and 4, but not able to properly generate modes that seem to be more restricted in the cantilevering deck extensions. From this observation, in addition to regarding the high accelerations recorded in the cantilevering deck extensions resulting from the purely documentation-based FE-model proven to be unrealistic, it is with good confidence possible to confirm that the documented bridge differs from the as-built structure. The thought cantilevering deck extensions seem not to be true cantilevers, having some degree of additional support on the underside. The experimental natural frequency of the cantilevering modes has, as discussed earlier in Section 8.5.2, given indications that the Oslo side of the bridge seems to be stiffer than the Hamar side. Thus, an assumption that the cantilevering deck extensions are further, unevenly supported beyond the location of the bearings resulting in the Oslo side being stiffer seems reasonable and justified by the gathered results.

9.2 Refining and Manual Tuning of Initial FE-model

As the initial FE-model was found to not generate modes with sufficient MAC correlation nor natural frequency correspondence, in addition to strong indications of the as-built structure not matching the documented structure, a closer visual inspection of the bridge was conducted. The goal of this inspection was to further investigate the cantilevering deck extensions to establish the actual boundary conditions of these that could possibly support the evidence found in the experimental data.

On further inspection, the cantilevering deck extensions were found to be resting directly on undocumented cast concrete slabs located underneath the deck extensions at both ends of the bridge. These concrete slabs are assumed to again be resting directly on soil/backfill within the abutments. The length and thickness of these slabs are not possible to positively conclude as there is no possibility to visually see all parts of the slabs. Assumingly, the thickness of the slabs is from the top of the abutments to the underside of the deck, whereas the length is from the back side of the bearings to the bridge ends. As far as can be seen, the width of the slabs extends between the insides of the bearings on both sides of the abutments. A visual presentation of the assumed extent of the concrete slabs underneath the deck extensions is presented in Figure 39. Furthermore, a picture of the concrete slab in relation to the bearings on the Oslo side is presented in Figure 40.

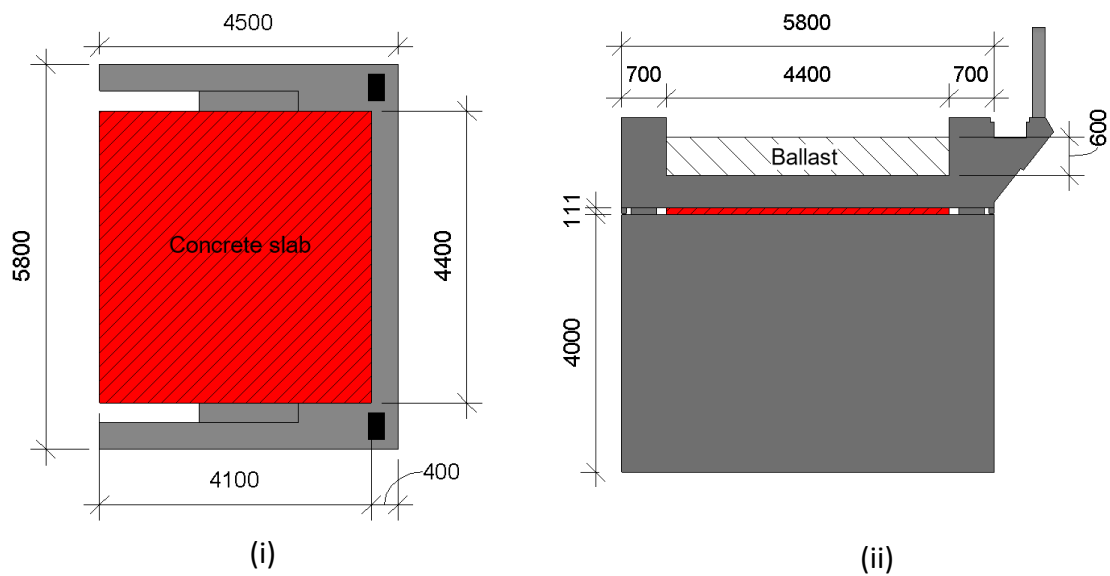


Figure 39. Concrete slabs underneath the deck extensions.



Figure 40. Concrete slab underneath deck extensions in relation to bearing.

The level of connectivity between the concrete slabs and the bridge deck is uncertain, but it is assumed that the deck is only resting on the concrete slabs without any anchoring. There is also assumed no anchoring between the abutments and the slabs, and that the slabs are not extending beneath the top of the abutments. The slabs are also assumed to be resting directly on soil/backfill, but the material- and mechanical properties of this are unknown. The substantial evidence from experimental results regarding a mismatch between the documented and as-built structure is confirmed from the visual inspection. By including the concrete slabs supporting the deck extensions as additional modeling parameters, the resulting modal parameters of the initial FE-model are assumed to be brought closer to the experimental results.

For including the structural effect of the concrete slabs in the initial FE-model, it was decided to model these as compression-only line-springs acting in the vertical direction from the location of the bearings to the bridge ends. For deciding and calculating the stiffness of these line-springs, hereinafter referred to as soil-springs, the “modulus of subgrade reaction” (k_s) for different soil/subgrade conditions is utilized. The modulus (or coefficient) of subgrade reaction is defined as “the pressure per unit deformation of the subgrade at a specified deformation or pressure level” [64]. Typical values of the modulus of subgrade reaction for different soil types are stated by Ubani et al. [65] and Bowles [66], which are presented in Table 11.

Table 11. Typical values of the modulus of subgrade reaction, k_s [65],[66].

Soil description	K_s [kN/m ² /m]
Humus soil or peat	5 000 – 15 000
Recent embankment	10 000 – 20 000
Fine or slightly compacted soil	15 000 – 30 000
Loose sand	4 800 – 16 000
Medium dense sand	9 600 – 80 000
Dense sand	64 000 – 128 000
Well compacted sand	50 000 – 100 000
Very well compacted sand	100 000 – 150 000
Loam or clay (moist)	30 000 – 60 000
Loam or clay (dry)	80 000 – 100 000
Clay with sand	80 000 – 100 000
Crushed stone with sand	100 000 – 150 000
Coarse crushed stone	200 000 – 250 000
Well compacted crushed stone	200 000 – 300 000

The resulting stiffness of the soil-springs at both the Oslo and Hamar side, k_{spO} and k_{spH} , respectively, were calculated using the concrete slabs' assumed width (4.4 m). Through an iterative process of manually tuning the stiffness of the soil-springs, starting at $k_s = 0$ (no contact) and increasing with 4 000 kN/m²/m increments, the effect of the soil-springs on the modal parameters were investigated. The soil-springs were initially adjusted symmetrically between the Oslo and Hamar side of the bridge and was later set to be unsymmetrical such that the Oslo side was made stiffer. In the final rendition of the initial FE-model, intended to be the starting point before the formal calibration process, the soil-spring at the Oslo side was set to 640 000 kN/m/m and 80 000 kN/m/m at the Hamar side. In this final rendition, the bridge deck cross-section geometry was also modified to represent the documented cross-section more accurately, as presented in Figure 9(i). The modified deck cross-sections are presented in Figure 41 with the basic measurements. The remaining modeling parameters are all left unchanged and in accordance with Table 5. A 2D-view of the refined FE-model from CSiBridge with soil-springs is presented in Figure 42.

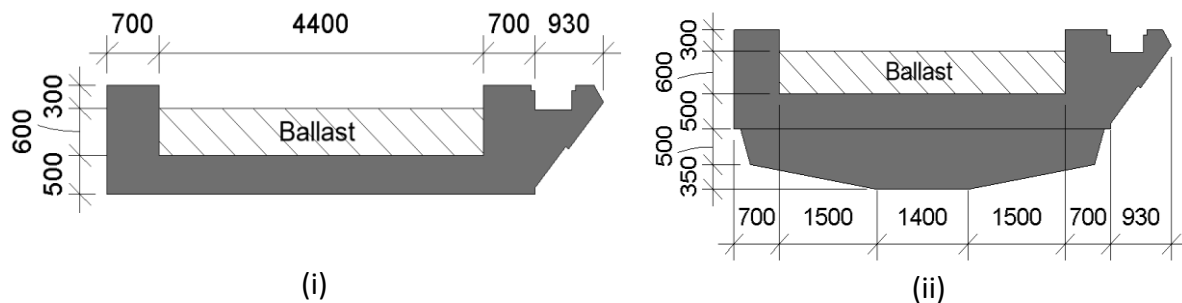


Figure 41. Modified deck cross-sections. (i) deck (ii) deck with column-cap.



Figure 42. 2D-view of refined FE-model with soil-springs.

10 Finite Element Model Updating

In the following sections, the results of the refinement and manual tuning of the initial FE-model, in addition to the formal updating process, are presented. Through sensitivity analyses of different modelling parameters, the sections assess and conclude on a set of applicable updating parameters, which are further investigated for the purpose of updating the manually tuned FE-model. Resultingly, the modal parameters and physical parameters are presented relative to their initial value so that the changes and improvements can be easily interpreted. Firstly, an extensive sensitivity analysis is conducted to enlighten the parameters that are of further interest.

The resulting modal parameters of the refined and manually tuned FE-model were found to be much closer to the experimental modal parameters, providing a more accurate representation of the as-built structure. With the inclusion of the unsymmetrical soil-springs supporting the deck extensions, Mode 1 and 2 had significant improvement regarding mode shape, and the natural frequency correspondence was increased for the third and fourth mode. In the initial FE-model without soil-springs, the mode shape of Mode 1 and 2 was not accurately captured as the cantilevering deck extensions were free to move. The soil-springs have effectively restricted the cantilevering motion for Mode 1 and 2 but have at the same time not restricted the motion too much such that Mode 3 and 4 are still well captured. The resulting modal parameters of the refined and manually tuned FE-model are presented and compared to the experimental modal parameters in Figure 43.

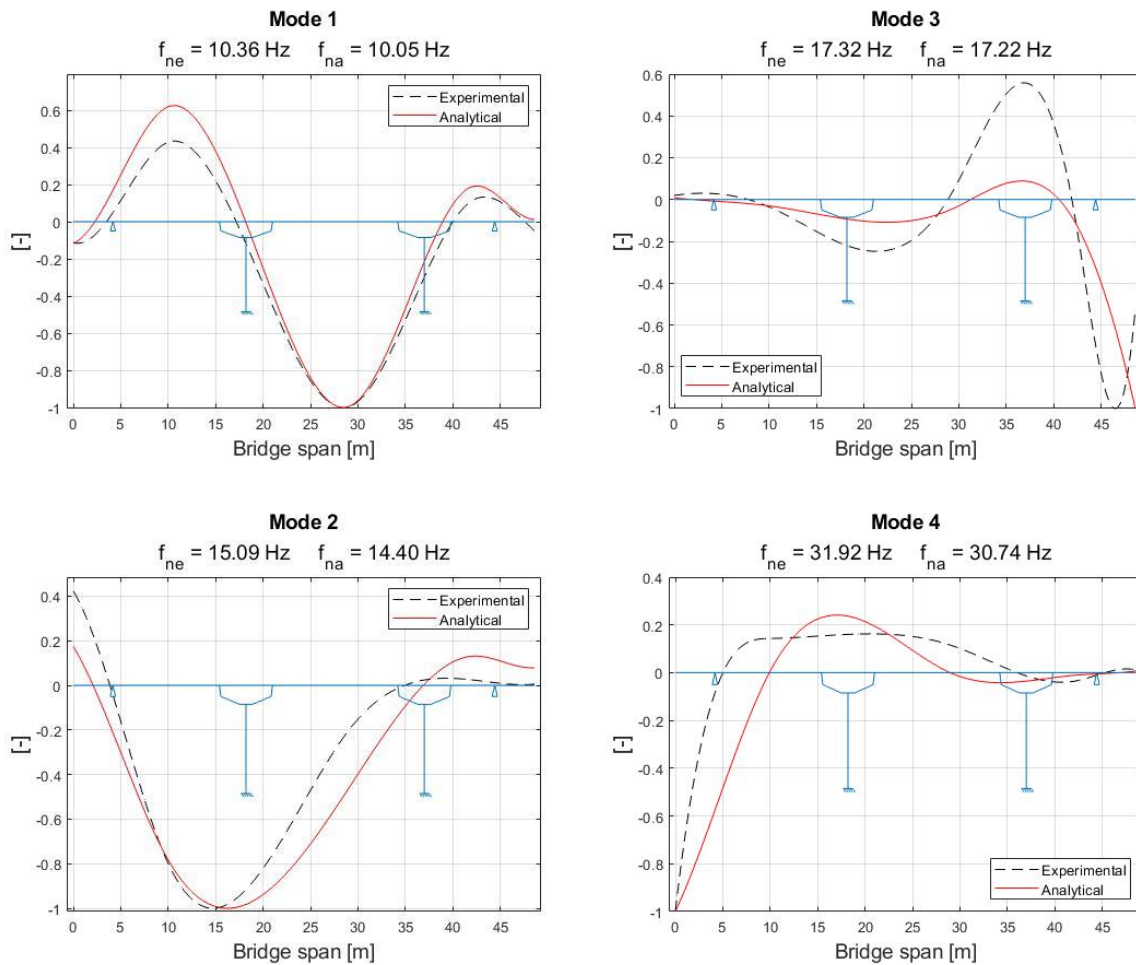


Figure 43. Experimental modes vs. modes from refined and manually tuned FE-model.

The resulting MAC correlation between the experimental and analytical modal parameters is presented in Figure 44, where an overall increase of correlation is shown except for Mode 4, which has decreased from 91 % to 89 %. The remaining modes have all experienced an increase in correlation where Mode 1 went from 66 % to 96 %, Mode 2 from 2 % to 78 %, and Mode 3 from 84 % to 86 %. The MAC correlation plot of Figure 44 also indicates a lower level of overlapping between the modes, assuring that the modes are clearly distinct. The natural frequency correspondence has also increased overall, as presented in Table 12, where especially Mode 3 and 4 have experienced the most significant increase in correspondence, going from a 21.5 % and 61.1 % error to 0.6 % and 3.7 % error, respectively.

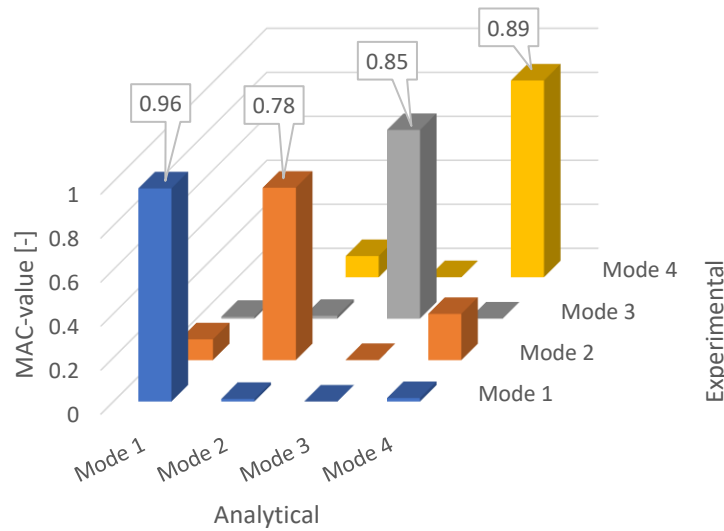


Figure 44. Experimental vs. analytical MAC correlation.

Table 12. Experimental vs. analytical natural frequencies.

	Mode 1	Mode 2	Mode 3	Mode 4
f_{ne} [Hz]	10.36	15.09	17.32	31.92
f_{na} [Hz]	10.05	14.40	17.22	30.74
Error [%]	3.0	4.6	0.6	3.7

Overall, both MAC correlation and natural frequency correspondence between the experimental and analytical results have increased as a result of including soil-springs in the FE-model to represent the effect of the concrete slabs supporting the deck extensions. The refined and manually tuned FE-model is now shown to have been brought closer to the as-built structure, where the overall MAC correlation and natural frequency error seen between the experimental and numerical results are considered to be within reasonable limits considering that this is before any formal updating of the model. By considering the “acceptable” 80 % lower limit for MAC correlation, as proposed by Ewins [63], this refined and manually tuned FE-model is concluded to be a good starting point and reference before further tuning and updating.

10.1 Sensitivity Analysis

An essential step in any FEMU process is identifying, selecting, and quantifying the FE-model’s sensitivity to the potential updating parameters. As presented in Chapter 6, “*Theoretical Background for Finite Element Model Updating*”, a sensitivity analysis followed by the

selection of updating parameters can be a complicated and challenging process that can be highly dependent on both past experience and engineering judgment by the analyst. To overcome these challenges, different methods for sensitivity analysis have been developed. In the following sections, the sensitivity analysis method utilized in this study, along with the final selection of updating parameters, will be presented.

The nine potential updating parameters selected for the updating process of the FE-model of the Stange Railway bridge were selected based on the perceived effect they could have on the modal parameters. These potential updating parameters are also those connected with the greatest uncertainty and are included in the FE-model as modeling parameters. The selected potential updating parameters are presented in Table 13, along with their individual lower- and upper bounds.

Table 13. Parameters selected for sensitivity analysis with lower and upper bounds.

	Parameter	Lower bound	Upper bound
1	Young's modulus of concrete bridge deck and girders [GPa]	27.0	44.0
2	Young's modulus of concrete columns [GPa]	27.0	44.0
3	Mass density of concrete bridge deck and girders [kg/m ³]	2 420.0	2 680.0
4	Mass density of concrete columns [kg/m ³]	2 420.0	2 680.0
5	Mass density of ballast [kg/m ³]	1 630.0	2 140.0
6	Stiffness of bearing spring Hamar [kN/m]	$1.02 * 10^6$	$6.11 * 10^6$
7	Stiffness of bearing spring Oslo [kN/m]	$1.02 * 10^6$	$6.11 * 10^6$
8	Stiffness of soil-spring Hamar [kN/m/m]	$2.20 * 10^6$	$1.32 * 10^6$
9	Stiffness of soil-spring Oslo [kN/m/m]	$2.20 * 10^6$	$1.32 * 10^6$

The limiting bounds for parameters 1 and 2, the Young's modulus of the concrete in the bridge deck, girders and columns, were taken from Table 3-1 in NS-EN 1992-1-1 [45]. The specified concrete quality used in the bridge is according to documentation B45, but as the strength and Young's modulus of concrete tends to increase with time [67], or decrease due to natural degradation, and the possibility of a lower quality concrete being used during construction, this parameter is uncertain. Thus, a lower- and upper bound for the concrete Young's modulus was decided based on the range of different concrete qualities specified in the standard. The bounds for mass density of the concrete used in the bridge deck, girders, and columns, represented by parameters 3 and 4, were adopted from a study by Chen et al. [12]. These are within a reasonable range of what could be expected for reinforced concrete and are thus perceived to be good estimations used for this case. The bounds for mass density of the

ballast, represented by parameter 5, is an uncertain parameter due to the different types of ballast used for railway infrastructure and as the documentation did not state any material properties for the ballast used on the Stange railway bridge. A typical range of mass density of railway ballast was determined based on a study by Ribeiro et al. [68]. After referring with a supplier of railway ballast in Norway, NorStone AS [69], the mass density of ballast typically used in Norway was confirmed to be within the range stated by Ribeiro et al. The upper- and lower bounds for the stiffness of the elastomeric bearings on the Hamar and Oslo side, represented by parameters 6 and 7, were challenging to define as it can be hard to predict the change in material properties of the elastomer as it ages. To decide on these bounds, the same relative change to the initial stiffness value as used by Chen et al. [12] was adopted as the structure in that study has a similar type of elastomeric bearings as the Stange railway bridge. The bounds for parameters 8 and 9, representing the stiffness of the soil-springs underneath the deck extensions on the Hamar and Oslo side, were calculated based on the typical modulus of subgrade reaction (k_s) seen for different types of soil/rock conditions, as presented in Table 11. Thus, a modulus of subgrade reaction of 5 000 kN/m²/m was used for calculating the lower bound and 300 000 kN/m²/m for calculating the upper bound.

After deciding on the potential updating parameters and their respective lower- and upper bounds, a sensitivity analysis of the FE-model with regards to these parameters was conducted. Firstly, the sensitivity of the FE-generated mode shapes with respect to change in the presented potential updating parameters was investigated and assessed using MAC values. For this, an individual FE analysis was first performed using the average values for all parameters, and the mode shapes of the four relevant modes were extracted. Then, FE analyses were performed where each parameter was individually adjusted to its lower- and upper bound, leaving all remaining parameters at average values, and the mode shapes were extracted. The mode shapes extracted using the lower- and upper bounds were then correlated to those extracted with average values using the MAC. The results of this sensitivity analysis are presented in Table 14. A MAC value close or equal to 1 indicates a mode shape with little or no sensitivity to change in the parameter in question. The further away the MAC value is from 1, the more sensitive the mode shape is to that parameter. It can be seen that all mode shapes are not sensitive to parameters 3, 4, and 5, as the MAC values are 1 for all cases of lower- and upper bounds. The mode shapes are shown to be slightly more sensitive

to parameters 1 and 2, but the greatest sensitivity is shown to be for parameters 6, 7, 8, and 9.

Table 14. Effect of parameters on the analytical mode shapes assessed using MAC.

Parameter	Bound	MAC values for each mode [-]			
		1 st	2 nd	3 rd	4 th
1	Lower	0.9964	0.9876	0.9977	0.9993
	Upper	0.9964	0.9735	0.9974	0.9995
2	Lower	0.9998	0.9996	1.0000	0.9984
	Upper	1.0000	0.9999	1.0000	0.9817
3	Lower	1.0000	1.0000	1.0000	1.0000
	Upper	1.0000	1.0000	1.0000	1.0000
4	Lower	1.0000	1.0000	1.0000	1.0000
	Upper	1.0000	1.0000	1.0000	1.0000
5	Lower	1.0000	1.0000	1.0000	1.0000
	Upper	1.0000	1.0000	1.0000	1.0000
6	Lower	0.9475	0.7154	0.9383	0.9934
	Upper	0.9981	0.9974	0.9942	0.9954
7	Lower	0.9873	0.9749	0.9998	0.9413
	Upper	0.9988	0.9967	1.0000	0.9931
8	Lower	0.9911	0.3695	0.8957	0.9999
	Upper	0.9998	0.9998	0.9905	0.9743
9	Lower	0.8209	0.3301	0.9999	0.7939
	Upper	0.9972	0.9967	1.0000	0.9521

The largest and most significant mode shape sensitivity is seen for the lower bound of parameters 8 and 9 for the second mode, having MAC values of 0.3695 and 0.3301, respectively. From the assessment of these modes, it was observed that the modes are barely recognizable compared to their “original” shapes and experimental counterparts. Generally, it was observed that when MAC values became lower than 0.6 – 0.5, it was difficult to recognize the modes. As discussed by Mosavi et al. [27], a MAC value of 0.5 in such a sensitivity analysis represents a dramatic change in mode shape, which is also found to be true for the case in this study. The negligible sensitivity of the mode shapes concerning parameters 3, 4, and 5 is in accordance with what could be expected prior to the sensitivity analysis, as the mode shapes are dependent on the relative distribution of mass and stiffness throughout the system. Thus, changing the mass density of the concrete or the ballast, which are uniformly distributed symmetrical masses, the relative distribution of mass is not changed, hence the mode shapes are not affected. The mode shapes are similarly shown not to be as sensitive to parameters 1 and 2 but have some impact as changing the Young’s

modulus of the concrete evidently has a more significant impact on the relative distribution of stiffness in the system.

After investigating the parameter sensitivity of the mode shapes, a second sensitivity analysis with the natural frequency as the target response was conducted. The method used for this was the same as for the mode shape sensitivity analysis, where the modal parameter of the average value was compared to the lower- and upper bounds. However, this time the resulting sensitivity is represented by the natural frequency error. A negative frequency error indicates that the natural frequency of the mode decreases compared to the average value of the respective parameter, and a positive error indicates an increase of the natural frequency. The resulting sensitivity analysis with respect to the natural frequency of the modes is presented in Table 15. Results of the sensitivity analysis with respect to natural frequency from Table 15 clearly show that all the FE-generated modal frequencies are not sensitive to change in parameter 4. The remaining modal natural frequencies are all shown, to some varying extent, to be sensitive to parameters 1 – 3 and 5 – 9, where the largest sensitivity is shown to be for the third and fourth mode when parameters 8 and 9 are changed.

Table 15. Effect of parameters on the analytical natural frequencies.

Parameter	Bound	Natural frequency error for each mode [%]			
		1 st	2 nd	3 rd	4 th
1	Lower	-9.00	-13.02	-2.52	-0.20
	Upper	7.67	7.81	2.17	0.49
2	Lower	-2.64	-1.88	-0.03	-0.05
	Upper	2.27	1.30	0.02	0.02
3	Lower	1.90	1.89	1.88	1.88
	Upper	-1.80	-1.79	-1.78	-1.78
4	Lower	0.00	0.00	0.00	0.00
	Upper	0.00	0.00	0.00	0.00
5	Lower	1.98	2.00	2.04	2.04
	Upper	-1.87	-1.88	-1.92	-1.92
6	Lower	-1.69	-1.00	-16.46	-0.03
	Upper	0.37	0.15	4.15	0.01
7	Lower	-2.70	-5.51	-0.01	-14.54
	Upper	0.67	1.63	0.00	5.72
8	Lower	-0.66	-0.93	-57.04	-0.01
	Upper	0.36	0.17	33.66	0.01
9	Lower	-4.22	-9.12	0.00	-52.47
	Upper	1.03	2.31	0.00	35.01

From the two separate sensitivity analyses, with mode shape and natural frequency as target response, respectively, how the structure depends on and reacts to the different parameters have been investigated and quantified. For future updating of the FE-model, this is an important factor to understand and of great help when interpreting the change of the modal parameters when the parameter values are adjusted and updated. Moving forward, it is evident that parameter 4, the mass density of the concrete in the columns, is a parameter that does not affect the mode shape nor the natural frequency of the modes. Thus, this parameter is excluded from further analysis.

10.2 FE-model Updating

Having completed the sensitivity analysis and quantified the FE-models sensitivity with respect to the selected updating parameters, the formal updating of the FE-model can commence. The method chosen for this process in this study is a two-step, iterative and manual process where the updating firstly will be conducted as an optimization problem with a limited number of parameters. Secondly, testing of an updating method using an objective function as described in Section 6.4 is performed.

The Stange railway bridge is a complex and somewhat unusual bridge considering its designed boundary conditions. These boundary conditions are additionally connected with uncertainty regarding the mechanical and stiffness properties of these. As a stated goal of this study, the identification and quantification of these boundary conditions are considered as a crucial step towards obtaining an FE-model that can better represent the actual structural behavior of the bridge. From the sensitivity analysis, it was found that the boundary conditions (parameters 6 – 9) are what most significantly influence the modal parameters in the case of the Stange railway bridge, thus these parameters are considered to be the most significant as they are shown to greatly affect the relative stiffness distribution in the structure. For the first step in the model updating process, being the manual optimization method, it was decided to prioritize and maximize the MAC correlation between the experimental and analytical mode shapes by using the parameters found to have the most significant influence on the mode shapes. The goal of this MAC optimization is to decide on the parameter values that generate the most ideal case concerning MAC correlation and then to conclude on these parameter values before further updating. By prioritizing the MAC correlation, the difference between the experimental and analytical mode shapes is minimized, which is perceived to be favorable

over correlating the natural frequencies. This is due to matching analytical and experimental mode pairs can be difficult, especially when there are closely spaced natural frequencies and more complex modes [63]. By then updating or optimizing solely based on the natural frequency correlation of the modes, the mode shapes can be altered to an extent where positive mode pairing is no longer practically possible. Prioritizing the mode shapes and MAC correlation over natural frequency in such an optimization method can also be argued for by assessing the theoretical representation for displacement as a function of time, as given by Equation 10 [55],

$$u(t) = \sum_{n=1}^N \varphi_n q_n(t) \quad (10)$$

Where Φ_n is a mode shape vector and $q_n(t)$ is a scalar as a function of the natural frequency and time. As the theoretical displacement shape of a structure at time t is a summation of the mode shape vectors multiplied with a scalar, which is dependent on the natural frequency, it can be argued that the mode shape is more important. To elaborate, if the natural frequency of a mode deviates from its accurate value will not influence the result as much since it is a scalar. In contrast, if the mode shape vector is incorrect or less accurate, the solution will be far from correct.

The MAC optimization process was initiated by estimating the optimal soil-spring ratio between the Hamar and Oslo side. As the soil-spring at the Oslo side is assumed to be stiffer than the Hamar side, it was decided to fix the modulus of subgrade reaction at an average reference value of 150 000 kN/m²/m while slowly increasing the soil-spring Hamar/Oslo ratio. Starting with a modulus of subgrade reaction of 0 kN/m²/m at the Hamar side, the value was firstly increased from 0 kN/m²/m to 150 000 kN/m²/m with 10 000 kN/m²/m per increment, and the analytical mode shape coordinates were extracted for each mode, at every increment. The analytical mode shapes were then correlated to the experimental mode shapes using the MAC, where the largest average MAC value was found to be at ratios between 0.3 and 0.4. Thus, the resolution of the increments was increased in this area, which resulted in an optimum ratio of 0.33 being identified. After the optimum soil-spring ratio was identified, the next MAC optimization step was to identify at which value of the soil-spring stiffness the average MAC value was maximized. This was done by slowly increasing the

modulus of subgrade reaction from the lower- to upper bound, starting at 5 000 kN/m²/m at the Hamar side and ending at 300 000 kN/m²/m at the Oslo side while maintaining the 0.33 ratio. As with the previous optimization step, the analytical mode shape coordinates were extracted from each iteration, and a MAC correlation was performed with respect to the experimental mode shapes. By increasing the increment resolution in areas of interest, the largest average MAC value was identified for the case with a modulus of subgrade reaction of 28 776 kN/m²/m at the Hamar side and 87 200 kN/m²/m at the Oslo side. This gave a soil-spring stiffness of 126 614 kN/m/m and 383 680 kN/m/m, respectively, which are included in the FE-model as compression-only line-springs extending from the bearings to the bridge end at both ends at both sides.

After concluding on both the optimal soil-spring stiffness ratio and values, the last parameters found to influence the mode shapes, the stiffness of the elastomeric bearings (parameters 6 and 7) was investigated. The mode shape MAC optimization was performed by slowly increasing the stiffness of the bearings from the lower- to upper bound symmetrically. It was considered performing trials of adjusting the stiffness properties of the bearings unsymmetrically. However, an unsymmetrical degradation of the bearings was perceived to be physically unrealistic as the bearings are all identical, the same age, and have all been subjected to the same environmental and mechanical loading. There is also no documentation or visual sign of any repair work or damage indicating a difference in the stiffness between the bearings. After adjusting the stiffness property of the bearings symmetrically and with constant increments from the lower- to upper bound, it was found that the MAC correlation of the mode shapes was not significantly increased or decreased. This is assumingly due to the symmetrical changes of the bearing stiffnesses do not significantly alter the overall relative stiffness distribution in the structure, which is necessary for the mode shapes to have any significant change. It was found that the theoretical stiffness property used as the reference value in the initial FE-model, which is in accordance with available documentation and bearing manufacturers' specifications, generated the most ideal case with regards to MAC correlation of the analytical and experimental mode shapes. In Table 16, the parameter values generating the most ideal case for mode shape MAC correlation are presented.

Table 16. Parameter values in the MAC-optimized FE-model.

Parameter		MAC-optimized FE-model
1	Young's modulus of concrete bridge deck and girders [GPa]	36.0
2	Young's modulus of concrete columns [GPa]	36.0
3	Mass density of concrete bridge deck and girders [kg/m ³]	2 548.5
4	Mass density of concrete columns [kg/m ³]	2 548.5
5	Mass density of ballast [kg/m ³]	1 800.0
6	Stiffness of bearing spring Hamar [kN/m]	1 629 630.0*
7	Stiffness of bearing spring Oslo [kN/m]	1 629 630.0*
8	Stiffness of soil-spring Hamar [kN/m/m]	126 614.0
9	Stiffness of soil-spring Oslo [kN/m/m]	383 680.0
*Total stiffness contribution from two elastomeric bearings		

Figure 45 presents the resulting MAC correlation between the experimental and analytical FE-computed mode shapes after MAC optimization of the analytical mode shapes. A general increase in MAC correlation can be observed for all modes when compared to previous results from before any updating, which are presented in Figure 44. The increase in MAC correlation is shown to be 1 % for Mode 1, 3 % for Mode 2, 1 % for Mode 3, and 3 % for Mode 4. The average MAC correlation of all modes after the manual mode shape MAC optimization method is 89 %. A visual comparison of these mode shapes and their experimental counterparts is presented in Figure 46.

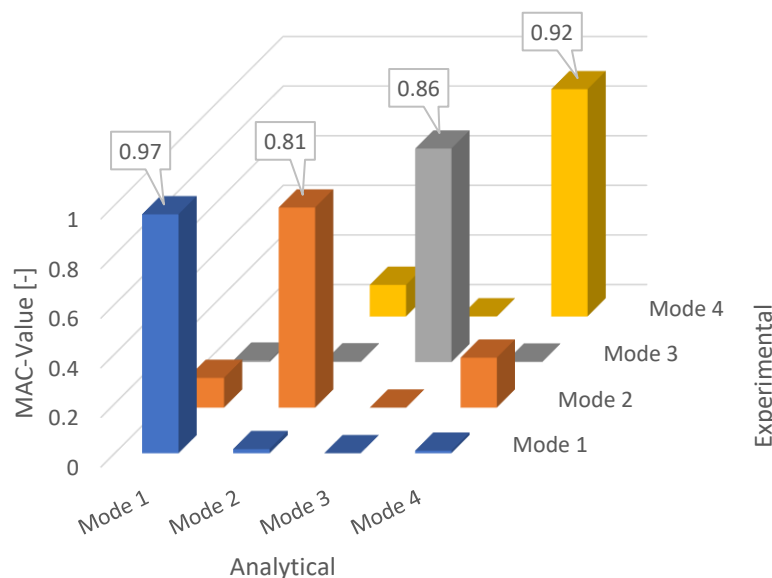


Figure 45. Correlation of experimental and analytical MAC-optimized mode shapes.

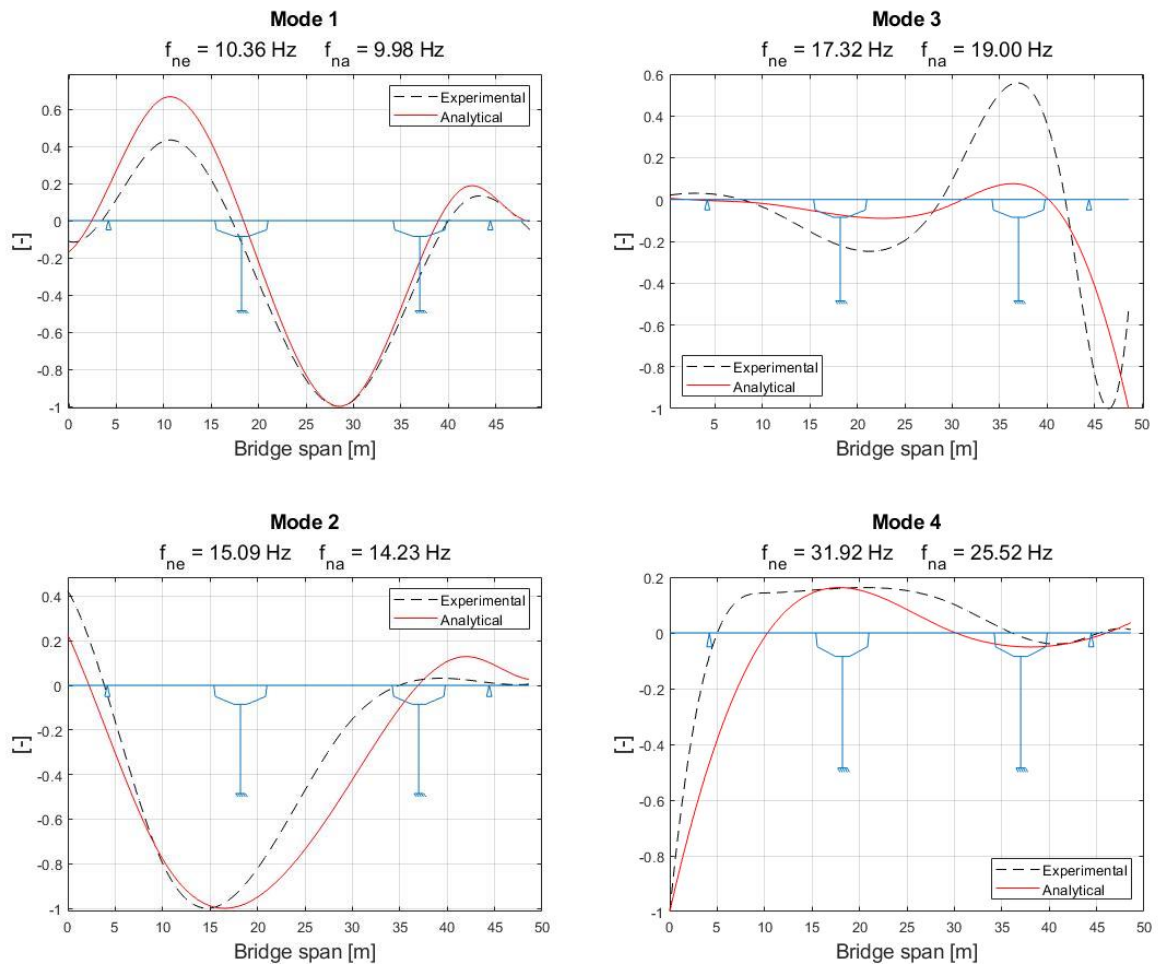


Figure 46. Experimental vs. analytical MAC-optimized modes.

Having prioritized the mode shape MAC correlation between the experimental and analytical modes has evidently had a negative effect on the natural frequency error of the modes, as presented in Table 17. This increase in frequency error was expected, but at the same time, also accepted.

Table 17. Natural frequencies of experimental and analytical MAC-optimized modes.

	Mode 1	Mode 2	Mode 3	Mode 4
f_{ne} [Hz]	10.36	15.09	17.32	31.92
f_{na} [Hz]	9.98	14.23	19.00	25.52
Error [%]	3.7	5.7	9.7	20.1

Prioritizing one modal response over another, resulting in improvements in the prioritized response, typically comes at the expense of the other responses [27]. The increase in

frequency error was accepted based on the average natural frequency error of all modes still being less than 10 %. A 10 % natural frequency error is perceived to be an acceptable error given the type of structure investigated and the level of uncertainty associated with it. Živanović et al. [10] discuss the natural frequency error experienced for different types and sizes of structures, where updating of smaller and less complicated bridge structures, such as footbridges, tend to have smaller frequency errors compared to large and more complex full-scale road and railway bridges. Živanović et al. further express that such larger structures tend to have many more parameters that are important for their dynamic behavior, but that these parameters can be difficult to incorporate with a sufficient level of detail in an FE-model, which could have a significant effect on the natural frequencies. The complexity and size of a structure is also discussed to affect the quality of the recorded experimental data, where data from smaller structures tend to be of higher quality. In addition to these complicating factors, Mosavi et al. [27] argue for the uncertainty of the extracted modes also being affected by what type of vibration data they are extracted from, where higher modes tend to be more uncertain as they often are not fully excited when using ambient vibrations. This could also affect results in this study as the extracted modes are based on free vibration data. However, as the MAC correlation is shown to be good also for the higher modes, the excitement of the modes is assumed to be sufficient and could not alone argue for a higher accepted frequency error. The discussed uncertainty factors regarding natural frequency have combined supported the accepted average frequency error in the results, and also seeing an increase in frequency error for higher modes is thus in accordance with what could be expected.

As the values for the updating parameters shown to most significantly affect the MAC correlation were decided through optimization of the MAC values, the second step of FEMU of the FE-model was conducted using an objective function and the remaining updating parameters. Prioritizing the MAC correlation had evidently negatively affected the natural frequency errors. Thus, it was decided to apply an objective function with natural frequency as target response using parameters 1, 2, 3, and 5 in an attempt to increase the natural frequency correspondence. The sensitivity-based and iterative FEMU procedure conducted for this purpose is as presented in the flowchart of Figure 5, following the theory and equations presented in Section 6.4. As a similar level of confidence in both responses and

parameters are assumed for this process, the weighing matrices \mathbf{C}_R and \mathbf{C}_P were both defined with an equal coefficient of 1 along the diagonals.

After the completion of several iterations, continuously updating the parameters and other required inputs for the objective function in each iteration, it was observed that the average natural frequency error of the modes did not improve. The updated parameter values (\mathbf{P}_u) did also show a close to negligible difference compared to parameter values of the previous iteration ($\mathbf{P}_{(i)}$). The natural frequency error of the individual modes was in two cases slightly decreased, whereas the remaining two modes saw an increase in the natural frequency error. This effect is partly assumed to be due to both the inherent geometrical properties of the bridge, being the unsymmetrical span-lengths, and the complexity of some of the modes. When using the given parameters, it is therefore reasonable that improvements in natural frequency correspondence of certain modes will be at the expense of the correspondence of other modes, combinedly not improving the average natural frequency correspondence. It is also possible that the updating parameters used for this FEMU procedure (parameters 1, 2, 3, and 5) do not have sufficient influence on either the relative mass- or stiffness distribution to greatly affect the natural frequency of the modes. One could also assume, due to the minimal changes seen for the updated parameter values, that the initial reference values used for these parameters, which corresponds to the available bridge documentation, are very good estimates and are thus possibly already the most ideal case considering the natural frequency correspondence. Very small or negligible differences in either the FE-model's modal parameters or the updated parameter values can indicate that convergence of the objective function is achieved, making further iterations unnecessary.

The parameters used for the mode shape MAC correlation optimization are shown to have a more significant influence on the natural frequency of the modes. Consequently, as these parameters prior to the sensitivity-based objective function FEMU were decided as a result of prioritizing the MAC correlation, major improvements of the average natural frequency correspondence were found to be challenging to achieve when using the presented method in this study. Thus, the results obtained from the manual mode shape MAC optimization will represent the final and updated FE-model. The results of the FE-model updating process for the identified four modes are presented in Table 18, comparing the experimental modal

parameters to the initial and updated analytical FE-computed modal parameters. For a flowchart presenting the complete process of FEMU applied in this study, see Appendix C.

Table 18. Results of the FE-model updating process for the identified modes.

Mode number	Experimental f_{ne} [Hz]	Initial analytical f_{na} [Hz]	Error [%]	Updated analytical f_{na} [Hz]	Error [%]	Initial MAC [-]	Updated MAC [-]
1	10.36	9.36	9.7	9.98	3.7	0.66	0.97
2	15.09	14.71	2.5	14.23	5.7	0.02	0.81
3	17.32	13.60	21.5	19.00	9.7	0.84	0.86
4	31.92	12.41	61.1	25.52	20.1	0.91	0.92
Average			23.7		9.8	0.61	0.89

Of the identified modes, a general increase of MAC correlation is seen for all modes. The largest increase in MAC correlation after FEMU is seen for Mode 1 and 2, with an increase of 31 % and 79 %, respectively. The average MAC correlation after updating is 89 %, which indicates consistent correspondence and well-correlated modes between the experimental and analytically computed mode shapes. The average natural frequency error is reduced from 23.7 % to 9.8 % between the initial and updated FE-model, which is perceived as an acceptable error given the limitations and uncertainties stated for this study. The modal analysis of the updated FE-model has proven the significance of these four identified dominant, recurring, and distinct modes. Cumulatively, for the first nine vertical modes within the investigated frequency range (< 40 Hz), the Modal Participating Mass Ratio of these modes represents 98 % of the total response, where the four presented modes cumulatively represent about 60 % of the total response. Given the level of correlation and total Modal Participating Mass Ratio presented for these four modes, the final and updated FE-model is perceived to be good and a closer true representation of the as-built structure.

11 Verification of FE Computed Accelerations and Displacements

Beyond the scope of the presented FEMU process and initial goals of this study, this chapter aims to investigate the applicability of the concluding, updated FE-model. Here, the goal is to investigate whether a simplified but yet sufficiently mode shape correlated FE-model is able to render the experimental accelerations and displacements obtained as responses to the passing passenger trains. Subsequently, a dynamic analysis was conducted using a suitable load model for high-speed trains. From the analysis, both accelerations and displacements

were compared to experimental responses and the standardized requirements. Firstly, the selected load model and the available information are presented.

Stated in Bane NOR's technical regulations, section 525 "Bruer og Konstruksjoner" [70], railways designed for speeds exceeding 200 km/h, load models according to section 6.4.6 in Eurocode 1 [59] should be used. Subsequently, for the continuous structure of the Stange railway bridge, with spans longer than 7 meters, HSLM-A is the applicable load model according to Eurocode 1, table 6.4 [59]. Moreover, the standard also expresses that the load model represents the loading from passenger trains at speeds exceeding 200 km/h and is thus a suitable load model for both the express- and local trains measured at Stange. However, as the Stange railway overpass is located close to Stange station, it is unlikely that the crossing passenger trains are traveling at such a speed. At which speed they are traveling is unknown and can vary, but Bane NOR has indicated a speed limit of 80 km/h when crossing the bridge. Thus, when setting up the dynamic analysis in CSiBridge, 80 km/h was assumed to be a reasonable and realistic reference speed for comparing the resulting accelerations with the experimental data. To keep the dynamic analysis simple, one of the ten possible load models (HSLM-A1-10) was selected. The selected load model, HSLM-A10, can be seen in Figure 47, where the corresponding number of coaches, distances, and loading are given in Table 19.

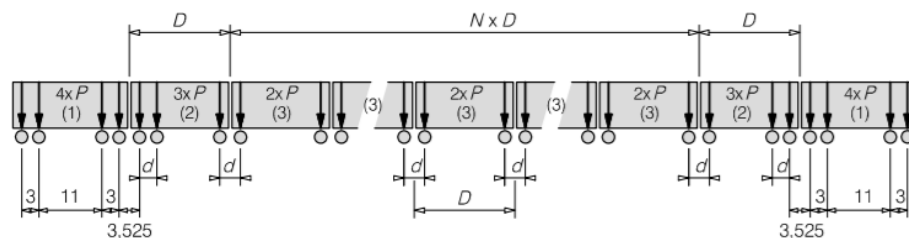


Figure 47. Load model HSLM-A [59].

Table 19. Load model HSLM-A10 [59].

Universal train	Number of intermediate coaches, N	Coach length, D [m]	Bogie axle spacing, d [m]	Point force, P [kN]
A10	11	27	2.0	210

To perform the dynamic analysis with the presented load model, a theoretical structural damping was calculated according to table 6.6 in Eurocode 1 [59]. For the prestressed

concrete bridge, with the longest span stretching up to 18 meters, the critical damping, ζ_{cr} , was set to 1.14 %. Furthermore, an additional damping, $\Delta\zeta$, as a function of span length was calculated according to Eurocode 1, equation 6.13 [59]. Resultingly, the total theoretical structural damping was then set equal to 1.32 % according to Eurocode 1, equation 6.12 [59]. The structural damping was further recalculated to mass- and stiffness-proportional damping coefficients δ and η , respectively, and incorporated in the updated FE-model by utilizing the relations presented in Equations 11 and 12 [71]. There, ω_i and ω_j are two specific natural frequencies assumed to have the same damping.

$$\delta = \frac{2\zeta}{\omega_i + \omega_j} \quad (11)$$

$$\eta = \omega_i \omega_j \delta \quad (12)$$

According to Figure 25, based on 92 train-crossings, the measured accelerations occurred in the range from 0.05 – 0.33 g. However, as these are extreme values, independent of train type and speed, the maximum accelerations obtained from the passenger trains (express and local) are assumed to be more consistent and representative. Thus, 0.05 - 0.26 g was set as a reference for comparison from the experimental data (see Figure 25), where 87 % of these had maximum acceleration located at Sensor 5.

Based on both experimental data and dynamic analysis, Table 20 presents the obtained accelerations from the assumed crossing speed, 80 km/h, the desired speed at Dovrebanen, 250 km/h, and their respective locations. It can be seen that from the reference points formed by the sensors, the maximum accelerations occur at Sensor 5 in all cases. It can also be seen that when the absolute maximum of the FE-model is investigated, the maximum accelerations occur beyond Sensor 5, on the far end towards Hamar. However, as there is no sensor at this location, the values are not directly comparable to the experimental data. Relative to the allowed accelerations of a railway bridge deck of 0.35 g, according to NS-EN 1990, section A2.4.4.2.1 (4) [37], the obtained accelerations from both experimental data and the dynamic analysis are all acceptable.

Table 20. Experimental vs. analytical accelerations.

Train speed [km/h]	Experimental data		Dynamic analysis	
	Max. Acceleration [g]	Location	Max. Acceleration [g]	Location
80*	0.05 – 0.26	Sensor 5	0.31	End Hamar side
			0.27	Sensor 5
250	-	-	0.21	End Hamar side
			0.19	Sensor 5

* 80 km/h is an assumed train crossing speed

By integrating the experimental accelerations twice, displacements as a function of time could be obtained. From then, the maximum displacements were extracted from each train crossing. Based on passenger trains only, the largest average maximum displacement was found in the mid-span, at Sensor 3. From the dynamic analysis, the same result was obtained; maximum displacement in the mid-span, at Sensor 3. According to Table 21, the obtained displacements from both experimental and analytical data are the same for all practical purposes: around 1 mm.

According to Bane NOR's technical regulations [70], section 525 "Bruer og Konstruksjoner", vertical displacements of the bridge deck should satisfy the comfort criteria set in NS-EN 1990, section A2.4.4.3 [37]. For the train speed given in Table 21, the maximum allowed displacement for the mid-span was set to 15 mm. It can be seen that both the experimental- and analytical displacements satisfy the criteria by a significant margin. Moreover, the obtained displacements also satisfy the stricter allowed displacement of 3.5 mm for the short, assumed cantilevering ends of 4.2 m.

Table 21. Experimental vs. analytical displacements.

Train speed [km/h]	Experimental data		Dynamic analysis	
	Average max. displacement [mm]	Location	Max. displacement [mm]	Location
80*	0.90	Sensor 3	1.14	Sensor 3
250	-	Sensor 3	1.18	Sensor 3

* 80 km/h is an assumed train crossing speed

The presented dynamic analysis has proven that the obtained accelerations and displacements are in an acceptable range relative to the standardized requirements. Moreover, the analytical updated FE-model is able to reproduce responses that correlate well

with those that are experimentally obtained. Even though there are a number of potential sources of error regarding the assumed train speed, the complexity of the model, and the load model, the results seem reasonable and can thus indicate that the mode shape correlated FE-model is efficient also in a dynamic analysis. Resultingly, the updated FE-model is able to reduce the maximum accelerations from 0.53 g to 0.31 g, and thus the measures conducted through the FEMU process evidently have a positive effect on rendering more accurate structural responses obtained through a dynamic analysis.

12 Conclusion

This study presents the implementation of a sensitivity-based, iterative, and manual FEMU process on the Stange railway overpass. Experimental operational condition, output-only acceleration data was successfully collected, which through use of the SSI-cov method implemented in MATLAB allowed for identification of four dominant, distinct and recurring modes within a realistic frequency range. An initial, purely documentation-based FE-model was developed using CSiBridge, and analytical modal analysis was performed to identify its modal parameters. Initial correlation of the experimental and analytically computed modal parameters indicated a low degree of correlation. However, through refinement and manual tuning of the FE-model, key modelling parameters were included, and the correlation of the modal parameters was significantly increased. Through a comprehensive sensitivity analysis of the FE-model's parameters, updating parameters found to greatly affect the relative mass- and stiffness distribution was identified. By implementing a manual and iterative mode shape MAC optimization method, the most ideal case regarding the relevant updating parameters was identified. Further FEMU was conducted using an objective function with natural frequency as target response. Combinedly, the manual tuning and FEMU process increased the average mode shape MAC correlation from 61 % to 89 % and reduced the average natural frequency error from 23.7 % to 9.8 %.

The updated FE-model is considered to have a very good average mode shape agreement and a reasonable average natural frequency error relative to the identified experimental modal parameters. The poor initial modal parameter correlation exemplified the common mismatch between documentation-based and as-built structures, but by including additional critical model parameters, this mismatch was minimized. For the case of the Stange railway overpass, the most critical model parameter was found to be the effect of the undocumented concrete slabs acting as additional supports underneath the initially assumed cantilevering bridge deck extensions. The more manual FEMU process utilized in this study has provided a greater understanding of the structure and its dynamic behavior, where the significant influence of its boundary conditions has been thoroughly investigated. The success of the complete FEMU process was found to depend on fair engineering judgment, but the chosen methods and processes have been proven to be manually manageable and successful, given the limitations imposed in this study.

Beyond the original goals of this study, a dynamic analysis with a suitable load model was performed to investigate if an updated FE-model with the level of complexity and with the level of modal parameter correlation achieved could provide accurate estimates of accelerations and displacements. The FE-computed accelerations and displacements were found to be within the requirements stated in standards and were also found to be close to the experimental results. Given the simplified FE-model and uncertainties surrounding the actual versus analytical load model, the FE-model is perceived to generate acceptable estimates of accelerations and displacements.

In relation to the stated overall goal of this study, which corresponds to the goals of initial work packages in the NEAR project, this study has successfully performed initial modal identification of the Stange railway overpass and developed a preliminary, updated FE-model. This achievement will lay the ground for further work in the NEAR project and provides the partners in Bane NOR with great value and effective, generally applicable methods for the structural assessment of railway bridges.

13 Future Work

The work presented in this study has proven to satisfactorily assess and reach the overall goal of conducting FEMU, form a preliminary, updated FE-model, and obtain a good understanding of the dynamic behavior of the Stange railway overpass. Furthermore, during the process of obtaining a high-fidelity FE-model, a set of recommendations for future work has been formed. The recommendations are based on observations regarding both experimental data and FE-modelling and should help facilitate future work on the bridge in focus as well as highlight key aspects for further development within system identification and FEMU.

As a part of performing system identification and thus extracting modal parameters, it was at an early stage observed that the number of sensors available led to a large amount of data processing. Even though the sensor locations were found to be suitable and effective, the limited amount of sensors led to extensive work in distinguishing modes. Thus, for future work, a sufficient amount of sensors/configurations is deemed necessary to distinguish modes and identify structural uncertainties at the bridge ends especially, but also to identify modes that the utilized configurations could not identify. The sensors should also be installed for a longer period of time to ensure good, representative data from all train types.

Even though the final, updated FE-model is found to be satisfactory, there are still discrepancies that can be improved. For the simplified FE-model used in this study, it was concluded that the selected parameters could not increase the correlation further. Thus, for future work, it is recommended to form a more complex FE-model utilizing, e.g., shell and/or solid elements and investigate parameters such as non-structural elements and a parameter representing the continuity of the railway track. Resultingly in the calibration process, setting up and running an automatic algorithm using specialized software is also seen as a point of interest to further improve the correlation.

Lastly, it is recommended to obtain more accurate train data and thus generate a better representation of the actual trains in the dynamic load model. In that way, the analytical dynamic analysis can be performed using the actual train speeds as it evidently had a significant effect on the accelerations of the bridge deck.

References

- [1] F. Hemez and C. Farrar, "A Brief History of 30 Years of Model Updating in Structural Dynamics," in *Special Topics in Structural Dynamics*, 1st ed., vol. 6, Springer International Publishing, 2014, pp. 53–71. doi: 10.1007/978-3-319-04729-4_6.
- [2] H.-P. Chen, *Structural Health Monitoring of Large Civil Engineering Structures*. John Wiley & Sons, 2018.
- [3] M. Friswell and J. E. Mottershead, *Finite element model updating in structural dynamics*, vol. 38. Springer Science & Business Media, 2013.
- [4] L. Deng and C. S. Cai, "Bridge Model Updating Using Response Surface Method and Genetic Algorithm," *Journal of Bridge Engineering*, vol. 15, no. 5, pp. 553–564, 2010, doi: 10.1061/(ASCE)BE.1943-5592.0000092.
- [5] T. H. T. Chan, Z. X. Li, Y. Yu, and Z. H. Sun, "Concurrent multi-scale modeling of civil infrastructures for analyses on structural deteriorating—Part II: Model updating and verification," *Finite Elements in Analysis and Design*, vol. 45, no. 11, pp. 795–805, 2009, doi: 10.1016/j.finel.2009.06.008.
- [6] B. Moaveni and I. Behmanesh, "Effects of changing ambient temperature on finite element model updating of the Dowling Hall Footbridge," *Engineering Structures*, vol. 43, pp. 58–68, 2012, doi: 10.1016/j.engstruct.2012.05.009.
- [7] W. Park, H.-K. Kim, and P. Jongchil, "Finite Element Model Updating for a Cable-Stayed Bridge Using Manual Tuning and Sensitivity-Based Optimization," *Structural Engineering International*, vol. 22, no. 1, pp. 14–19, 2012, doi: 10.2749/101686612X13216060212870.
- [8] Y. Ding and A. Li, "Finite Element Model Updating for the Runyang Cable-Stayed Bridge Tower Using Ambient Vibration Test Results," *Advances in Structural Engineering*, vol. 11, no. 3, pp. 323–335, 2008, doi: 10.1260/136943308785082599.
- [9] W.-X. Ren and H.-B. Chen, "Finite element model updating in structural dynamics by using the response surface method," *Engineering Structures*, vol. 32, no. 8, pp. 2455–2465, 2010, doi: 10.1016/j.engstruct.2010.04.019.
- [10] S. Živanović, A. Pavic, and P. Reynolds, "Finite element modelling and updating of a lively footbridge: The complete process," *Journal of Sound and Vibration*, vol. 301, no. 1–2, pp. 126–145, 2007, doi: 10.1016/j.jsv.2006.09.024.
- [11] I. Olofsson *et al.*, "Assessment of European railway bridges for future traffic demands and longer lives – EC project 'Sustainable Bridges,'" *Structure and Infrastructure Engineering*, vol. 1, pp. 93–100, 2005, doi: 10.1080/15732470412331289396.
- [12] X. Chen, P. Omenzetter, and S. Beskhyroun, "Calibration of the Finite Element Model of a Twelve-Span Prestressed Concrete Bridge Using Ambient Vibration Data," in *7th European Workshop on Structural Health Monitoring*, Nantes, France, 2014, pp. 1388–1395. doi: 10.13140/2.1.1497.7603.
- [13] E. Reynders, "System Identification Methods for (Operational) Modal Analysis: Review and Comparison," *Archives of Computational Methods in Engineering*, vol. 19, no. 1, pp. 51–124, 2012, doi: 10.1007/s11831-012-9069-x.
- [14] Á. Cunha and E. Caetano, "Experimental Modal Analysis of Civil Engineering Structures," *SOUND AND VIBRATION*, vol. 40, no. 6, pp. 12–20, 2006.
- [15] T. Holtet, "Dette skal bli Norges lengste jernbanebru," *Jernbanemagasinet*, 2020. <http://jernbanemagasinet.no/artikler/dette-skali-bli-norges-lengste-jernbanebru/> (accessed Mar. 31, 2021).
- [16] E. Erduran, "NEAR: Next Generation Finite Element Calibration Methods for Railway Bridges," Oslo Metropolitan University, Dept. of Civil Eng. and Energy Tech., Oslo, Norway, 2020.
- [17] H. Arksey and L. O'Malley, "Scoping studies: towards a methodological framework," *International Journal of Social Research Methodology*, vol. 8, no. 1, pp. 19–32, 2005, doi: 10.1080/1364557032000119616.

- [18] F. Lorenzoni, N. De Conto, F. da Porto, and C. Modena, "Ambient and free-vibration tests to improve the quantification and estimation of modal parameters in existing bridges," *J Civil Struct Health Monit*, vol. 9, no. 5, pp. 617–637, 2019, doi: 10.1007/s13349-019-00357-4.
- [19] M. Hiatt *et al.*, "Finite Element Model Updating of a PSC Box Girder Bridge Using Ambient Vibration Test," *Advanced Materials Research*, vol. 168–170, pp. 2263–2270, 2010, doi: 10.4028/www.scientific.net/AMR.168-170.2263.
- [20] P. Omenzetter *et al.*, "Forced and ambient vibration testing of full scale bridges," The LRF Centre for Safety and Reliability Engineering, Aberdeen, UK, UNI/578, 2013. doi: 10.13140/2.1.1168.5448.
- [21] A. C. Altunışık, A. Bayraktar, B. Sevim, and F. Birinci, "Vibration-based operational modal analysis of the Mikron historic arch bridge after restoration," *Civil Engineering and Environmental Systems*, vol. 28, no. 3, pp. 247–259, 2011, doi: 10.1080/10286608.2011.588328.
- [22] S. Qin, Y.-L. Zhou, H. Cao, and M. A. Wahab, "Model Updating in Complex Bridge Structures using Kriging Model Ensemble with Genetic Algorithm," *KSCCE Journal of Civil Engineering*, vol. 22, no. 9, pp. 3567–3578, 2018, doi: 10.1007/s12205-017-1107-7.
- [23] O. S. Bursi, A. Kumar, G. Abbiati, and R. Ceravolo, "Identification, Model Updating, and Validation of a Steel Twin Deck Curved Cable-Stayed Footbridge," *Computer-Aided Civil and Infrastructure Engineering*, vol. 29, no. 9, pp. 703–722, 2014, doi: 10.1111/mice.12076.
- [24] Ø. W. Petersen and O. Øiseth, "Sensitivity-based finite element model updating of a pontoon bridge," *Engineering Structures*, vol. 150, no. 1, pp. 573–584, 2017, doi: <https://doi.org/10.1016/j.engstruct.2017.07.025>.
- [25] Z. Li, J. Fu, Q. Liang, H. Mao, and Y. He, "Modal identification of civil structures via covariance-driven stochastic subspace method," *Mathematical Biosciences and Engineering*, vol. 16, no. 5, p. 5709, 2019, doi: 10.3934/mbe.2019285.
- [26] A. Otto, "OoMA Toolbox." <https://se.mathworks.com/matlabcentral/fileexchange/68657-ooma-toolbox> (accessed Mar. 09, 2021).
- [27] A. A. Mosavi, H. Sedarat, S. M. O'Connor, A. Emami-Naeini, and J. Lynch, "Calibrating a high-fidelity finite element model of a highway bridge using a multi-variable sensitivity-based optimisation approach," *Structure and Infrastructure Engineering*, vol. 10, no. 5, pp. 627–642, 2014, doi: 10.1080/15732479.2012.757793.
- [28] S. Sehgal and H. Kumar, "Structural Dynamic Model Updating Techniques: A State of the Art Review," *Archives of Computational Methods in Engineering*, vol. 23, no. 3, pp. 515–533, 2016, doi: 10.1007/s11831-015-9150-3.
- [29] H. Moravej, S. Jamali, T. H. T. Chan, and A. Nguyen, "Finite element model updating of civil engineering infrastructures: a literature review," in *Proceedings of the 8th International Conference on Structural Health Monitoring of Intelligent Infrastructure (SHMII 2017)*, Red Hook, NY, USA, 2018, vol. 2, pp. 1099–1110.
- [30] R. Allemang, "The modal assurance criterion - Twenty years of use and abuse," *Sound & vibration*, vol. 37, pp. 14–23, 2003.
- [31] R. J. Allemang and D. L. Brown, "A Correlation Coefficient for Modal Vector Analysis," in *Proceedings of the 1st International Modal Analysis Conference*, Orlando, Florida, 1982, pp. 110–116.
- [32] Y. B. Yang and Y. J. Chen, "Direct versus iterative model updating methods for mass and stiffness matrices," *International Journal of Structural Stability and Dynamics*, vol. 10, 2010, doi: 10.1142/S0219455410003518.
- [33] J. Brownjohn, P. Moyo, P. Omenzetter, and Y. Lu, "Assessment of Highway Bridge Upgrading by Dynamic Testing and Finite-Element Model Updating," *Journal of Bridge Engineering*, vol. 8, no. 3, p. 12, 2003, doi: 10.1061/(ASCE)1084-0702(2003)8:3(162).
- [34] "Norge i bilder." <https://www.norgebilder.no/> (accessed Mar. 18, 2021).

- [35] *Google Maps*.
https://www.google.no/maps/@60.7196906,11.1930592,3a,90y,47.12h,94.32t/data=!3m6!1e1!3m4!1sJOahgDnPjqNEDQy_3aqAXw!2e0!7i16384!8i8192 (accessed Feb. 13, 2020).
- [36] Rambøll and Sweco, "Utbygging Eidsvoll – Hamar (UEH) Undergang for Fv222 ved Stange stasjon, kapasitetsvurdering," UEH-55-A-25144, 2020.
- [37] "Eurocode: Basis of structural design," NS-EN 1990:2002+A1:2005+NA:2016, 2016.
- [38] C. Freudenrich, "How Space Shuttles Work," *HowStuffWorks*, 2001.
<https://science.howstuffworks.com/space-shuttle.htm> (accessed Mar. 22, 2021).
- [39] M. P. Collins, D. Mitchell, and E. C. Bentz, "Shear design of concrete structures," in *iStructE*, London, 2008, pp. 32–39.
- [40] SAP2000, *Computers & Structures, Inc.* 2019.
- [41] Ansys. <https://www.ansys.com/> (accessed Apr. 06, 2020).
- [42] CSI Bridge, *Computers & Structures, Inc.* 2010.
- [43] J. M. W. Brownjohn, P.-Q. Xia, H. Hao, and Y. Xia, "Civil structure condition assessment by FE model updating: methodology and case studies," *Finite Elements in Analysis and Design*, vol. 37, no. 10, pp. 761–775, 2001, doi: 10.1016/S0168-874X(00)00071-8.
- [44] W. E. Daniell and J. H. G. Macdonald, "Improved finite element modelling of a cable-stayed bridge through systematic manual tuning," *Engineering Structures*, vol. 29, no. 3, pp. 358–371, 2007, doi: 10.1016/j.engstruct.2006.05.003.
- [45] "Eurocode 2: Design of concrete structures - Part 1-1: General rules and rules for buildings," NS-EN 1992-1-1:2004+A1:2014+NA:2018, 2018.
- [46] "Concrete — Specification, performance, production and conformity," NS-EN 206:2013+A1:2016+NA:2020, 2020.
- [47] L. Bornet, A. Andersson, J. Zwolski, and J.-M. Battini, "Influence of the ballasted track on the dynamic properties of a truss railway bridge," *Structure and Infrastructure Engineering*, vol. 11, no. 6, pp. 796–803, 2015, doi: 10.1080/15732479.2014.912242.
- [48] "Lagersystemer," *Brosjyrer - Kataloger*. <http://www.spennteknikk.no/brosjyrer-kataloger/> (accessed Nov. 25, 2020).
- [49] R. D. Cook, D. S. Malkus, M. E. Plesha, and R. J. Witt, *Concepts and Applications of Finite Element Analysis*, 4th ed. John Wiley & Sons, 2001.
- [50] "Unquake." <https://www.unquake.co> (accessed Feb. 26, 2021).
- [51] "Analog Devices." <https://www.analog.com/en/index.html> (accessed Feb. 26, 2021).
- [52] "Products." <https://www.unquake.co/en/products> (accessed Feb. 26, 2021).
- [53] "Grafiske togruter, fastlagt rutetermin R21." <https://www.banenor.no/kundeportal/ruter-og-sportilgang/grafiske-togruter2/> (accessed Mar. 09, 2021).
- [54] MATLAB, *MathWorks*. R2020a, 2020.
- [55] A. Chopra, *Dynamics of Structures*, 4th ed. Pearson Education Limited, 2015.
- [56] M. Ülker-Kaustell and R. Karoumi, "Application of the continuous wavelet transform on the free vibrations of a steel–concrete composite railway bridge," *Engineering Structures*, vol. 33, pp. 911–919, 2011, doi: 10.1016/j.engstruct.2010.12.012.
- [57] B. Peeters, "System Identification and Damage Detection in Civil Engineering," PhD thesis, Department of Civil Engineering, K.U.Leuven, 2000.
- [58] M. Majka and M. Hartnett, "Effects of speed, load and damping on the dynamic response of railway bridges and vehicles," *Computers & Structures*, vol. 86, no. 6, pp. 556–572, 2008, doi: 10.1016/j.compstruc.2007.05.002.
- [59] "Eurocode 1: Actions on structures - Part 2: Traffic loads on bridges," NS-EN 1991-2:2003+NA:2010, 2010.
- [60] "Cubic spline data interpolation - MATLAB spline - MathWorks Nordic." <https://se.mathworks.com/help/matlab/ref/spline.html> (accessed Mar. 25, 2021).
- [61] M. Pastor, M. Binda, and T. Harčarik, "Modal Assurance Criterion," *Procedia Engineering*, vol. 48, pp. 543–548, 2012, doi: 10.1016/j.proeng.2012.09.551.

- [62] M. Nieto, M. Elsayed, and D. Walch, "Modal Participation Factors And Their Potential Applications In Aerospace: A Review," presented at the CSME International Congress 2018, Toronto, Canada, 2018. doi: 10.25071/10315/35254.
- [63] D. J. Ewins, "Model validation: Correlation for updating," *Sadhana*, vol. 25, no. 3, pp. 221–234, 2000, doi: 10.1007/BF02703541.
- [64] K. R. Arora, *Soil Mechanics and Foundation Engineering*, 6th ed. Standard Publishers Distributions, 2004.
- [65] O. U. Ubani, C. M. O. Nwaiwu, J. I. Obiora, and E. O. Mezie, "Effect of soil compressibility on the structural response of box culverts using finite element approach," *Nigerian journal of technology*, vol. 39, no. 1, pp. 42–51, 2020, doi: 10.4314/njt.v39i1.5.
- [66] J. E. Bowles, *Foundation Analysis and Design*, 5th ed. McGraw-Hill, 1997.
- [67] P. Gjerp, S. Smepllass, M. Maage, B. Pedersen, B. Kristiansen, and J. Injar, *Betong - regelverk, teknologi og utførelse*, 1st ed. Byggenæringens Forlag AS, 2015.
- [68] D. Ribeiro, R. Calçada, R. Delgado, M. Brehm, and V. Zabel, "Finite element model updating of a bowstring-arch railway bridge based on experimental modal parameters," *Engineering Structures*, vol. 40, pp. 413–435, 2012, doi: 10.1016/j.engstruct.2012.03.013.
- [69] "NorStone AS." <https://www.norstone.no/en/home> (accessed Apr. 28, 2021).
- [70] "Bruer og konstruksjoner/Prosjektering og bygging/Laster – Teknisk regelverk." https://trv.banenor.no/wiki/Bruer_og_konstruksjoner/Prosjektering_og_bygging/Laster#.C3.98vrige_lastemodeller_.28HSLM_A_og_HSLM_B.29 (accessed May 18, 2021).
- [71] "Damping coefficients - Technical Knowledge Base - Computers and Structures, Inc. - Technical Knowledge Base." <https://wiki.csiamerica.com/display/kb/Damping+coefficients> (accessed May 18, 2021).

Appendices

Appendix A – Literature List

Table A.1. Literature list.

Title	Author(s)	Year	Source
A Multiscale Finite Element Model Validation Method of Composite Cable-Stayed Bridge Based on Structural Health Monitoring System	Zhong et al.	2015	Shock and Vibration
A multistage FE updating procedure for damage identification in large-scale structures based on multiobjective evolutionary optimization	Perera and Ruiz	2008	Mechanical Systems and Signal Processing
Ambient and free-vibration tests to improve the quantification and estimation of modal parameters in existing bridges	Lorenzoni et al.	2019	Journal of Civil Structural Health Monitoring
Assessment of Highway Bridge Upgrading by Dynamic Testing and Finite-Element Model Updating	Brownjohn et al.	2003	Journal of Bridge Engineering
Automated modal identification using principal component and cluster analysis: Application to a long-span cable-stayed bridge	Mao et al.	2019	Structural control and health monitoring
Bayesian Finite Element Model Updating and Assessment of Cable-Stayed Bridges Using Wireless Sensor Data	Asadollahi et al.	2018	Sensors
Bridge model updating using response surface method and genetic algorithm	Deng and Cai	2010	Journal of Bridge Engineering
Calibrating a high-fidelity finite element model of a highway bridge using a multi-variable sensitivity-based optimisation approach	Mosavi et al.	2013	Structure and Infrastructure Engineering
Calibration of the Finite Element Model of a Twelve-Span Prestressed Concrete Bridge Using Ambient Vibration Data	Chen et al.	2014	7th European Workshop on Structural Health Monitoring, Jul 2014, Nantes, France
Candidate model construction of a cable-stayed bridge using parameterised sensitivity-based finite element model updating	Park et al.	2015	Structure and Infrastructure Engineering
Civil structure condition assessment by FE model updating: Methodology and case studies	Brownjohn et al.	2001	Finite Elements in Analysis and Design
Concurrent multi-scale modeling of civil infrastructures for analyses on structural deteriorating—Part II: Model updating and verification	Chan et al.	2009	Finite Elements in Analysis and Design
Effects of changing ambient temperature on finite element model updating of the Dowling Hall Footbridge	Moaveni and Behmanesh	2012	Engineering Structures
Experimental and numerical approaches for structural assessment in new footbridge designs (SFRSCC–GFPR hybrid structure)	Sánchez-Aparicio et al.	2015	Composite Structures
FE Model Updating on an In-Service Self-Anchored Suspension Bridge with Extra-Width Using Hybrid Method	Xia et al.	2017	Applied Sciences

Field-testing and numerical simulation of vantage steel bridge	El-Sisi et al.	2020	Journal of Civil Structural Health Monitoring
Finite element model updating and validating of Runyang Suspension Bridge based on SHMS	Hao et al.	2005	Journal of Southeast University
Finite Element Model Updating for a Cable-stayed Bridge Using Manual Tuning and Sensitivity-based Optimization	Park et al.	2012	Structural engineering international
Finite element model updating for the Runyang Cable-stayed Bridge tower using ambient vibration test results	Ding and Li	2008	Advances in Structural Engineering
Finite element model updating in structural dynamics by using the response surface method	Ren and Chen	2010	Engineering Structures
Finite Element Model Updating of a PSC Box Girder Bridge Using Ambient Vibration Test	Hiatt et al.	2011	Advanced Materials Research
Finite element model updating of bridge structures based on sensitivity analysis and optimization algorithm	Minshui and Hongping	2008	Wuhan University Journal of Natural Sciences
Finite Element Model Updating of Civil Engineering Infrastructures: A review literature	Moravej et al.	2017	The 8th International Conference on Structural Health Monitoring of Intelligent Infrastructure Brisbane, Australia
Finite element model updating of existing steel bridge based on structural health monitoring	He et al.	2008	Journal of Central South University of Technology
Finite element model updating and structural damage identification using OMAX data	Reynders et al.	2010	Mechanical systems and signal processing
Finite element model updating for structures with parametric constraints	Zhang et al.	2000	Earthquake engineering & structural dynamics
Finite element model updating of a bowstring-arch railway bridge based on experimental modal parameters	Ribeiro et al.	2012	Engineering Structures
Finite Element Model Updating of Canonica Bridge Using Experimental Modal Data and Genetic Algorithm	Liu et al.	2018	Structural engineering international
Finite Element Model Updating of Senyuva Historical Arch Bridge Using Ambient Vibration Tests	Bayraktar et al.	2009	The Baltic journal of road and bridge engineering
Finite element model validation of bridge based on structural health monitoring—Part I: Response surface-based finite element model updating	Zong et al.	2015	Journal of Traffic and Transportation Engineering
Finite element modelling and updating of a lively footbridge: The complete process	Živanović et al.	2007	Journal of Sound and Vibration
Finite-Element Model Updating and Dynamic Responses of Reconstructed Historical Timber Bridges using Ambient Vibration Test Results	Altunişik et al.	2020	Journal of Performance of Constructed Facilities
Finite-Element Analysis and Vibration Testing of a Two-Span Masonry Arch Bridge	Bayraktar et al.	2010	Journal of Performance of Constructed Facilities
Full-scale bridge finite-element model calibration using measured frequency-response functions	Sipple and Sanayei	2015	Journal of Bridge Engineering

Identification of soil-structure interaction effect in a portal frame railway bridge through full-scale dynamic testing	Zangeneh et al.	2018	Engineering Structures
Identification, model updating, and validation of a steel twin deck curved cable-stayed footbridge	Bursi et al.	2014	Computer-Aided Civil and Infrastructure Engineering
Improved finite element modelling of a cable-stayed bridge through systematic manual tuning	Daniell and Macdonald	2007	Engineering Structures
Influence of the ballasted track on the dynamic properties of a truss railway bridge	Bornet et al.	2015	Structure and Infrastructure Engineering
Long-term structural health monitoring system for a FRP composite highway bridge structure	Guan et al.	2007	Journal of Intelligent Material Systems and Structures
Modal identification, model updating and nonlinear analysis of a reinforced concrete bridge	El-Borgi et al.	2008	Journal of Vibration and Control
Modal parameter identification of a three-storey structure using frequency domain techniques FDD and EFDD and time domain technique SSI: Experimental studies and simulations	Mohammadi and Nasirshoabi	2017	Journal of Vibroengineering
Modal parameter identification of concrete filled steel tube arch bridge based on stochastic subspace method	Li-xian and Sheng-kui	2014	Advanced Materials Research
Model calibration in the presence of resonant non-structural elements	Matta and De Stefano	2015	Journal of Civil Structural Health Monitoring
Model identification of bridges using measurement data	Robert-Nicoud et al.	2005	Computer-aided civil and infrastructure engineering
Model updating for structural health monitoring using static and dynamic measurements	Schommer et al.	2017	Procedia Engineering
Model Updating in Complex Bridge Structures using Kriging Model Ensemble with Genetic Algorithm	Qin et al.	2018	KSCE Journal of Civil Engineering
Model updating of a dynamic model of a composite steel-concrete railway viaduct based on experimental tests	Malveiro et al.	2018	Engineering Structures
Model updating of an existing bridge with high-dimensional variables using modified particle swarm optimization and ambient excitation data	Xia et al.	2020	Measurement: Journal of the International Measurement Confederation
Model Updating of Railway Bridge Using in Situ Dynamic Displacement Measurement under Trainloads	Feng and Feng	2015	Journal of Bridge Engineering
Model updating of a historic concrete bridge by sensitivity- and global optimization-based Latin Hypercube Sampling	Ferrari et al.	2019	Engineering structures
Non-destructive modal parameter identification of historical timber bridges using ambient vibration tests after restoration	Altunışık et al.	2019	Measurement: Journal of the International Measurement Confederation
Parameter selection in finite-element-model updating by global sensitivity analysis using gaussian process metamodel	Wan et al.	2015	Journal of structural engineering

Performance of a tied-arch reinforced concrete railway bridge: Rating, safety assessment, and bond length evaluation	Uzgider et al.	2009	Journal of Performance of Constructed Facilities
Railway bridge structural health monitoring and fault detection: State-of-the-art methods and future challenges	Vagnoli et al.	2018	Structural Health Monitoring
Recent progress and future trends on damage identification methods for bridge structures	An et al.	2019	Structural Control and Health Monitoring
Review of the application of finite element model updating to civil structures	Wang et al.	2014	Key Engineering Materials
Sensitivity-based finite element model updating of a pontoon bridge	Petersen and Øiseth	2017	Engineering Structures
Stochastic model updating utilizing Bayesian approach and Gaussian process model	Wan and Ren	2016	Mechanical Systems and Signal Processing
Structural Condition Assessment of Birecik Highway Bridge Using Operational Modal Analysis	Bayraktar et al.	2016	International Journal of Civil Engineering
Structural Dynamic Model Updating Techniques: A State of the Art Review	Sehgal and Kumar	2015	Archives of Computational Methods in Engineering
Structural Identification of a Concrete-Filled Steel Tubular Arch Bridge via Ambient Vibration Test Data	Zhou et al.	2017	Journal of Bridge Engineering
Structural model updating of an in-service bridge using dynamic data	Garcia-Palencia et al.	2015	Structural Control and Health Monitoring
Structural model updating using dynamic data	García-Palencia and Santini-Bell	2014	Journal of Civil Structural Health Monitoring
Structural safety assessment of bowstring type RC arch bridges using ambient vibration testing and finite element model calibration	Türker and Bayraktar	2014	Measurement: Journal of the International Measurement Confederation
Structural condition assessment of a bridge pier: A case study using experimental modal analysis and finite element model updating	Mao et al.	2019	Structural control and health monitoring
Structural Identification for Performance Prediction Considering Uncertainties: Case Study of a Movable Bridge	Gokce et al.	2013	Journal of Structural Engineering
Structural identification of a tied arch bridge using parallel genetic algorithms and ambient vibration monitoring with a wireless sensor network	Whelan et al.	2018	Journal of civil structural health monitoring
Substructure based approach to finite element model updating	Weng et al.	2011	Computers & structures
System identification and model updating of highway bridges using ambient vibration tests	Sabamehr et al.	2018	Journal of civil structural health monitoring
System Identification Methods for (Operational) Modal Analysis: Review and Comparison	Reynders	2012	Archives of Computational Methods in Engineering
Vibration-based operational modal analysis of the Mikron historic arch bridge after restoration	Altunişik et al.	2011	Civil engineering and environmental systems

Operational Condition Monitoring of the Stange Railway Overpass

Objective: Collection of operational condition acceleration data from the Stange railway overpass.

Location: Stange railway bridge, Norway.

Date: 15.12.2020 – 17.12.2020.



Figure B.1. Stange railway overpass.

Sensor Hardware

Sensor hardware utilized consisted of 5 complete sets of Unquake accelerographs, including datalogger unit, accelerometer, GPS unit, 5V USB powerbank, 16-32 GB SD-memory card, and required cables/wiring. Prior to departure to Stange, all sensor hardware was tested for correct operation, labeled, and individually stored in plastic containers for transportation.

Hardware Installation

Sensor hardware supplier recommend that accelerometers are secured on thin steel plates using high-powered magnets, where the steel plate is mounted directly on the concrete surface using a fast setting, high-strength adhesive. Due to recent snowfall and freezing temperatures at the time of hardware installation, a thin layer of frost and ice covering the vertical concrete surfaces on the bridge prevented proper installation of the steel plates using only adhesives. To secure a proper bond between the concrete surface and steel plates, a concrete drill was used to install expansive concrete bolts. To secure the correct placement and orientation of the accelerometers, a tape measure and level were used. At some locations where the concrete surface was not perfectly level in the vertical axis, steel shims were used

in addition to the steel plates and were adjusted and fastened using additional adhesive and concrete bolts.

Workflow of hardware installation:

1. Measuring layout for sensor placement and marking each location (both sensor setups)
2. Installation of steel plates
3. Setup of datalogger, accelerometer, and GPS unit at each location for the first setup
4. Re-checking location measurements and securing correct orientation of accelerometers
5. Connecting power-supply and checking for correct operation

Measuring the sensor layout and Installation of the steel plates were the most labor-intensive steps and took roughly 1.5 hours where four people were working. For additional weather protection of the datalogger and powerbank units, the hardware was placed in fully enclosed plastic boxes during operation. Figure B.2 and B.3 show the datalogger, accelerometer, and GPS unit setup.



Figure B.2. Datalogger and accelerometer setup.



Figure B.3. Accelerometer and GPS unit setup.

As the rail line was active, we were given 20-minute windows to work to allow for passing trains. A representative from Bane NOR was acting as a security supervisor during the work and had constant communication with railway administration to coordinate the work on the

line. Prior to departure, all people involved had to go through an online security course to be allowed to perform work on an active rail line.

Sensor Operation

After installation of the hardware, the operational monitoring was initiated for sensor configuration one at approx. 10:20, Tuesday 15.12.2020. The monitoring in configuration one was continued until 08:39 the following day, giving approx. 22 hours of continuous monitoring for the first setup. At this time, two of the sensors were moved to a new location (setup 2) in addition to all dataloggers being reset. Monitoring for configuration two was initiated at approx. 08:50, Wednesday 16.12.2020 and completed at approx. 07:36 the following day, giving approx. 23 hours of continuous monitoring for configuration two. Combined between the setups, approx. 45 hours of acceleration data were obtained.

Weather data observed from 15.12.2020 – 17.12.2020 showed a minimum temperature of $-6,0^{\circ}\text{C}$ and a maximum temperature of $0,6^{\circ}\text{C}$ during monitoring. Only light precipitation was recorded during monitoring, but this is not assumed to have affected the measurements.

Preliminary Quality Assurance of Data

After ending monitoring and dismantling all hardware, a basic preliminary quality assurance of collected acceleration data was performed. This included control of timestamps and format of data, in addition to taking data backups of all collected data.

Appendix C – Complete FEMU Process

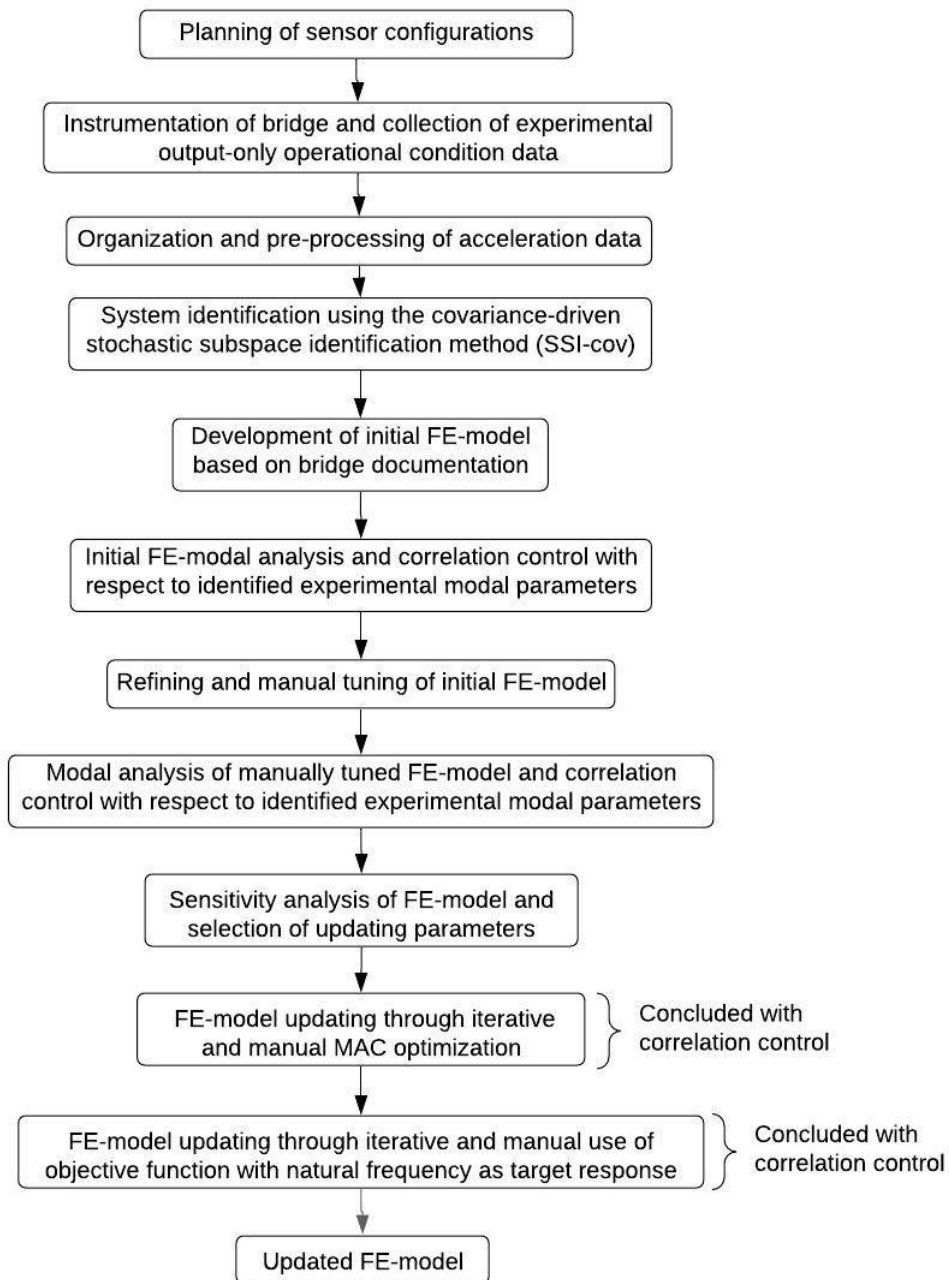


Figure C.1. Complete FEMU process flowchart.